NASA TECHNICAL NOTE

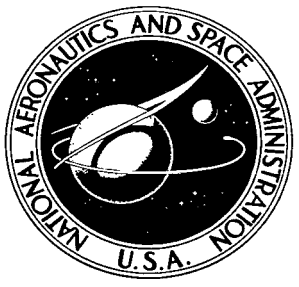

NASA TN D-7004

NASA TN D-7004

WIND-TUNNEL INVESTIGATION OF A JET TRANSPORT AIRPLANE CONFIGURATION WITH AN EXTERNAL-FLOW JET FLAP AND INBOARD POD-MOUNTED ENGINES

by Delma C. Freeman, Jr., Lysle P. Parlett, and Robert L. Henderson

Langley Research Center
Hampton, Va. 23365

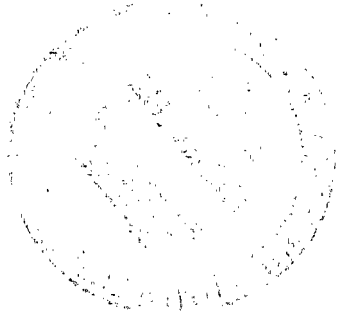

NATIONAL AERONAUTICS AND SPACE ADMINISTRATION • WASHINGTON, D. C. • DECEMBER 1970

1. Report No.	2. Government Accession No.	3. Recipient's Catalog No.
NASA TN D-7004		

4. Title and Subtitle	5. Report Date
WIND-TUNNEL INVESTIGATION OF A JET TRANSPORT AIRPLANE CONFIGURATION WITH AN EXTERNAL-FLOW JET FLAP AND INBOARD POD-MOUNTED ENGINES	December 1970
	6. Performing Organization Code

7. Author(s)	8. Performing Organization Report No.
Delma C. Freeman, Jr., Lysle P. Parlett, and Robert L. Henderson	L-7403
	10. Work Unit No. 721-01-11-06
9. Performing Organization Name and Address: NASA Langley Research Center, Hampton, Va. 23365	11. Contract or Grant No.
12. Sponsoring Agency Name and Address: National Aeronautics and Space Administration, Washington, D.C. 20546	13. Type of Report and Period Covered: Technical Note
	14. Sponsoring Agency Code

15. Supplementary Notes

16. Abstract

A wind-tunnel investigation has been conducted to determine the aerodynamic and stability and control characteristics of a jet transport airplane configuration with an external-flow jet flap and four pod-mounted engines. Major emphasis of the investigation was placed on determining the effectiveness of close-inboard mounting of the engines as a means of reducing the large engine-out moments inherent in an external-flow jet-flap system and of evaluating the use of asymmetric blowing on drooped ailerons or the use of differential flap deflection as a means of providing trim to offset the engine-out moments.

17. Key Words (Suggested by Author(s))	18. Distribution Statement
External-flow jet flap High-lift devices STOL configurations	Unclassified – Unlimited

19. Security Classif. (of this report)	20. Security Classif. (of this page)	21. No. of Pages	22. Price*
Unclassified	Unclassified	120	$3.00

*For sale by the Clearinghouse for Federal Scientific and Technical Information
Springfield, Virginia 22151

WIND-TUNNEL INVESTIGATION OF A JET TRANSPORT AIRPLANE CONFIGURATION WITH AN EXTERNAL-FLOW JET FLAP AND INBOARD POD-MOUNTED ENGINES

By Delma C. Freeman, Jr., Lysle P. Parlett,
and Robert L. Henderson
Langley Research Center

SUMMARY

A wind-tunnel investigation has been conducted to determine the aerodynamic and stability and control characteristics of a jet transport airplane configuration with an external-flow jet flap and four pod-mounted engines. Major emphasis of the investigation was placed on determining the effectiveness of close-inboard mounting of the engines as a means of reducing the large engine-out moments inherent in an external-flow jet-flap system and of evaluating the use of asymmetric blowing on drooped ailerons or the use of differential flap deflection as a means of providing trim to offset the engine-out moments.

The results of the investigation indicated that with the location of pod-mounted engines fairly close inboard, it was possible to achieve sizable reductions in engine-out moments. The use of either asymmetric blowing over drooped ailerons or differential flap deflection offered a means of achieving roll trim for engine-out conditions over the normal operational angle-of-attack range, but neither method was able to trim the much larger rolling asymmetries that occurred when the wing with an engine inoperative stalled first. The combination of aileron blowing and spoilers provided roll trim capability up to the stall angle of attack but the roll asymmetries exceeded this capability beyond the stall. For either method of roll trim, the rudder, with boundary-layer control, was capable of trimming the asymmetric yawing moments. The close-inboard engine arrangement showed no particular adverse effect on longitudinal stability or trim but did produce some detrimental effect on lift.

INTRODUCTION

Recent interest in the development of jet-powered STOL transport aircraft has led to serious consideration of the external-flow jet flap as a means of producing the high lift required for STOL operation. Early experimental work (refs. 1 to 3) demonstrated the feasibility of this concept for producing high lift but interest in the idea decreased

mainly because of the problems of high temperature on the aircraft structures. The more recent development of the high-bypass turbofan engines with relatively cool exhaust has minimized this problem and made the concept much more feasible from structural considerations.

In the application of the jet-flap concept to STOL aircraft, consideration must be given to stability and control at very low speeds, particularly in terms of safe operation with a critical engine inoperative. There is very little experimental information of this type available from which basic problem areas can be identified and from which effective design features can be established for practical hardware applications. Because of the need for this type of information, some recent stability and control investigations have been conducted on high-thrust-weight-ratio jet STOL aircraft configurations equipped with external-flow jet flaps. (See refs. 4 and 5.) The results of these investigations confirmed the fact that high lift could be generated with this concept but pointed out that the engine-out moments associated with an engine failure were too large to be trimmed out by conventional aileron and rudder control. In an effort to provide some additional information on the engine-out problem, the present investigation was undertaken with the major objectives of studying means of reducing the engine-out moments and of providing some means other than spoilers, which have a severe lift penalty, for offsetting engine-out rolling moments. The model used in this investigation was the same as that used in references 5 and 6 and had a swept wing located high on the fuselage and a horizontal tail located high on the vertical tail. The engine arrangement used in the present study differed from that tested earlier in that the outboard engines were moved inboard and located next to the inboard engines in a clustered arrangement to simulate a configuration with engines mounted together in a single pod. The model was equipped with blowing systems on the ailerons, rudder, and elevator to provide increased control effectiveness at the high lift conditions generated in the tests.

The present investigation consisted of tests over an angle-of-attack and angle-of-sideslip range for several thrust coefficients and for several flap deflections. In tests made under various engine-out conditions, the effectiveness of asymmetric blowing over a drooped aileron and the effectiveness of differential flap deflection were evaluated as a means of achieving roll trim. In addition to the static force tests, flow-survey measurements were made in the vicinity of the horizontal tail to determine the downwash variation for a jet-flap configuration operating at very high lift coefficients.

SYMBOLS

The longitudinal data are referred to the stability-axis system and the lateral data are referred to the body-axis system. (See fig. 1.) The origin of the axes was at the center of gravity (0.33 mean aerodynamic chord) shown in figure 2.

In order to facilitate international usage of the data presented, dimensional quantities are presented both in U.S. Customary Units and in the International System of Units (SI). Equivalent dimensions were determined by using the conversion factors given in reference 7.

b wing span, ft (m)

C_D drag coefficient, F_D/qS

C_L lift coefficient, F_L/qS

C_l rolling-moment coefficient, M_X/qSb

$C_{l_\beta} = \frac{\partial C_l}{\partial \beta}$, per deg

C_m pitching-moment coefficient, $M_Y/qS\bar{c}$

$C_{m_{i_t}} = \frac{\partial C_m}{\partial i_t}$, per deg

C_n yawing-moment coefficient, M_Z/qSb

$C_{n_{i_v}} = \frac{\partial C_n}{\partial i_v}$, per deg

$C_{n_\beta} = \frac{\partial C_n}{\partial \beta}$, per deg

C_Y side-force coefficient, F_Y/qS

$C_{Y_\beta} = \frac{\partial C_Y}{\partial \beta}$, per deg

C_μ engine gross-thrust coefficient, $\dot{m}V_E/qS$

$C_{\mu,a}$ aileron blowing jet-momentum coefficient, $F_{R,a}/qS$

$C_{\mu,e}$ elevator blowing jet-momentum coefficient, $F_{R,e}/qS$

$C_{\mu,r}$ rudder blowing jet-momentum coefficient, $F_{R,r}/qS$

c local wing chord, in. (cm)

$\bar{c}$	mean aerodynamic chord, in. (cm)
F_A	axial force, lb (N)
F_D	drag force, lb (N)
F_L	lift force, lb (N)
F_N	normal force, lb (N)
F_R	resultant force, lb (N)
$F_{R,a}$	resultant force for aileron blowing, lb (N)
$F_{R,e}$	resultant force for elevator blowing, lb (N)
$F_{R,r}$	resultant force for rudder blowing, lb (N)
F_X	force along X-axis, positive forward, lb (N)
F_Y	side force, positive to the right, lb (N)
F_Z	force along Z-axis, positive down, lb (N)
i_t	horizontal-tail incidence angle, deg
i_v	vertical-tail incidence angle, deg
M_X	rolling moment, ft-lb (m-N)
M_Y	pitching moment, ft-lb (m-N)
M_Z	yawing moment, ft-lb (m-N)
$\dot{m}$	engine mass-flow rate, slugs/sec (kg/sec)
q	free-stream dynamic pressure, $\frac{1}{2}\rho V^2$, lb/ft^2 (N/m^2)
q_t	dynamic pressure at the tail, $\frac{1}{2}\rho V_t^2$, lb/ft^2 (N/m^2)

S	wing area, ft^2 (m^2)
T	thrust, lb (N)
V	free-stream velocity, ft/sec (m/sec)
V_E	engine exit velocity, ft/sec (m/sec)
V_t	velocity at tail, ft/sec (m/sec)
X,Y,Z	body reference axes
X_S,Y_S,Z_S	stability reference axes
z	tail height (measured from top of fuselage to horizontal tail), in. (cm)
α	angle of attack, deg
β	angle of sideslip, deg
δ_a	aileron deflection, positive when trailing edge is down, deg
δ_e	elevator deflection, positive when trailing edge is down, deg
δ_{f1}	deflection of forward segment of trailing-edge flap (referenced to wing root chord), deg
δ_{f2}	deflection of aft segment of trailing-edge flap (referenced to wing root chord), deg
δ_j	jet deflection, deg
δ_r	rudder deflection, positive when trailing edge is to the left, deg
δ_s	spoiler deflection, deg
ϵ	downwash angle measured with respect to the free stream, deg
η	flap turning efficiency, $\frac{\sqrt{F_A{}^2 + F_N{}^2}}{T}$

ρ air density, slugs/ft^3 (kg/m^3)

$1 - \frac{\partial \epsilon}{\partial \alpha}$ downwash factor

Subscripts:

L left

R right

WIND TUNNEL

The tests were made in the 30- by 60-foot (9.1- by 18.3-m) open-throat test section of the Langley full-scale tunnel with the model mounted about 10 feet (3.05 m) above the ground board. The model was so small in proportion to the tunnel test section that no wind-tunnel wall corrections were needed or applied. Normal corrections for flow angularity were applied.

MODEL AND APPARATUS

The investigation was conducted on the four-engine, high-wing, jet-transport model illustrated by the three-view drawing of figure 2(a). The model was the same as that used in reference 6 except that the outboard engine was moved inboard to a location adjacent to the inboard engine, the leading-edge slats were replaced with leading-edge flaps, and the chord of the aft segment of the trailing-edge flap was doubled. The dimensional characteristics of the model are given in table I. A detailed sketch of the flap assembly and engine-pylon arrangement is shown in figure 2(b). Details of the leading-edge flap configuration and the jet-exhaust deflectors employed during the tests are presented in figures 2(c) and 2(d), respectively. Details of the aileron blowing system are presented in figure 2(e). The model was equipped with a conventional spoiler located on the wing and also with a small-chord spoiler located on the flap. (See figs. 2(a) and 2(b).) Photographs of the model mounted for static force tests in the Langley full-scale tunnel are presented in figure 3.

To facilitate model configuration changes and to insure accurate flap deflection angles, the wing of the model was designed with removable trailing edges. To convert the model from the clean configuration to each of the flap-deflected configurations, the clean trailing edges were replaced with trailing-edge flaps constructed with fixed gaps, overlaps, and deflection angles. The leading-edge flaps were designed so that they could be fastened to the wing leading edge at fixed positions when desired.

The model engines represented turbofans with a bypass ratio of approximately 8 to 1. These engines were installed at -3° incidence so that for the basic condition the jet exhaust impinged directly on the trailing-edge flap system. In addition, in an attempt to achieve better spreading and to improve the turning efficiency of the jet-flap system, several jet-exhaust deflectors (see fig. 2(d)) were tested. The engine turbines were driven by compressed air and turned fans which produced the desired thrust.

All the model control surfaces (elevator, aileron, and rudder) were equipped with blowing. The blowing system consisted of a simple tube arrangement located at the rear of the wing or tail and just in front of the controls. Compressed air was supplied to the tubes internally and forced over the control surface through a series of small holes spaced equally along the tube. The holes were quite small and far apart with the result that the blowing system was not effective for boundary-layer control. This system was used on all surfaces and is illustrated in the horizontal-tail cross section shown in figure 2(a). In tests with the ailerons drooped to simulate full-span flaps, it was necessary to alter the aileron shape with a simple bent-sheet-metal arrangement so that the ailerons conformed to the basic flap contour. (See fig. 2(e).) This alteration was necessary in order to prevent a break in continuity of the flap system when the ailerons were drooped because the model used in the tests was an existing model which had an aileron hinge offset from that of the basic flaps.

All the tests were made with an internal strain-gage balance and conventional sting which entered the rear of the fuselage.

TESTS AND PROCEDURES

In preparation for the tests, engine calibrations were made to determine gross thrust as a function of engine speed, in rpm, in the static condition – at zero angle of attack with the thrust deflectors off and with flaps undeflected. For the actual tests the engine rotational speed was set to give the desired thrust, then these settings were held constant through the ranges of angles of attack or sideslip.

Jet deflection angles and flap turning efficiency were determined from measurements of normal and axial forces made in the static thrust condition with flaps deflected. The static thrust used in computing turning efficiency was taken directly from the engine calibrations at the appropriate rpm.

During the wind-on tests, six-component longitudinal and lateral static force data were measured at flap deflections (fig. 2(b)) of $20^{\circ}/40^{\circ}$, $25^{\circ}/50^{\circ}$, and $30^{\circ}/60^{\circ}$ for a range of engine gross-thrust coefficient C_{μ} (total of all engines) from 0 to 4.24, and through an angle-of-attack range from -5° to 30°. Tests were made at various horizontal-tail incidence angles, at various deflections of aileron, rudder, and elevator, and for various

amounts of blowing over each of the control surfaces. The amount of blowing over the ailerons was established by the amount required over one aileron to produce roll trim in the engine-out condition at $\alpha = 0^{o}$. Under conditions of symmetric thrust, one-half the mass flow rate as established above was applied to each aileron as a lift-augmenting device. The mass flow rates for each of the blown surfaces was evaluated by measuring the force produced by the respective jets in the wind-off condition. Sideslip runs were made over a range of sideslip angles from -20^{o} to 20^{o}. All wind-on tests were made at a free-stream dynamic pressure of approximately 3 lb/ft^2 (144 N/m^2) which corresponds to a velocity of 50 ft/sec (15.2 m/sec) and to a Reynolds number, based on the mean aerodynamic chord, of 0.35×10^6.

In addition to the force tests, a few flow survey measurements were made in the vicinity of the horizontal tail to determine the downwash variation with changes in thrust coefficient. The measurements were made with a simple vane of balsa wood which was free to pivot for alinement with the local flow. The flow angle was indicated through the use of a potentiometer connected to the wooden vane.

PRESENTATION OF DATA

The data obtained in the investigation are presented in the following figures:

	Figure
Static turning data	4
Longitudinal characteristics, tail off:	
$\delta_{f1}/\delta_{f2} = 30^{o}/60^{o}$	5
$\delta_{f1}/\delta_{f2} = 25^{o}/50^{o}$	6
$\delta_{f1}/\delta_{f2} = 20^{o}/40^{o}$	7
Drag polar plots of model	8
Longitudinal characteristics, tail on:	
$\delta_f = 0^{o}$; $\delta_e = 0^{o}$	9
$\delta_{f1}/\delta_{f2} = 30^{o}/60^{o}$; $\delta_e = -50^{o}$	10
$\delta_{f1}/\delta_{f2} = 25^{o}/50^{o}$; $\delta_e = -50^{o}$	11
$\delta_{f1}/\delta_{f2} = 20^{o}/40^{o}$; $\delta_e = -50^{o}$	12
Longitudinal characteristics with spoiler deflection	13
Longitudinal characteristics with aileron blowing	14
Horizontal-tail lift characteristics	15
Downwash angles at the tail:	
$\delta_{f1}/\delta_{f2} = 30^{o}/60^{o}$	16
$\delta_{f1}/\delta_{f2} = 20^{o}/40^{o}$	17
Summary of downwash flow studies	18

Figure

Dynamic pressure at the tail 19
Variation of lateral characteristics with β 20
Lateral stability characteristics:
$\delta_{f1}/\delta_{f2} = 30^o/60^o$ 21
$\delta_{f1}/\delta_{f2} = 20^o/40^o$ 22
$\delta_{f1}/\delta_{f2} = 0^o$; $C_\mu = 0$; $C_{\mu,a} = 0$ 23
Lateral and longitudinal characteristics:
Left outboard engine inoperative; $\delta_{f1}/\delta_{f2} = 30^o/60^o$; $\delta_e = -50^o$; $i_t = 0^o$; $\delta_a = 60^o$; $C_{\mu,a} = 0$ 24
Left inboard engine inoperative; $\delta_{f1}/\delta_{f2} = 30^o/60^o$; $\delta_e = -50^o$; $i_t = 0^o$; $\delta_a = 60^o$; $C_{\mu,a} = 0$ 25
Left outboard engine inoperative:
$\delta_{f1}/\delta_{f2} = 25^o/50^o$; $i_t = 0^o$; $\delta_e = -50^o$; $\delta_a = 50^o$ 26
$\delta_{f1}/\delta_{f2} = 20^o/40^o$; $i_t = 0^o$; $\delta_e = -50^o$; $\delta_a = 40^o$ 27
Asymmetric aileron blowing; $\delta_{f1}/\delta_{f2} = 30^o/60^o$; $i_t = 0^o$; $\delta_e = -50^o$; $\delta_{a_L} = 60^o$; $\delta_{a_R} = 0^o$; $C_{\mu,a_R} = 0$ 28
Left inboard engine inoperative; asymmetric aileron blowing; $\delta_{f1}/\delta_{f2} = 30^o/60^o$; $i_t = 0^o$; $\delta_e = -50^o$; $\delta_{a_L} = 60^o$; $\delta_{a_R} = 60^o$; $C_{\mu,a_R} = 0$ 29
Left outboard engine inoperative; asymmetric aileron blowing:
$\delta_{f1}/\delta_{f2} = 30^o/60^o$; $i_t = 0^o$; $\delta_e = -50^o$; $\delta_{a_L} = 60^o$; $\delta_{a_R} = 60^o$ 30
$\delta_{f1}/\delta_{f2} = 25^o/50^o$; $i_t = 0^o$; $\delta_e = -50^o$; $\delta_{a_L} = 50^o$; $\delta_{a_R} = 0^o$; $C_{\mu,a_R} = 0$ . . 31
$\delta_{f1}/\delta_{f2} = 25^o/50^o$; $i_t = 0^o$; $\delta_e = -50^o$; $\delta_{a_L} = 50^o$; $\delta_{a_R} = 50^o$ 32
Left outboard engine inoperative; differential flap deflection; $(\delta_{f1}/\delta_{f2})_L = 30^o/60^o$; $(\delta_{f1}/\delta_{f2})_R = 20^o/40^o$; $i_t = 0^o$; $\delta_e = -50^o$; $\delta_{a_L} = 60^o$; $\delta_{a_R} = 40^o$ 33
Left inboard engine inoperative; differential flap deflection; $(\delta_{f1}/\delta_{f2})_L = 30^o/60^o$; $(\delta_{f1}/\delta_{f2})_R = 20^o/40^o$; $i_t = -50^o$; $\delta_{a_L} = 60^o$; $\delta_{a_R} = 40^o$ 34
Left outboard engine inoperative; differential flap deflection; engines spread out; $(\delta_{f1}/\delta_{f2})_L = 30^o/60^o$; $(\delta_{f1}/\delta_{f2})_R = 20^o/40^o$; $i_t = 0^o$; $\delta_e = -50^o$; $\delta_{a_L} = 60^o$; $\delta_{a_R} = 40^o$; $C_{\mu,a_R} = 0$ 35
Left inboard engine operative; differential flap deflection; engines spread out; $(\delta_{f1}/\delta_{f2})_L = 30^o/60^o$; $(\delta_{f1}/\delta_{f2})_R = 20^o/40^o$; $i_t = 0^o$; $\delta_e = -50^o$; $\delta_{a_L} = 60^o$; $\delta_{a_R} = 40^o$ 36
Left inboard engine inoperative; asymmetric aileron blowing; $\delta_{f1}/\delta_{f2} = 20^o/40^o$; $i_t = 0^o$; $\delta_e = -50^o$; $\delta_{a_L} = 40^o$; $\delta_{a_R} = 40^o$ 37

Figure

Spoiler effectiveness; $\delta_s = 60^o$; $i_t = 0^o$; $\delta_e = -50^o$; $\delta_a = 60^o$; $\delta_{f1}/\delta_{f2} = 30^o/60^o$ 38
Spoiler effectiveness, wing and flap spoilers; $\delta_s = 60^o$; $i_t = 0^o$; $\delta_e = -50^o$; $\delta_a = 40^o$; $\delta_{f1}/\delta_{f2} = 20^o/40^o$ 39
Rudder effectiveness:
$\delta_r = -42^o$; $\delta_{f1}/\delta_{f2} = 30^o/60^o$; $i_t = 0^o$; $\delta_e = -50^o$; $\delta_a = 60^o$ 40
$\delta_r = -42^o$; $\delta_f = 0^o$; $i_t = 0^o$; $\delta_e = 0^o$ 41
Variation of lateral characteristics with vertical-tail incidence 42

RESULTS AND DISCUSSION

Lift Characteristics

In the investigation reported in reference 5 a number of exhaust deflectors were used on the external-flow jet-flap arrangement to determine their effectiveness in spreading and turning the jet. From these tests, in which the model had engines spread out along the wing, it was found that deflectors mounted on the bottom of the engine improved the turning efficiency of the system. In the present study, in which the engines were clustered together and mounted inboard along the wing, the same deflectors were also tested to check their effectiveness in this different system. The results of these tests, presented in figure 4 in terms of the ratio of normal force to thrust F_N/T against the ratio of axial force to thrust F_A/T, show that the turning efficiency was not significantly altered by the addition of the deflectors over that for the condition with deflectors off. On the basis of these static turning tests and on the results of preliminary wind-on tests measured with the deflectors on and off, which generally confirmed the results of the static turning tests, the present investigation was conducted with deflectors off.

Basic longitudinal data for the model in the tail-off configuration with flap deflections of $30^o/60^o$, $25^o/50^o$, and $20^o/40^o$ are presented in figures 5, 6, and 7, respectively. The leading-edge flaps were extended for all test conditions. These figures show that the stall angle and the maximum lift coefficient increased with increasing thrust coefficient and that the effects of power on the lift characteristics were more pronounced at the higher flap deflections. The data of figure 5(a) show that lift coefficients up to about 9 (untrimmed) could be produced for a gross-thrust coefficient of 4.24. As would be expected because of the rearward location of the flap loads, high lift coefficients are accompanied by large nose-down moments.

A comparison of the data of figures 5(a), 5(b), and 5(c) shows the effect of drooping the ailerons to represent a configuration with full-span flaps. The data of figure 5(b) show that with the ailerons drooped and no blowing, there was some loss in maximum lift,

probably because of flow separation on the ailerons. With blowing over the ailerons (fig. 5(c)), however, there were substantial gains in lift at low and moderate angles of attack but generally no appreciable change in maximum lift over that with the ailerons undeflected. Actually, the ailerons were built with a different hinge line from that of the flaps, and it was necessary to alter the wing-tip flaps with a bent-sheet-metal arrangement to conform to the flap contour. This arrangement made a relatively poor wing-tip flap, but it was believed that with some blowing, the arrangement was good enough to determine the relative effects of full-span flaps.

Since the model of the present investigation is identical with that of reference 5 except for the change in engine location from a configuration with the engines spread out along the span to one with the engines clustered in an inboard arrangement, the question naturally arises as to the relative effectiveness of the two engine arrangements. The data of figure 8(a) provide a direct indication of the relative aerodynamic performance of these two arrangements in the form of drag polar plots. These data are presented for trim lift coefficients with the center-of-gravity location of $0.33\bar{c}$ in both cases. As would be expected from a consideration of spanwise load distribution, the configuration having the spread-out engine arrangement shows somewhat better performance than does the one with the clustered arrangement. The data of figure 8(b) show that aileron deflection in combination with some aileron blowing results in some improvement in performance over that with ailerons undeflected. The lower maximum lift coefficient that occurred for the drooped ailerons can probably be attributed to the fact that the leading-edge treatment, which was tailored to the undeflected aileron condition, was badly out of adjustment with ailerons deflected and resulted in flow separations.

Longitudinal Stability and Trim With Symmetric Thrust

The longitudinal stability and trim characteristics with horizontal tail on are plotted in figures 9 to 12 for various symmetric thrust levels, flap settings, and horizontal-tail incidence angles. Data showing lift characteristics with symmetrical spoiler deflection are presented in figure 13, and data showing the effects of increased aileron blowing are presented in figure 14. Data obtained with the horizontal tail alone are presented in figure 15, and data obtained in flow surveys in the vicinity of the horizontal tail are presented in figures 16 to 18. The variation of dynamic pressure at the tail with engine thrust is shown in figure 19.

The data of figure 9 show that the model with undeflected flaps was stable up through the stall. A comparison of these data with the pitching-moment data of figure 10 for flap deflections of $30^{\circ}/60^{\circ}$ shows that the flap-down configuration was also stable and could be trimmed in pitch even at the highest thrust settings by the application of blowing to the horizontal tail used in the tests. A comparison of the data of figures 10(b) and 10(c)

shows that adding blowing to the tail provided additional trim capability to the tail without any appreciable effect on the stability characteristics of the model.

The data of figure 10(f) show a comparison of the pitching-moment data of the present investigation with data from reference 5. This plot shows that changing the engines from a spread-out arrangement (ref. 5) to the inboard, clustered arrangement of the present investigation produced only small changes in the stability characteristics of the model. Included in this plot are data with wing-tip blowing, and as expected, these data show an increase in diving moment with blowing, but there was no appreciable change in stability characteristics. The data of figures 11 and 12 show that changing the flap deflections to $25^{\circ}/50^{\circ}$ or $20^{\circ}/40^{\circ}$ introduced no significant changes in the stability and trim characteristics noted for the flap deflection of $30^{\circ}/60^{\circ}$ in figure 10.

A comparison of the data for a symmetrical spoiler deflection of 30° (fig. 13(c)) with data for the spoilers undeflected (fig. 10(b)) shows that the spoilers produce decremental lift changes of only about 0.6 at the higher thrust conditions. These tests indicate that in using conventional spoilers for lift control, much higher spoiler deflections are required on a jet-flap airplane configuration to produce given changes in vertical acceleration than on more conventional configurations operating at more conventional lift coefficients.

The data of figure 14 show that increases in maximum lift coefficient can be achieved with a small amount of blowing over the ailerons. For example, for a $C_{\mu,a}$ of about 0.12 on the ailerons, the maximum lift coefficient of the configuration was increased by an increment of about 1.0 above that obtained with no aileron blowing without any appreciable increase in C_D at the higher engine thrusts. This increase in maximum lift coefficient probably results mainly from achieving flow attachment on the ailerons.

The results of tests to determine the lift characteristics of the horizontal tail (fig. 15) show that the tail with a leading-edge flap and double-slotted trailing-edge flaps had a maximum lift coefficient of about 2.2 with no blowing. The maximum lift coefficient was increased up to 2.9 by blowing over the trailing-edge flaps with $C_{\mu,e} = 0.022$. The utilization of blowing on the model tail was not meant to imply that blowing would be needed in full-scale operation, but rather was intended to give lift on the model tail which would be representative of that of a geometrically similar tail at full-scale Reynolds number without blowing. The lift curve estimated for full-scale operation, included in figure 15, shows that a maximum tail lift coefficient of 2.5 could be expected at full-scale Reynolds number.

The results of flow surveys to measure the downwash characteristics in the vicinity of the horizontal tail (figs. 16 and 17) indicate that the variation of downwash angle with tail spanwise station is not very large except for horizontal-tail locations near the

fuselage. For these locations the downwash angle is reduced considerably from the root to the tip station. A summary of the downwash measurements in terms of the downwash factor $1 - \frac{\partial \epsilon}{\partial \alpha}$ (presented in fig. 18) shows that the horizontal tail is markedly more effective in stablizing the model if it is in the high location. For this location (z/c = 1.50) the value of $1 - \frac{\partial \epsilon}{\partial \alpha}$ varies only from about 0.5 to 0.7 over the entire range of C_μ. Figure 19 shows the ratio of the dynamic pressure at the tail to the free-stream dynamic pressure as a function of the engine thrust used in the tests. This ratio was determined from the following expressions:

For the horizontal tail,

$$\frac{q_t}{q} = \frac{\left(C_{m_{i_t}}\right)_{\text{power on}}}{\left(C_{m_{i_t}}\right)_{\text{power off}}}$$

and for the vertical tail,

$$\frac{q_t}{q} = \frac{\left(C_{n_{i_v}}\right)_{\text{power on}}}{\left(C_{n_{i_v}}\right)_{\text{power off}}}$$

The results of figure 19 show that the dynamic pressure at the tail increased with increases in thrust coefficient. The higher local dynamic pressure occurred in the vicinity of the horizontal tail where ratios of q_t/q are shown to be 1.4 for the higher values of C_μ.

Lateral Stability With Symmetric Thrust

The static lateral stability characteristics of the configuration under conditions of symmetric thrust are presented in figures 20 to 23. Figure 20 shows that the variations of the lateral characteristics with sideslip angle are fairly linear.

Figures 21 to 23 show the variation with angle of attack of the static lateral stability derivatives as determined from tests at 5° and -5° sideslip. These data show that the tail-on configuration had positive directional stability $\left(C_{n_\beta}\right)$ and positive effective dihedral $\left(-C_{l_\beta}\right)$ at any test condition below the stall. The application of power is shown to increase markedly the directional stability at flap deflections of $30^\circ/60^\circ$ and $20^\circ/40^\circ$. Figure 21(b) shows that the vertical tail remained effective for producing directional stability up through the stall. The reduction in directional stability above the stall, which is indicated by the data of figures 21(b) and 22(b), is a result of the large increase in instability of the wing-fuselage configuration.

Lateral and Longitudinal Characteristics With Asymmetric Thrust

Lateral characteristics obtained for the model with asymmetric thrust (one engine inoperative) are presented in figures 24 to 27. The lateral characteristics for all engines operating are also presented for comparison. Because in a powered-lift system engine failure also results in loss of lift, plots of the lateral characteristics with one engine out are accompanied by the corresponding longitudinal data.

The data of figures 24(b) and 25(a) show that large rolling moments accompany an engine-out condition; and even though the engines were clustered together at an inboard location for the present study, the rolling moments produced by the outboard engine were significantly larger than those of the inboard engine. At the stall the moments become much larger because the stall occurs at a lower angle of attack on the wing with the inoperative engine. The corresponding lift data (figs. 24(c) and 25(b)) when compared with the four-engine lift data of figure 10(b) show that the engine failure would produce a loss in lift coefficient of about 1.0. As expected, reducing the flap deflections from $30^{\circ}/60^{\circ}$ to $20^{\circ}/40^{\circ}$ reduced the engine-out rolling moments but increased the engine-out yawing moments. (Compare figs. 24(b) and 27(b).)

Control of Asymmetric Thrust Condition

One of the objectives of the present investigation was to evaluate an aileron blowing system for possible use in trimming out the large rolling moments associated with an engine-out condition. Data presented in figures 28 to 32 and 37 were obtained with one engine inoperative and with asymmetric blowing on the ailerons to achieve roll trim. In figures 33 to 36, the effects of differential flap deflection with and without aileron blowing are presented. The lateral control moments which could be produced by two spoiler systems are shown in figures 38 and 39, and the lateral moments which could be produced by rudder deflection and by changes in vertical-tail incidence are presented in figures 40 to 42. Since the aerodynamic performance of the engine-out configuration is extremely important in determining safe boundaries of flight operation, plots of the lateral characteristics are accompanied by the corresponding longitudinal data.

One of the most significant points noted in the data of figures 28 to 32 is that aileron blowing offers a promising means of achieving roll trim for an engine-out condition in the low angle-of-attack range. As the angle of attack is increased to the stall, however, the engine-out wing stalls first, and near an angle of attack of 20°, the rolling moments become very large. Increased aileron blowing tends to increase the lift performance of the engine-out configuration and to delay the onset of tip stall, but offers no decrease in the large rolling moment at the stall angle of attack.

The lateral characteristics for the engine-out condition with differential flap deflection (figs. 33 to 36) are generally similar to those for aileron blowing in that roll trim can

be achieved at low angles of attack but large rolling moments occur at the stall. In addition, large adverse yawing moments are introduced with differential flap deflections. The addition of aileron blowing to this system offered no significant decrease in the rolling moment at the stall. A comparison of the data of figures 33 to 34 with figures 35 to 36 shows that roll trim could be achieved in either the clustered or spread-engine arrangement. It should be noted, however, that it was necessary to apply more aileron blowing and to decrease the deflection of the right aileron to zero to produce roll trim in the spread-engine condition.

Figure 38 shows that conventional spoilers (located on the wing just forward of the flap system) are capable of producing rolling moments of about 0.14. The conventional spoilers in combination with a small-chord spoiler on the flap itself, however, increased the rolling moments due to spoiler deflection up to about 0.20 (fig. 38(c)). Comparison of longitudinal data for spoiler operation (fig. 38(d)) with data for spoilers undeflected (fig. 10(b)) indicates that spoiler deflection decreased the lift coefficients by approximately 1.0.

One of the most significant points to be made about the lateral-control data in figures 40 to 42 is that blowing over the rudder increased the yawing-moment coefficient produced by rudder deflection from about 0.07 up to 0.2 for C_μ of about 0.02. This is enough rudder effectiveness to trim the largest yawing moments encountered in engine-out conditions with corrective roll trim applied.

SUMMARY OF RESULTS

From the results of a wind-tunnel investigation of a jet transport airplane configuration with an external-flow jet flap and inboard pod-mounted engines, the following results were obtained:

1. The location of pod-mounted engines fairly close inboard showed some detrimental effect on lift but showed no particular adverse effects on longitudinal stability and trim and appeared to offer an effective means of obtaining sizable reductions in the engine-out moments associated with an engine failure.

2. The use of asymmetric blowing over a drooped aileron or the use of differential flap deflection appeared to offer a means of achieving roll trim for engine-out conditions over the normal operational angle-of-attack range, but was not able to trim the much larger asymmetries that occurred when the wing with an engine inoperative stalled first. The combination of aileron blowing and spoilers provided roll trim capability up to the stall angle of attack but the roll asymmetries exceeded this capability beyond the stall.

3. For either method of roll trim of the engine-out condition, the rudder with blowing was capable of trimming the yawing-moment asymmetries.

Langley Research Center,
National Aeronautics and Space Administration,
Hampton, Va., October 14, 1970.

REFERENCES

1. Campbell, John P.; and Johnson, Joseph L., Jr.: Wind-Tunnel Investigation of an External-Flow Jet-Augmented Slotted Flap Suitable for Application to Airplanes With Pod-Mounted Jet Engines. NACA TN 3898, 1956.

2. Johnson, Joseph L., Jr.: Wind-Tunnel Investigation of the Static Longitudinal Stability and Trim Characteristics of a Sweptback-Wing Jet-Transport Model Equipped With an External-Flow Jet-Augmented Flap. NACA TN 4177, 1958.

3. Johnson, Joseph L., Jr.: Wind-Tunnel Investigation of a Small-Scale Sweptback-Wing Jet-Transport Model Equipped With an External-Flow Jet-Augmented Double Slotted Flap. NASA MEMO 3-8-59L, 1959.

4. Parlett, Lysle P.; and Shivers, James P.: Wind-Tunnel Investigation of an STOL Aircraft Configuration Equipped With an External-Flow Jet Flap. NASA TN D-5364, 1969.

5. Parlett, Lysle P.; Freeman, Delma C., Jr.; and Smith, Charles C., Jr.: Wind-Tunnel Investigation of a Jet Transport Airplane Configuration With High Thrust-Weight Ratio and an External-Flow Jet Flap. NASA TN D-6058, 1970.

6. Freeman, Delma C., Jr.; Grafton, Sue B.; and D'Amato, Richard: Static and Dynamic Stability Derivatives of a Model of a Jet Transport Equipped With External-Flow Jet-Augmented Flaps. NASA TN D-5408, 1969.

7. Mechtly, E. A.: The International System of Units – Physical Constants and Conversion Factors (Revised). NASA SP-7012, 1969.

TABLE I.- DIMENSIONS OF MODEL

Wing:	
Area, ft^2 (m^2)	7.87 (0.731)
Span (to theoretical tip), in. (cm)	95.08 (241.51)
Aspect ratio	7.75
Length of mean aerodynamic chord, in. (cm)	13.22 (33.59)
Distance from nose of model to quarter-chord point of mean aerodynamic chord, in. (cm)	40.54 (102.98)
Spanwise station of mean aerodynamic chord, in. (cm)	19.33 (49.10)
Root chord, in. (cm)	19.49 (49.50)
Tip chord (theoretical tip), in. (cm)	6.54 (16.62)
Break-station chord, in. (cm)	12.08 (30.67)
Spanwise station of break, in. (cm)	20.16 (51.20)
Sweep of quarter-chord line:	
Inboard panel, deg	24.08
Outboard panel, deg	25.00
Dihedral of quarter-chord line:	
Inboard panel, deg	-3.50
Outboard panel, deg	-3.50
Incidence of mean aerodynamic chord, deg	4.50
Incidence of root chord, deg	6.00
Geometric twist:	
Root, deg	0.0
Break station, deg	-1.5
Tip, deg	-3.5
Vertical tail:	
Area, ft^2 (m^2)	1.67 (0.155)
Span, in. (cm)	20 (50.8)
Aspect ratio	1.66
Sweep angles:	
Leading edge, deg	38
Trailing edge, deg	31
Root chord, in. (cm)	14 (35.6)
Tip chord, in. (cm)	10.15 (25.9)
Horizontal tail:	
Area, ft^2 (m^2)	2.88 (0.268)
Span, in. (cm)	46.76 (118.77)
Length of mean aerodynamic chord, in. (cm)	9.52 (24.18)
Incidence	Variable

TABLE I.- DIMENSIONS OF MODEL – Concluded

Engines:	
Spanwise location of inboard engines, in. (cm)	10.47 (26.59)
Spanwise location of outboard engines, in. (cm)	14.47 (36.75)
Incidence of all engine center lines relative to X-axis, deg	-3.00
Moment reference:	
Longitudinal location, distance from nose of model, in. (cm)	41.61 (105.69)
Vertical location, distance from top of fuselage at wing, in. (cm)	4.92 (12.49)
Control-surface dimensions:	
Rudder:	
Span, in. (cm)	16 (40.6)
Chord, upper end, parallel to X-axis, in. (cm)	4.3 (10.9)
Chord, lower end, parallel to X-axis, in. (cm)	6 (15.2)
Hinge-line location, percent chord	57
Sweep of hinge line, deg	34
Elevator:	
Span, in. (cm)	17.31 (43.99)
Chord, outboard, in. (cm)	1.66 (4.21)
Chord, inboard, in. (cm)	3.31 (8.40)
Hinge-line location, percent chord	73
Sweep of hinge line, deg	16.5
Aileron:	
Span, in. (cm)	13.35 (33.90)
Chord, outboard, in. (cm)	4.5 (11.43)
Chord, inboard, in. (cm)	3.25 (8.26)
Hinge-line location, percent chord	50

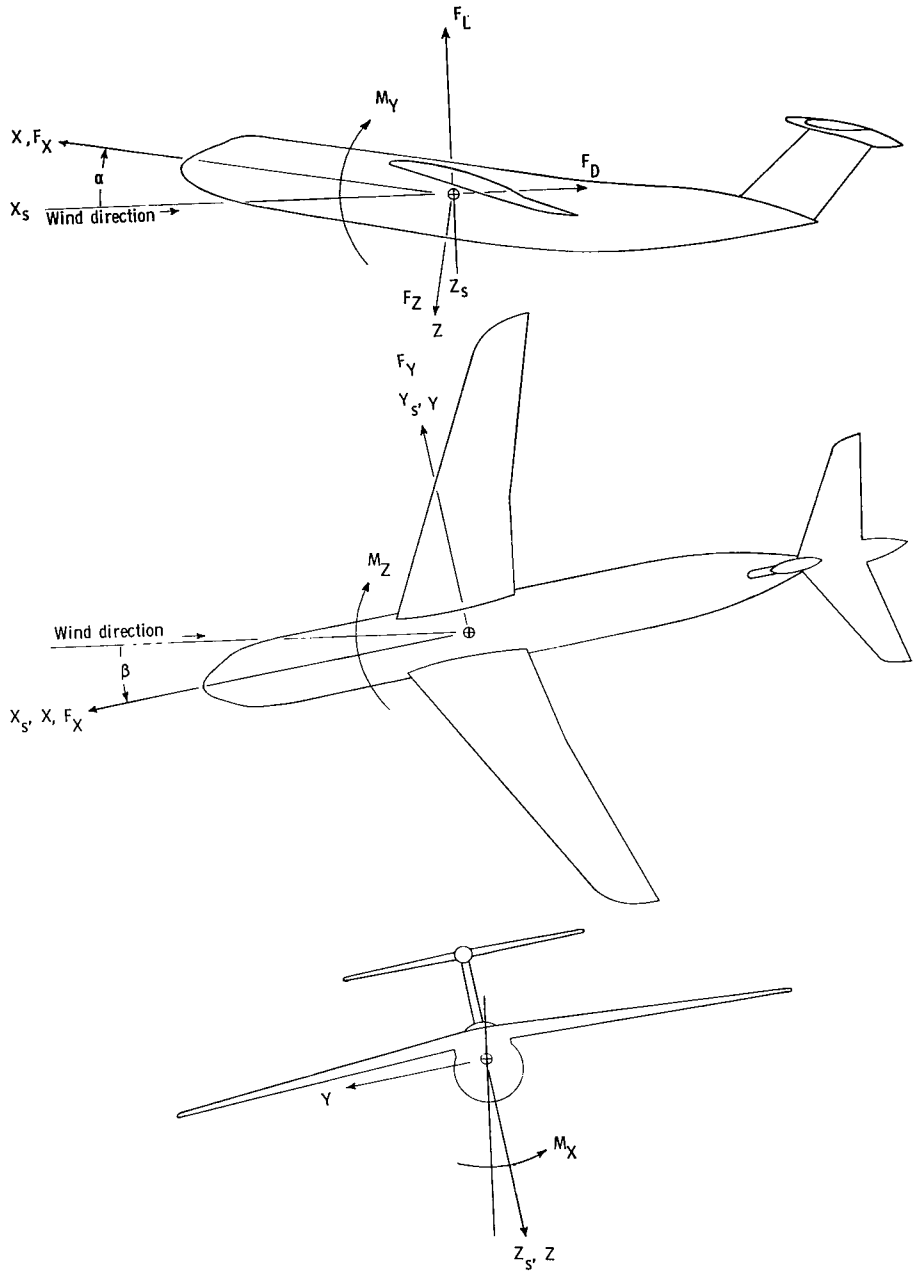

Figure 1.- Axis system used in presentation of data. Arrows indicate positive direction of moments, axes, and angles.

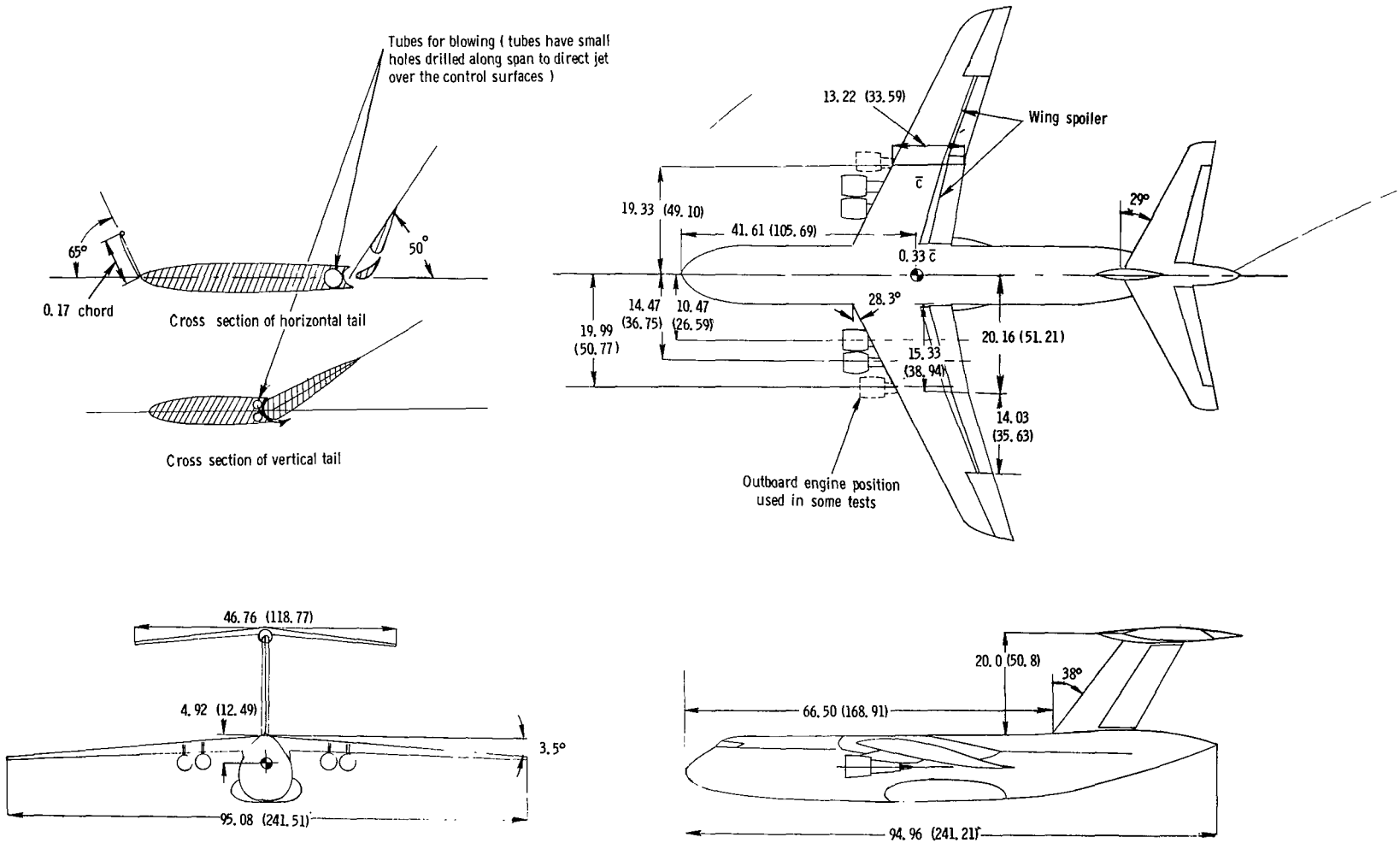

(a) Three-view drawing of complete model. All linear dimensions are in inches (cm).

Figure 2.- Drawings of model used in investigation.

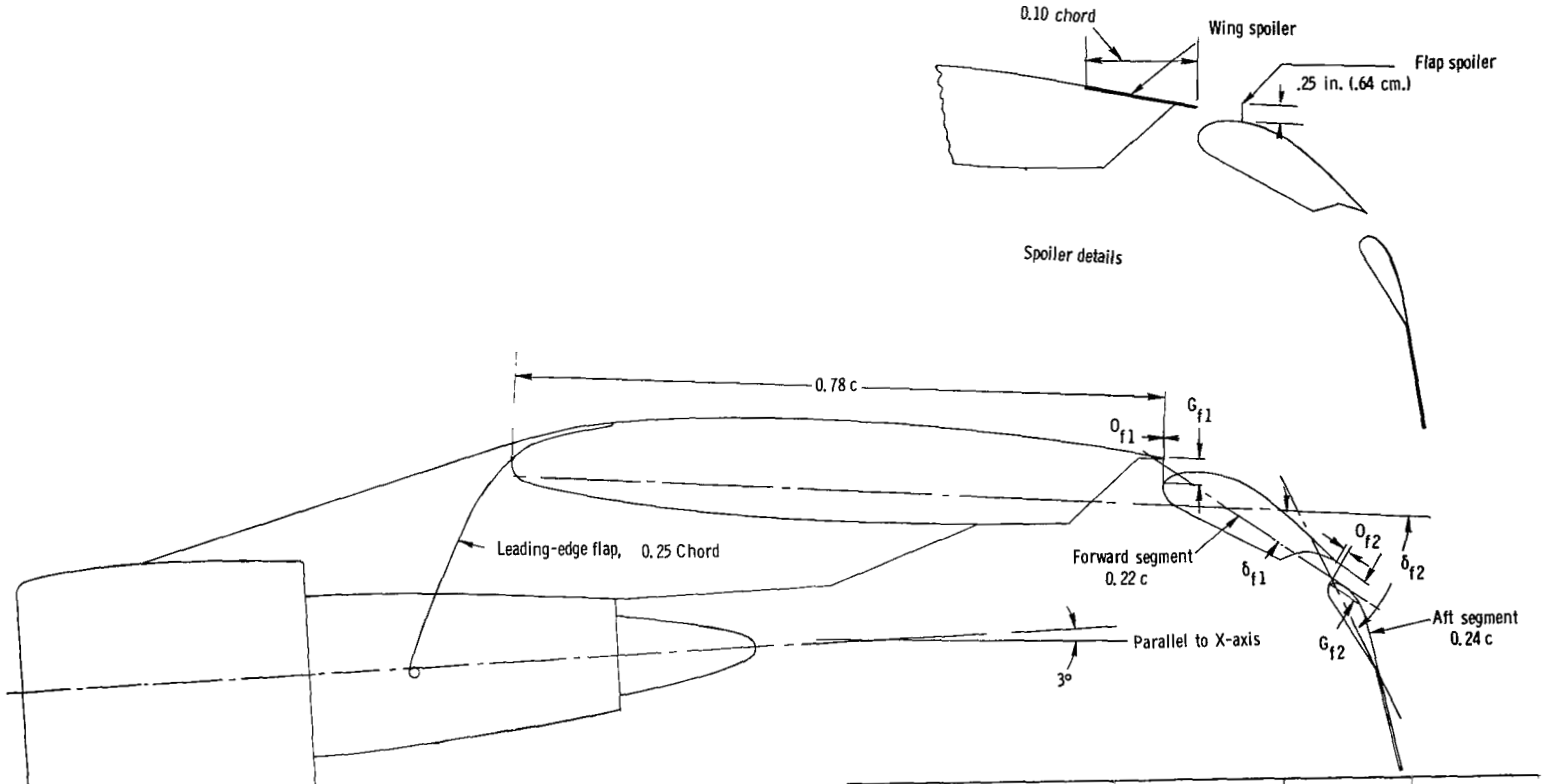

δ_{f1}/δ_{f2} deg/deg	Forward-segment gap, G_{f1}, percent c	Forward-segment overlap, O_{f1}, percent c	Aft-segment gap, G_{f2}, percent c	Aft-segment overlap, O_{f2}, percent c
20/40	5.0	0	2.5	0.5
30/60	3.0	0	2.5	.5

(b) Flap assembly and engine-pylon details.

Figure 2.- Continued.

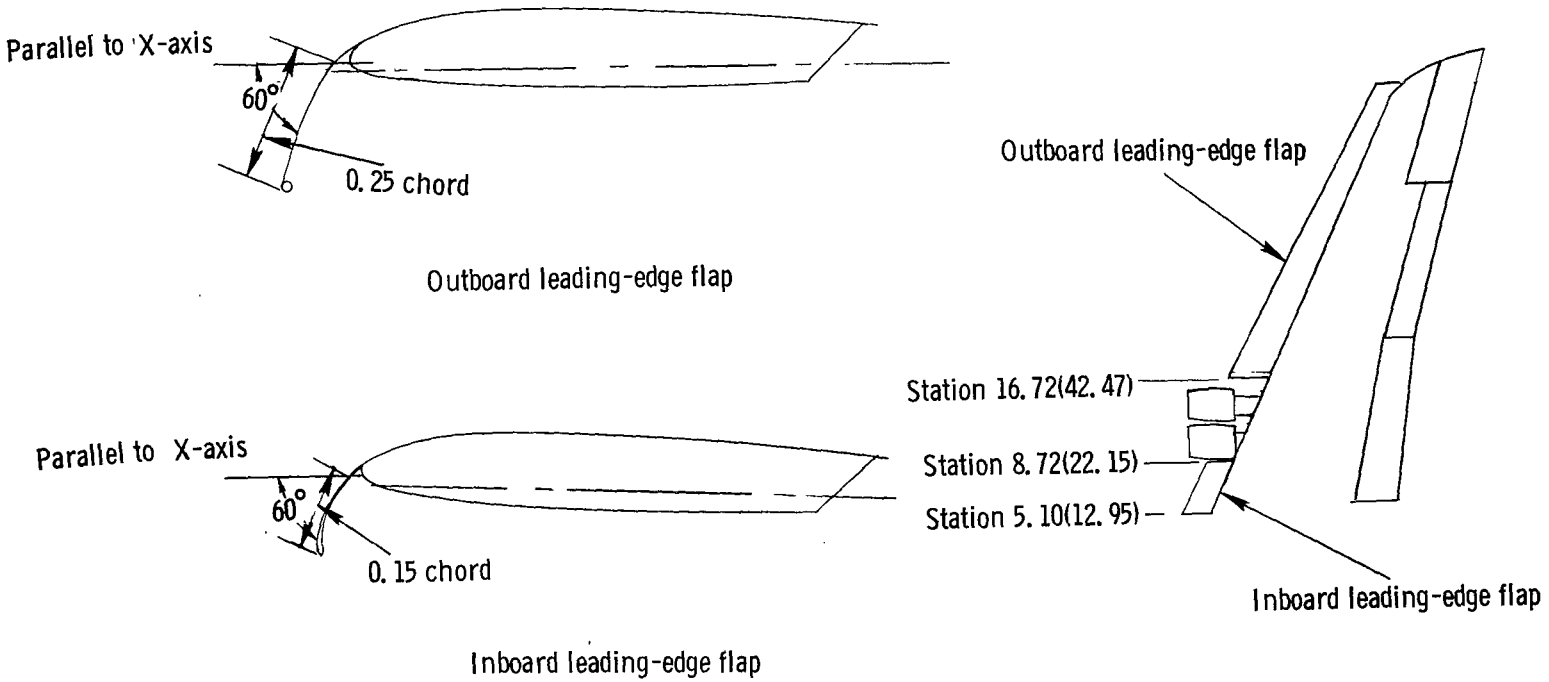

(c) Leading-edge flap details. All dimensions are in inches (cm).

Figure 2.- Continued.

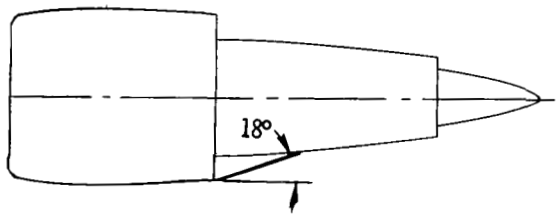

Deflector 1

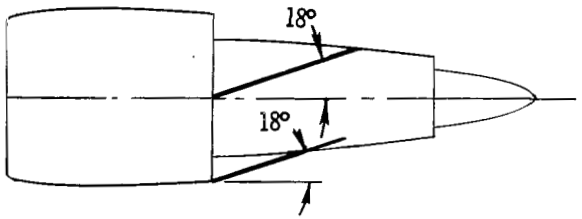

Deflector 2

Combination of deflector 1 and upper vane

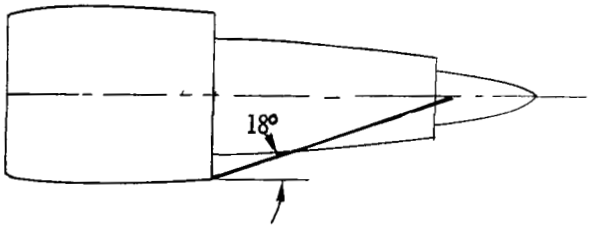

Deflector 3

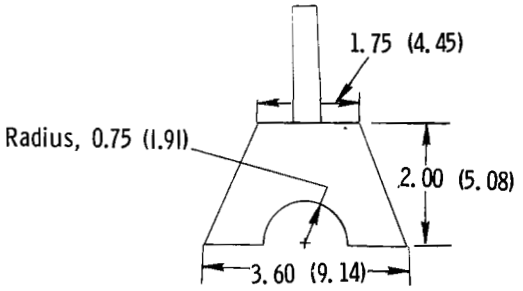

Deflector 1

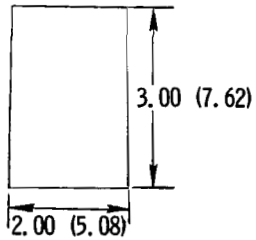

Upper vane of deflector 2

2 required for engine

(1right hand and 1 left hand)

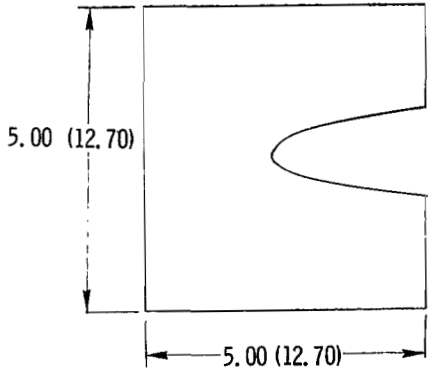

Deflector 3

Top view of deflectors

(d) Detail drawing of jet-exhaust components. Linear dimensions are in inches (cm).

Figure 2.- Continued.

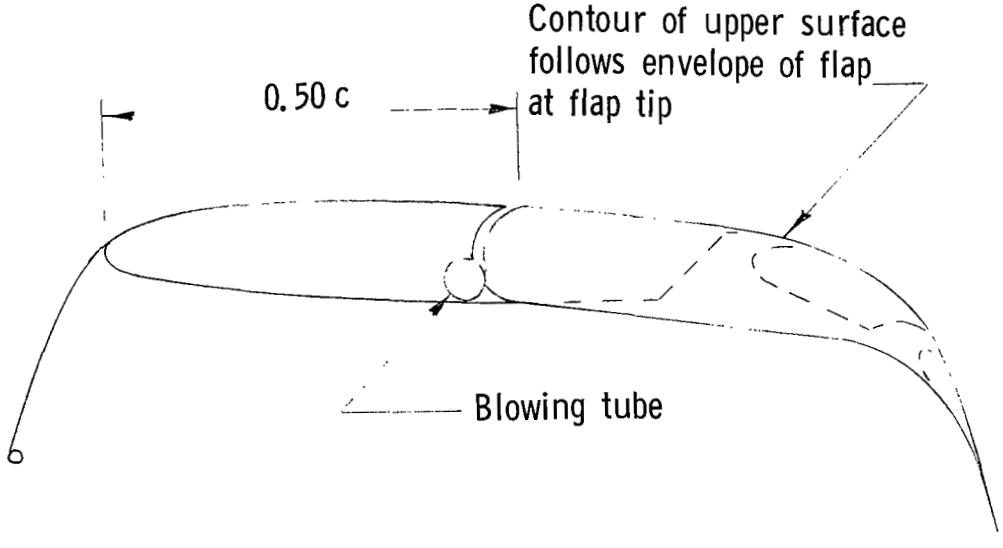

(e) Aileron detail.

Figure 2.- Concluded.

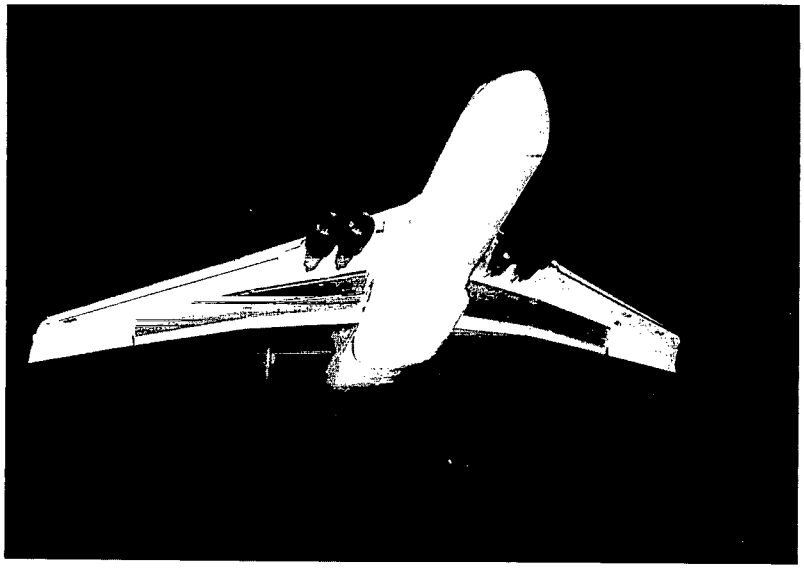

L-70-1063

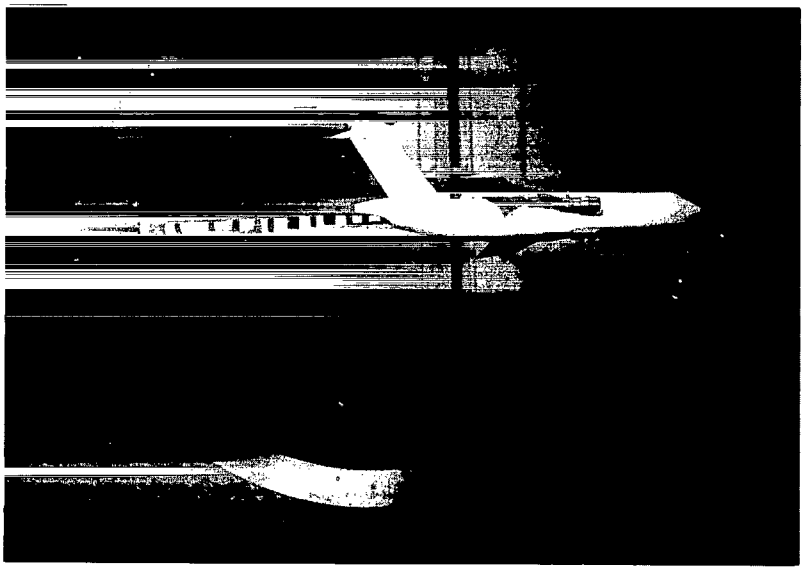

L-70-1066

Figure 3.- Photographs of model mounted for tests.

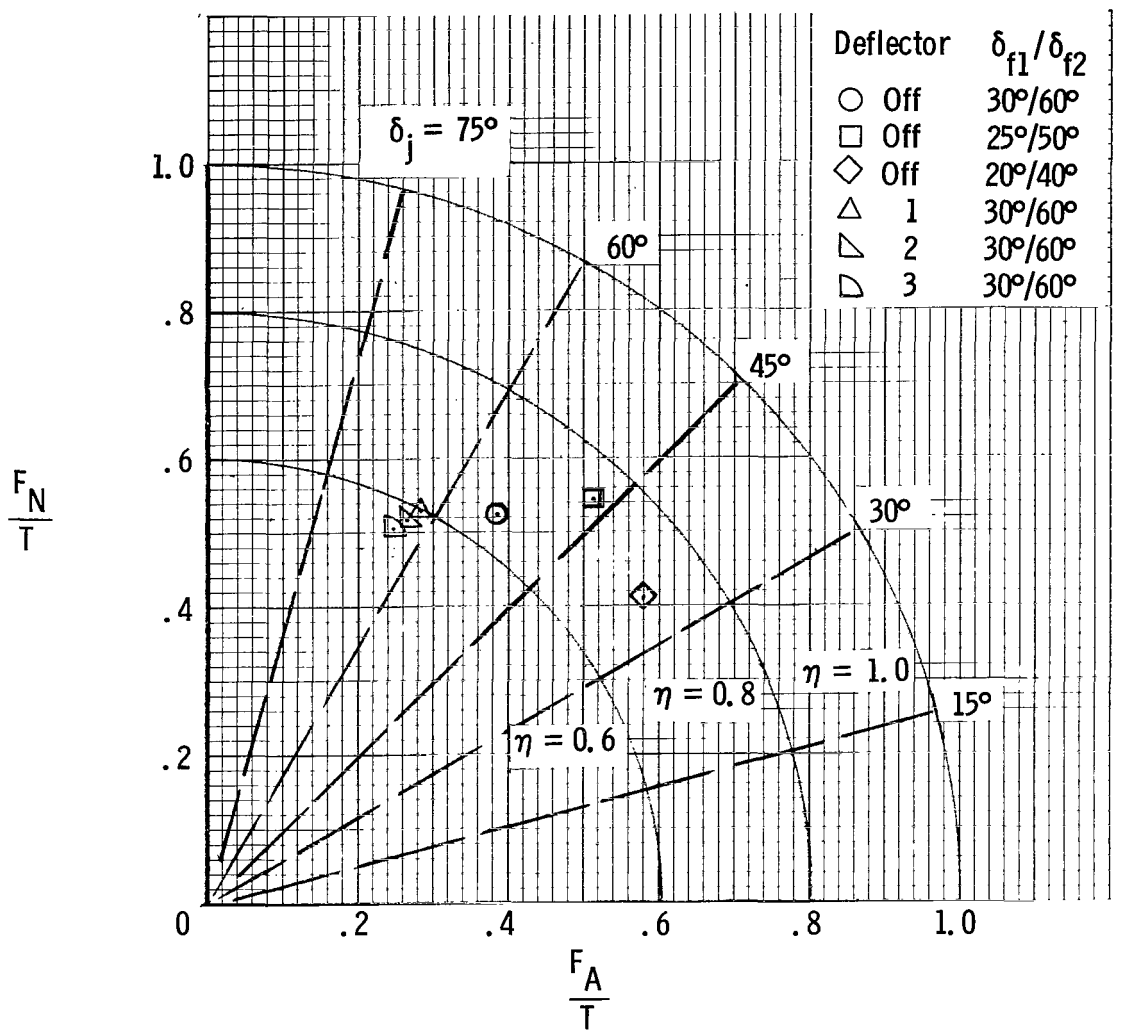

Figure 4.- Summary of static turning efficiency and turning angle.

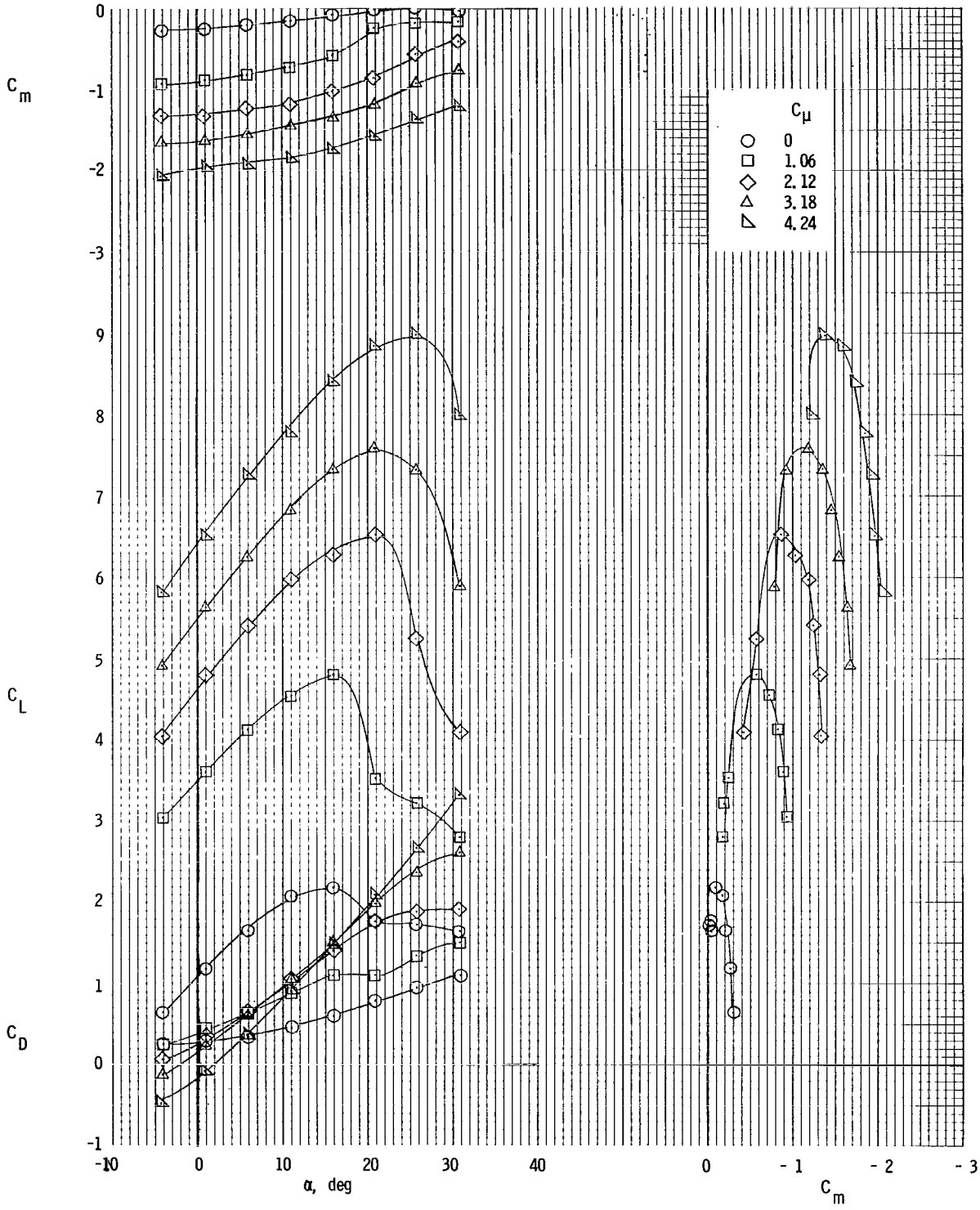

(a) $\delta_a = 0^o$.

Figure 5.- Longitudinal characteristics of model. Tail off. $\delta_{f1}/\delta_{f2} = 30^o/60^o$.

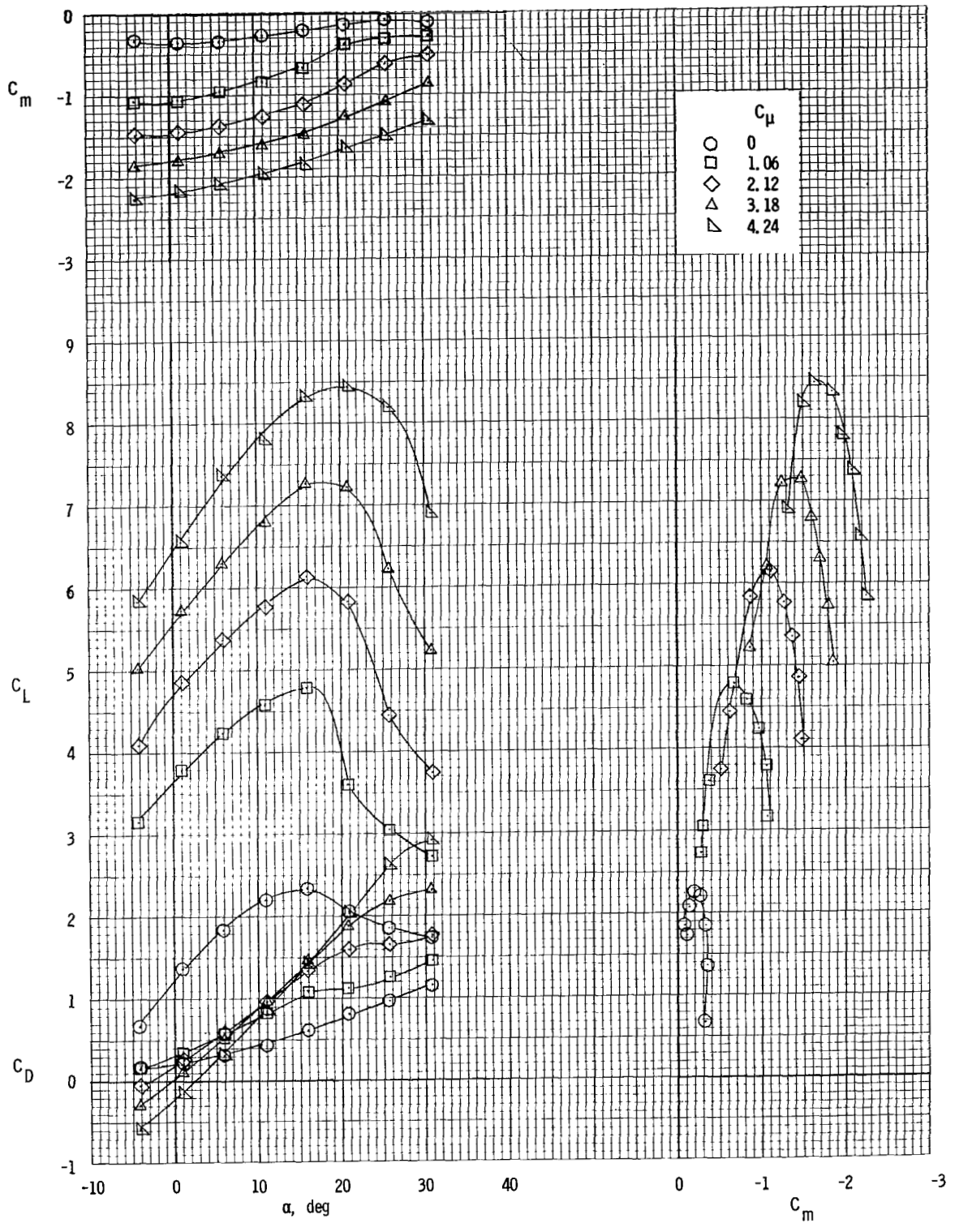

(b) $\delta_a = 60^o$; $C_{\mu,a} = 0$.

Figure 5.- Continued.

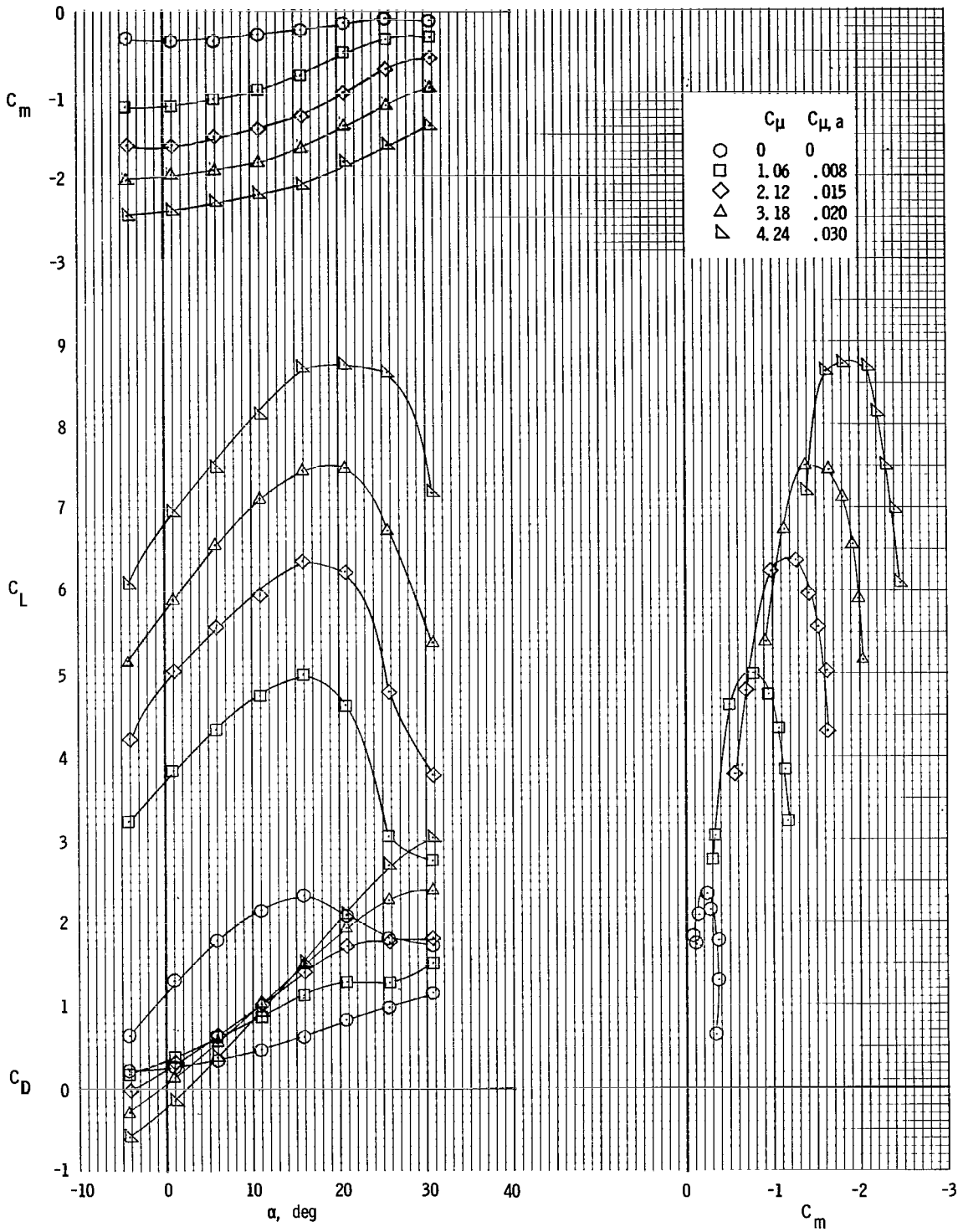

(c) $\delta_a = 60^o$; $C_{\mu,a}$ as shown.

Figure 5.- Concluded.

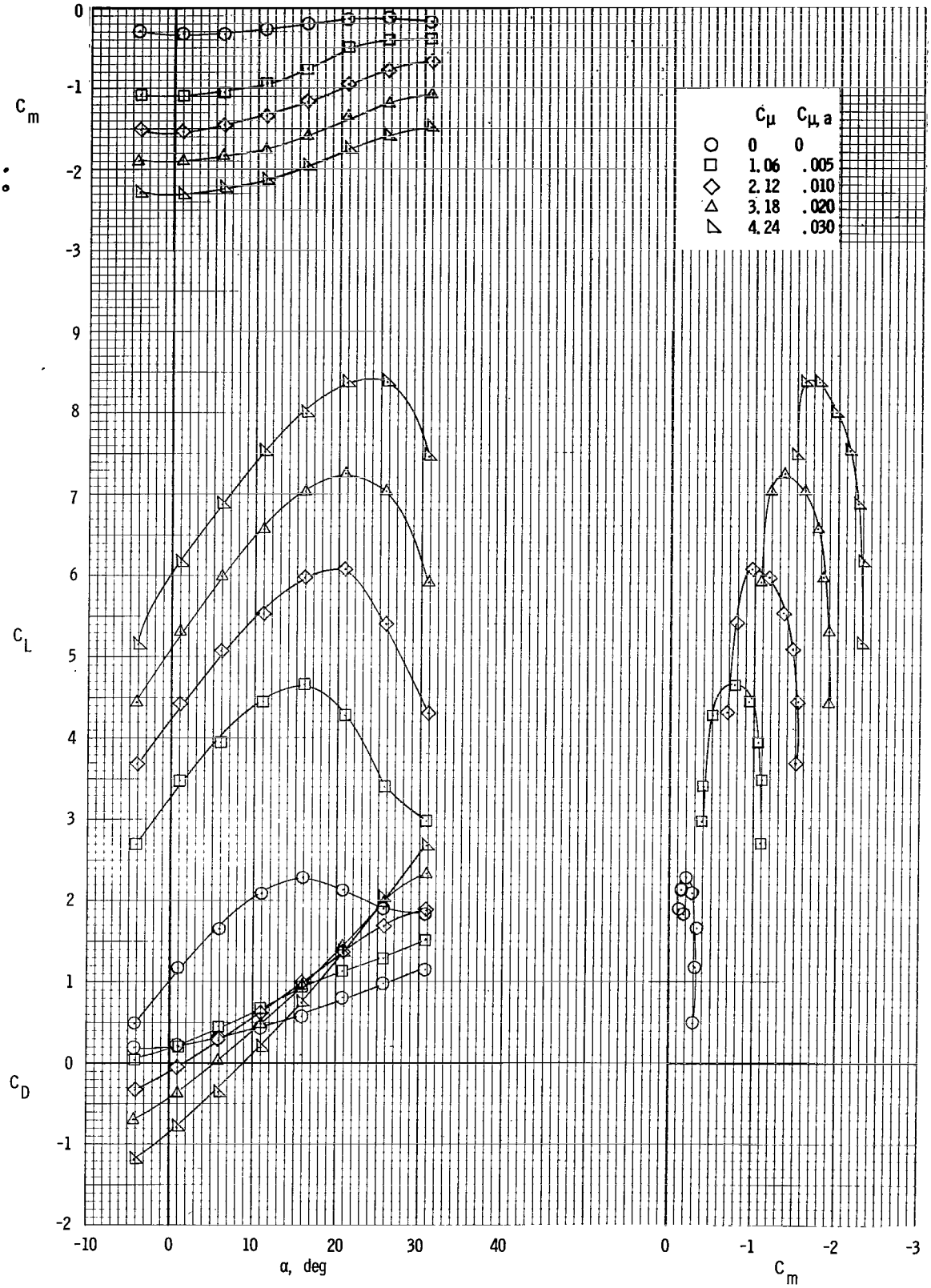

Figure 6.- Longitudinal characteristics of model. Tail off; $\delta_{f1}/\delta_{f2} = 25^o/50^o$; $\delta_a = 50^o$.

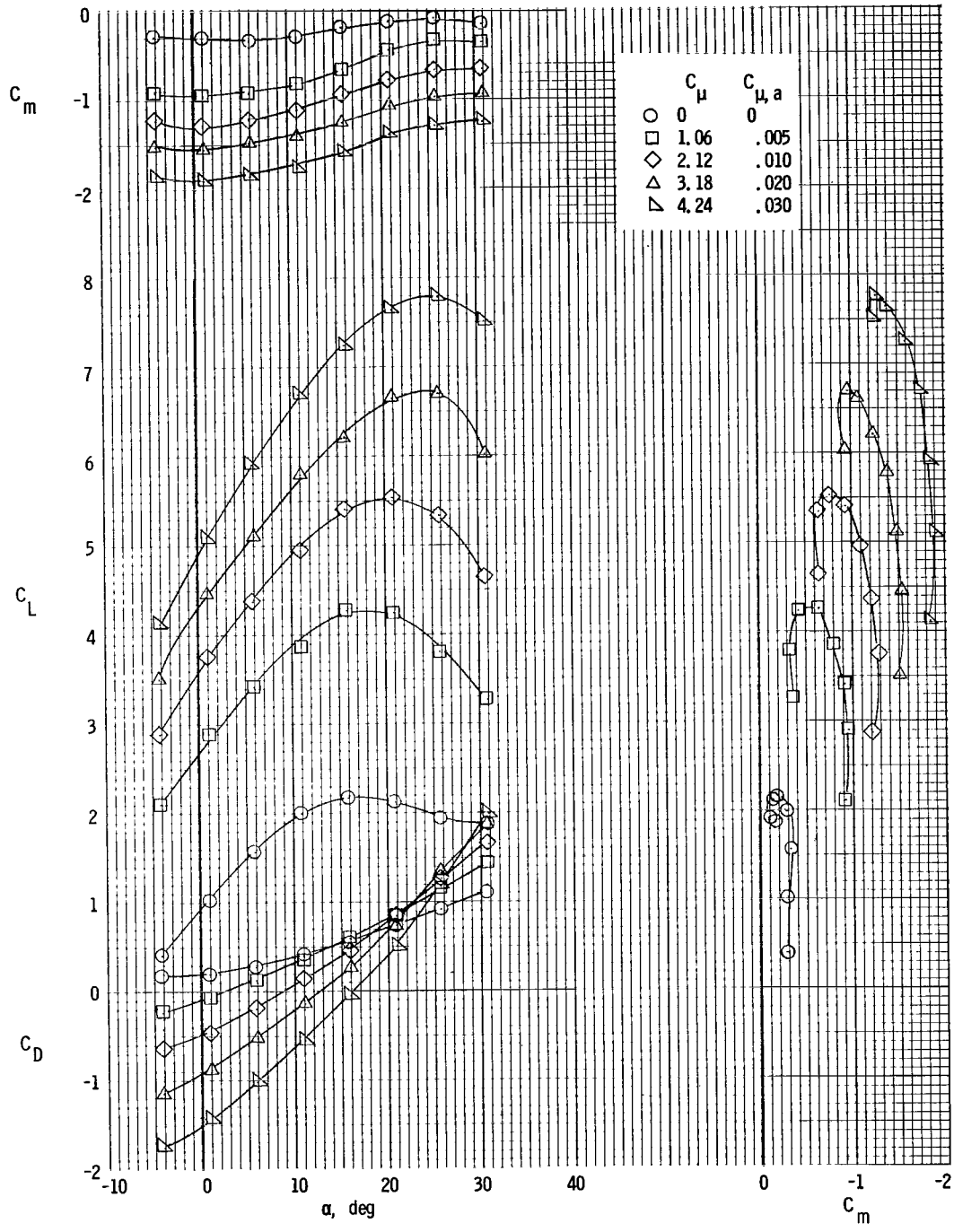

Figure 7.- Longitudinal characteristics of model. Tail off; $\delta_{f1}/\delta_{f2} = 20^o/40^o$; $\delta_a = 40^o$.

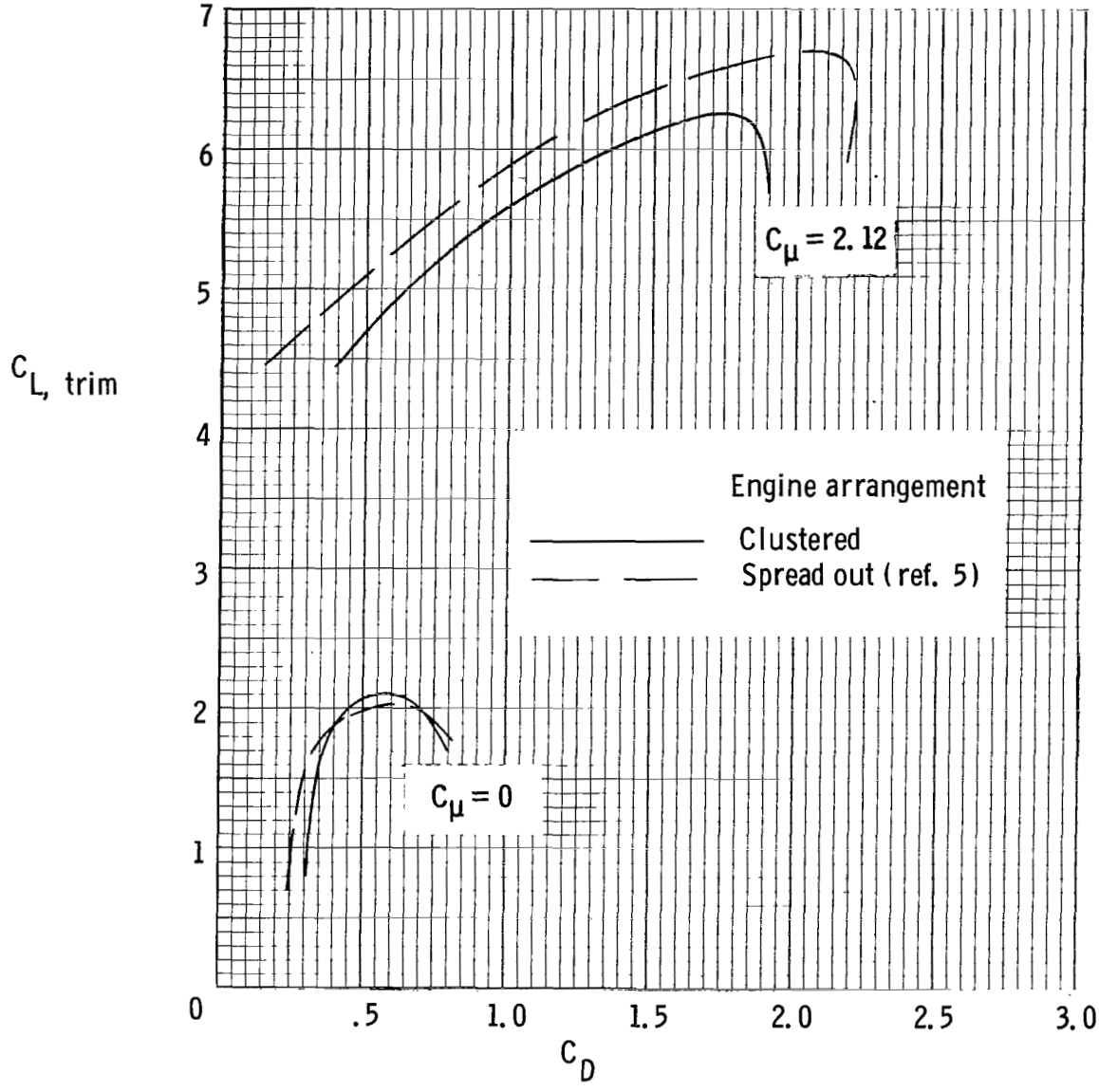

(a) Effect of engine arrangement. $\delta_a = 0^o$.

Figure 8.- Drag polars of model. $\delta_{f1}/\delta_{f2} = 30^o/60^o$.

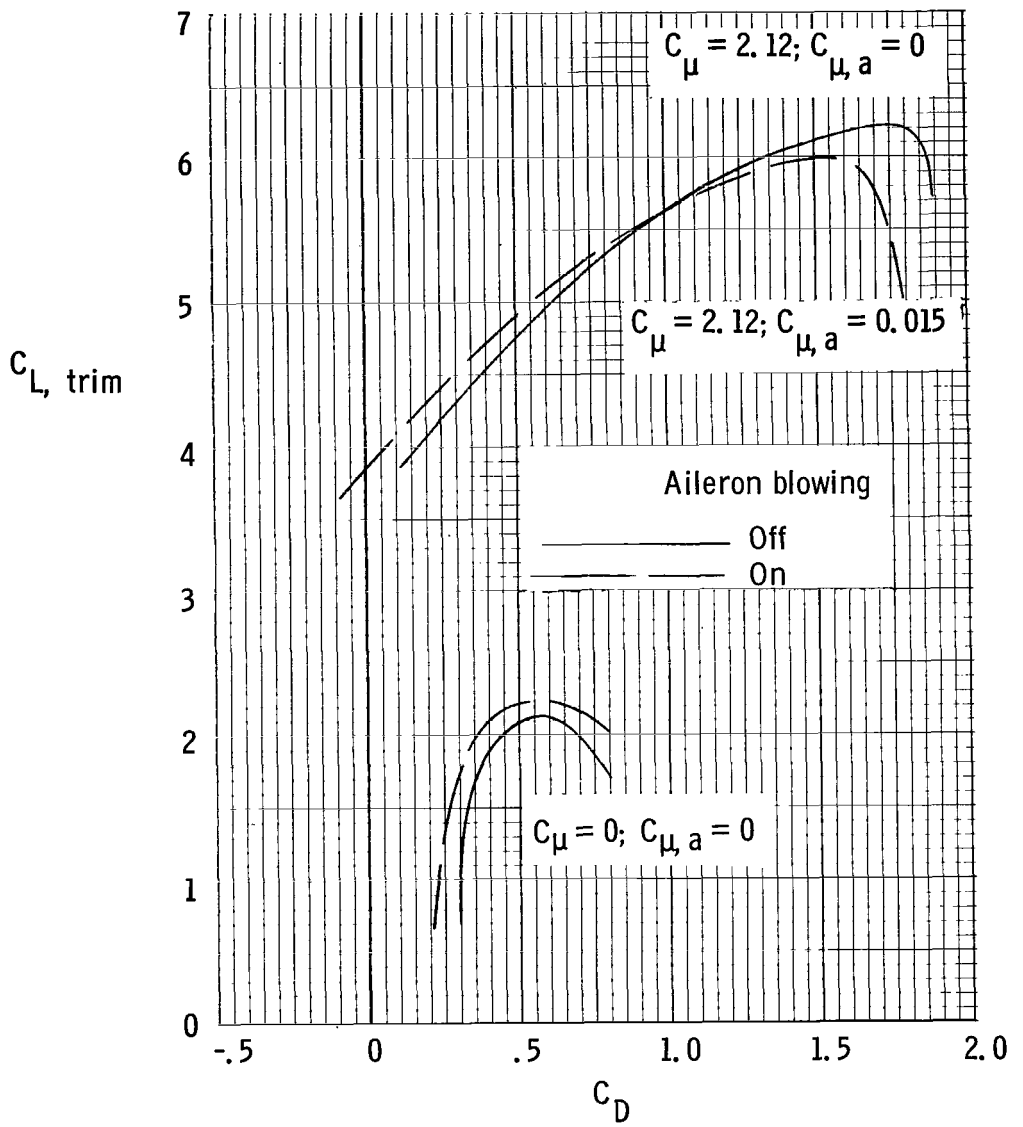

(b) Combined effect of aileron deflection and aileron blowing. $\delta_a = 60^o$; clustered engines.

Figure 8.- Concluded.

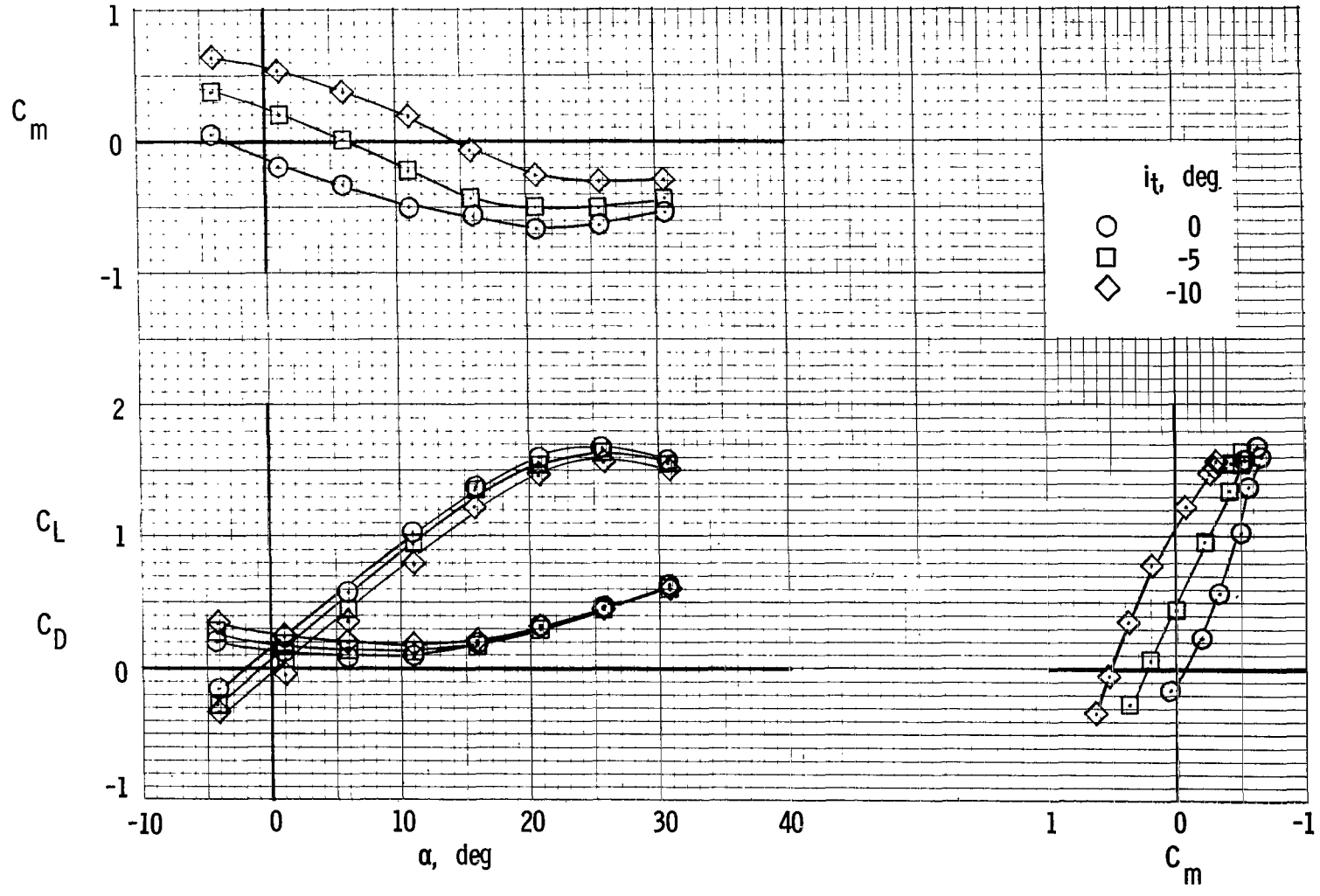

Figure 9.- Longitudinal characteristics. Tail on; $\delta_f = 0^o$; $\delta_e = 0^o$.

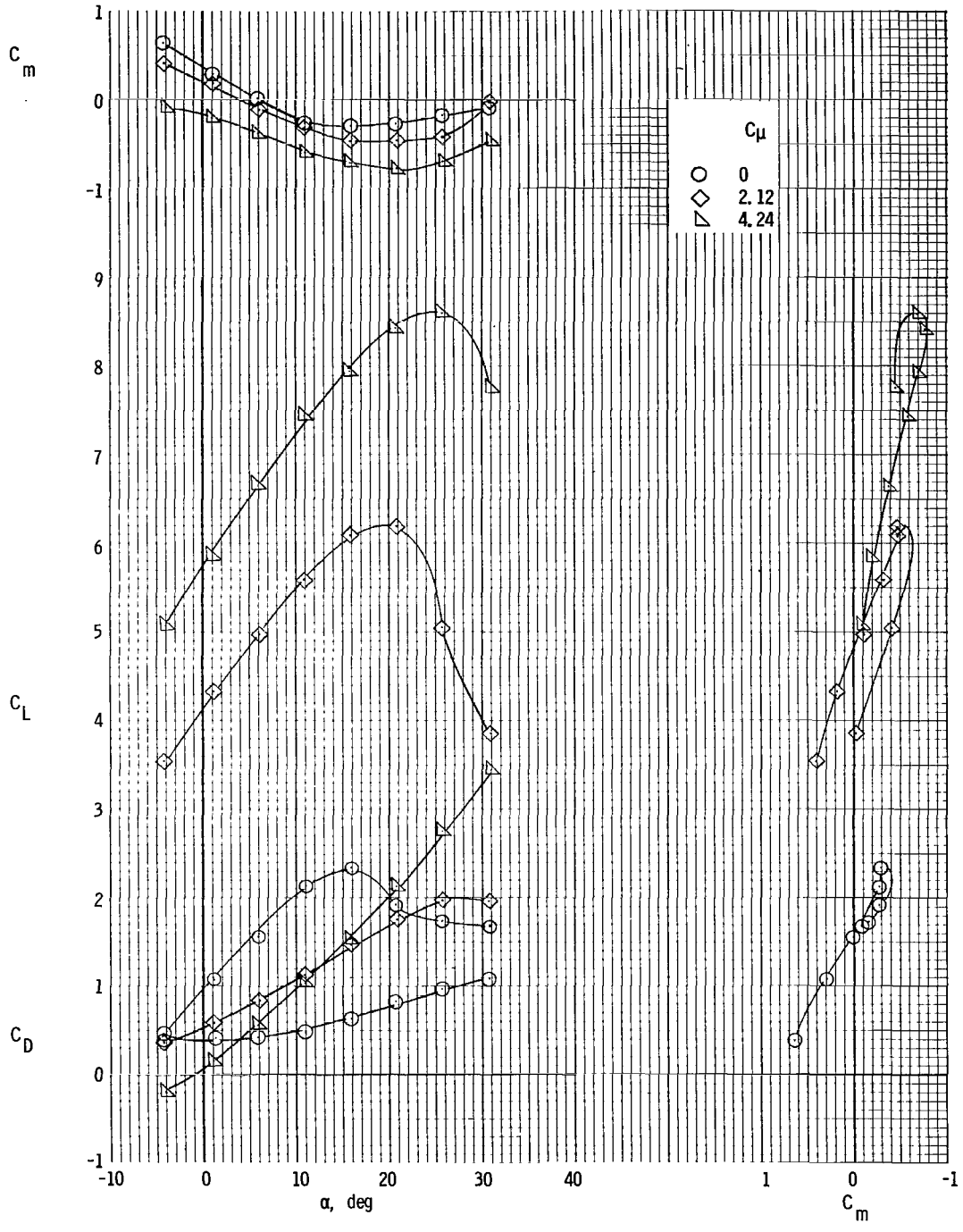

(a) $i_t = 0^o$; $\delta_a = 0^o$.

Figure 10.- Longitudinal characteristics. Tail on; $\delta_{f1}/\delta_{f2} = 30^o/60^o$; $\delta_e = -50^o$.

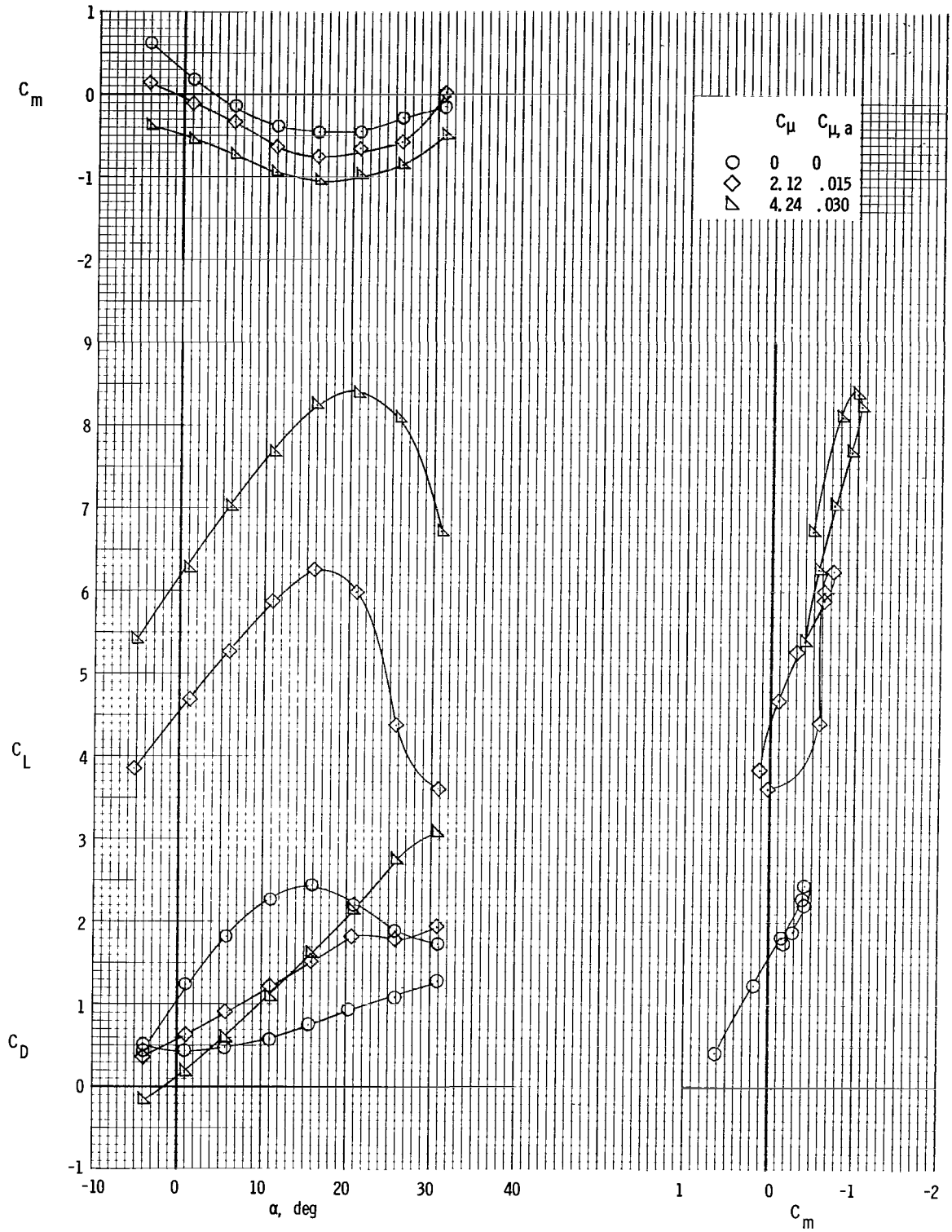

(b) $i_t = 0^o$; $\delta_a = 60^o$.

Figure 10.- Continued.

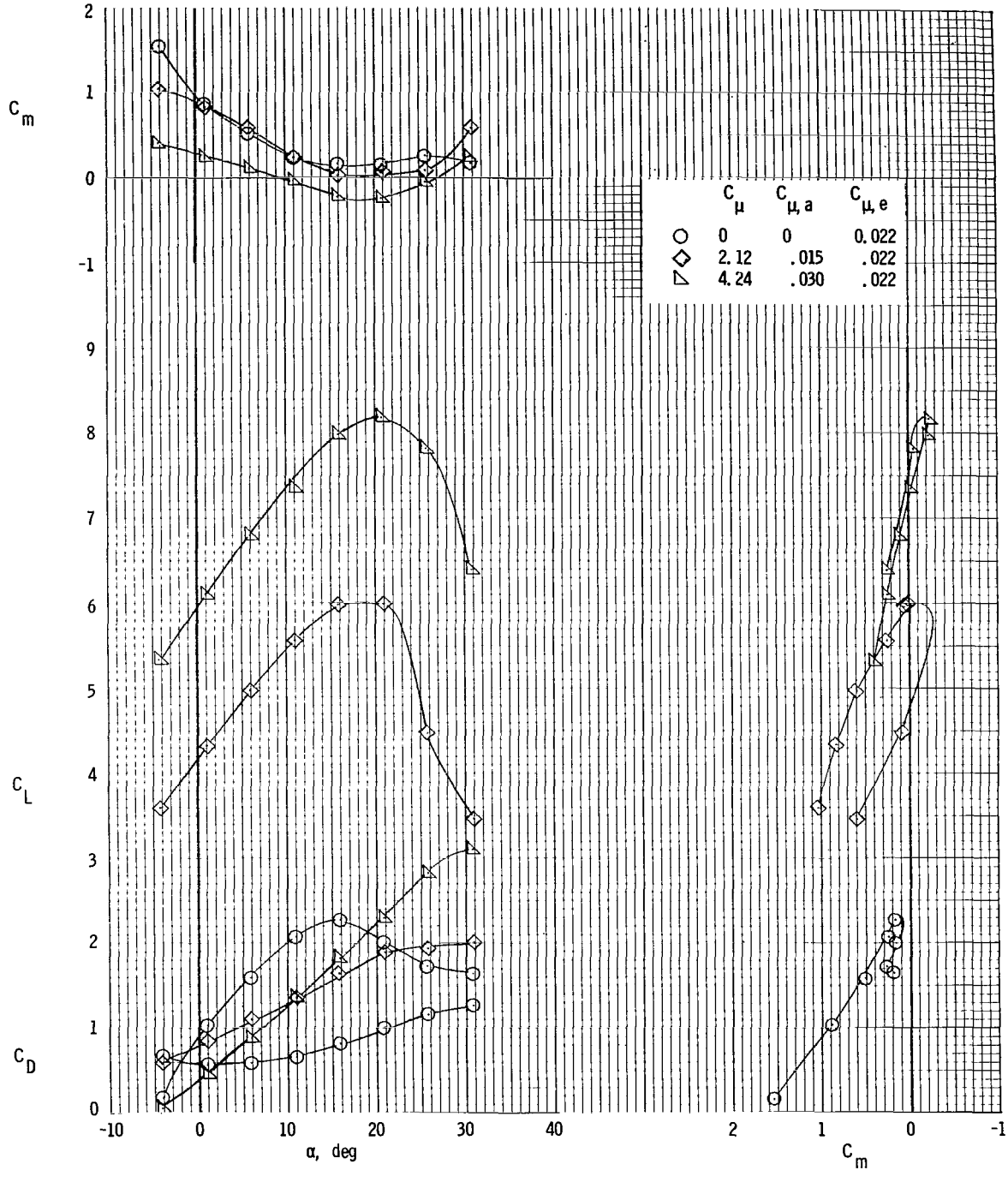

(c) $i_t = 0^o$; $\delta_a = 60^o$.

Figure 10.- Continued.

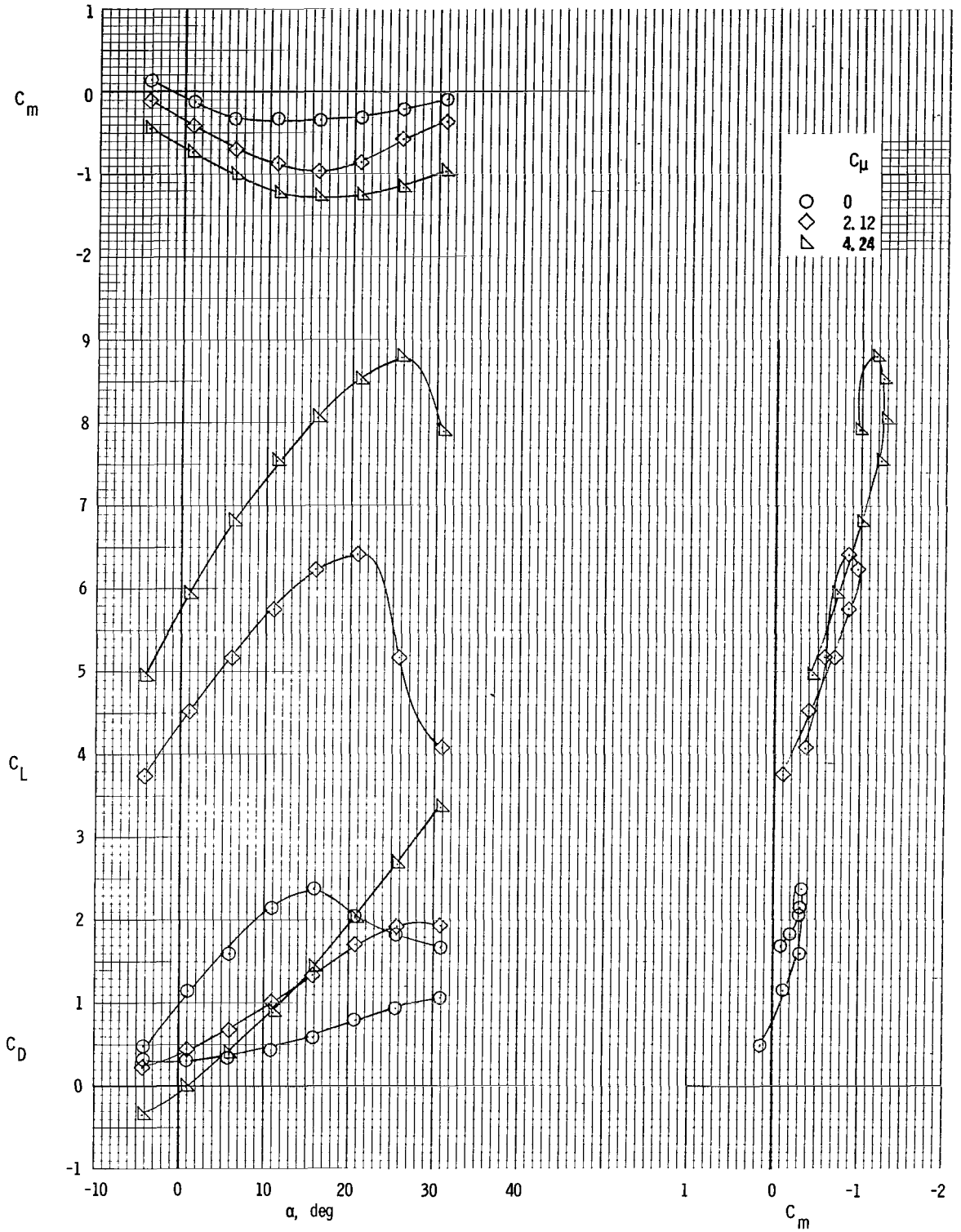

(d) $i_t = 5^o$; $\delta_a = 0^o$.

Figure 10.- Continued.

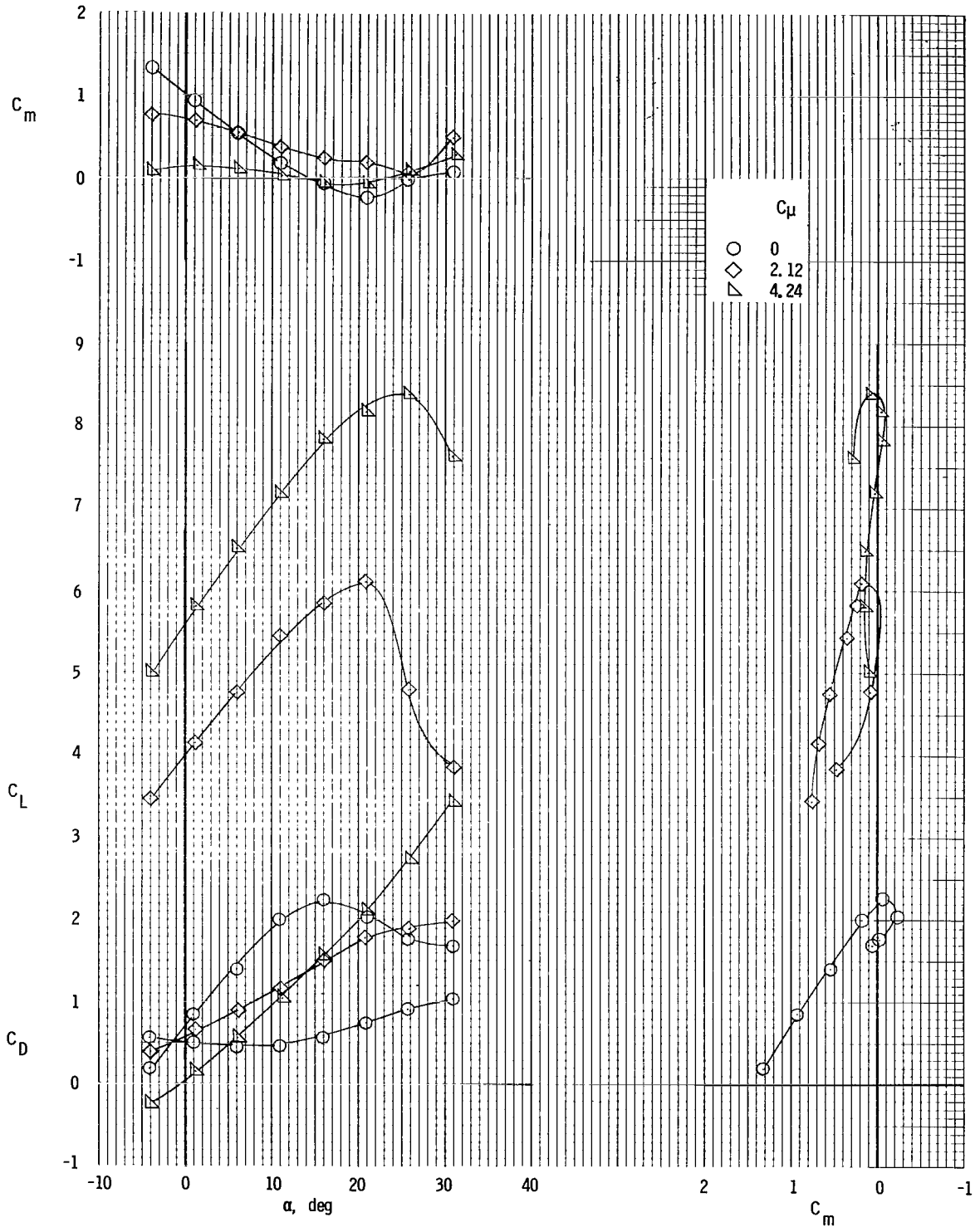

(e) $i_t = -5^o$; $\delta_a = 0^o$.

Figure 10.- Continued.

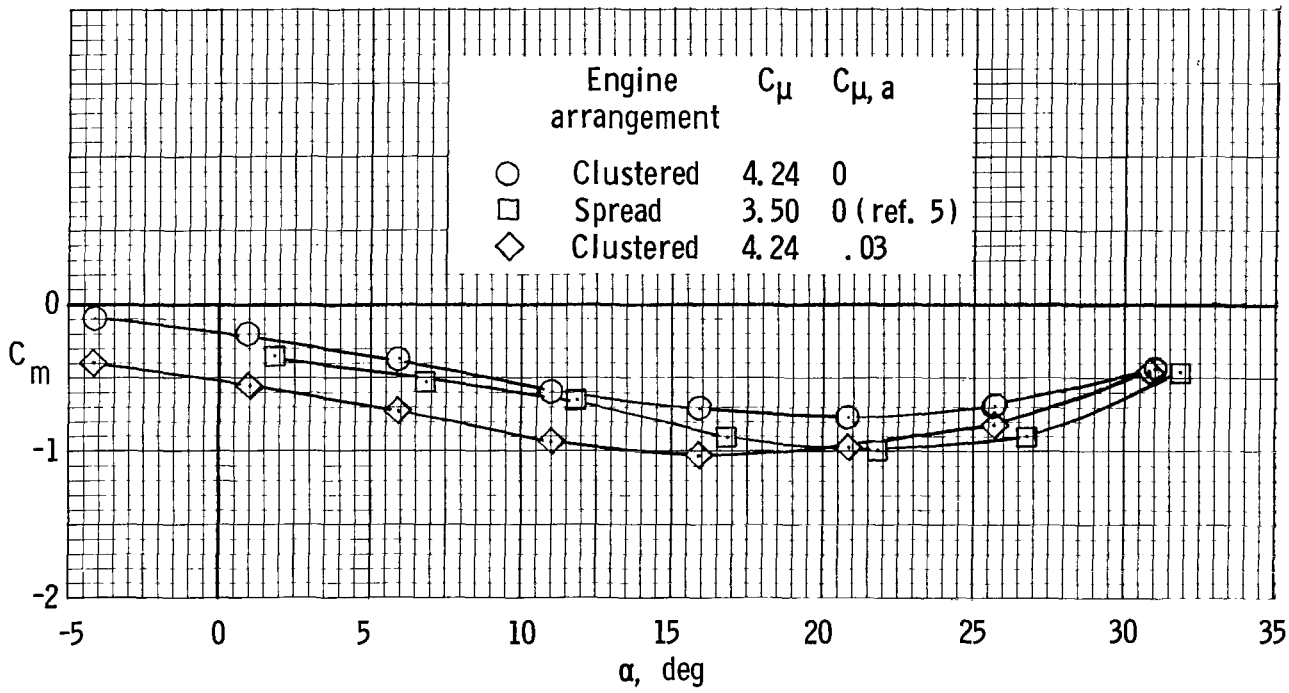

(f) Pitch characteristics. Center of gravity at $0.33\bar{c}$.

Figure 10.- Concluded.

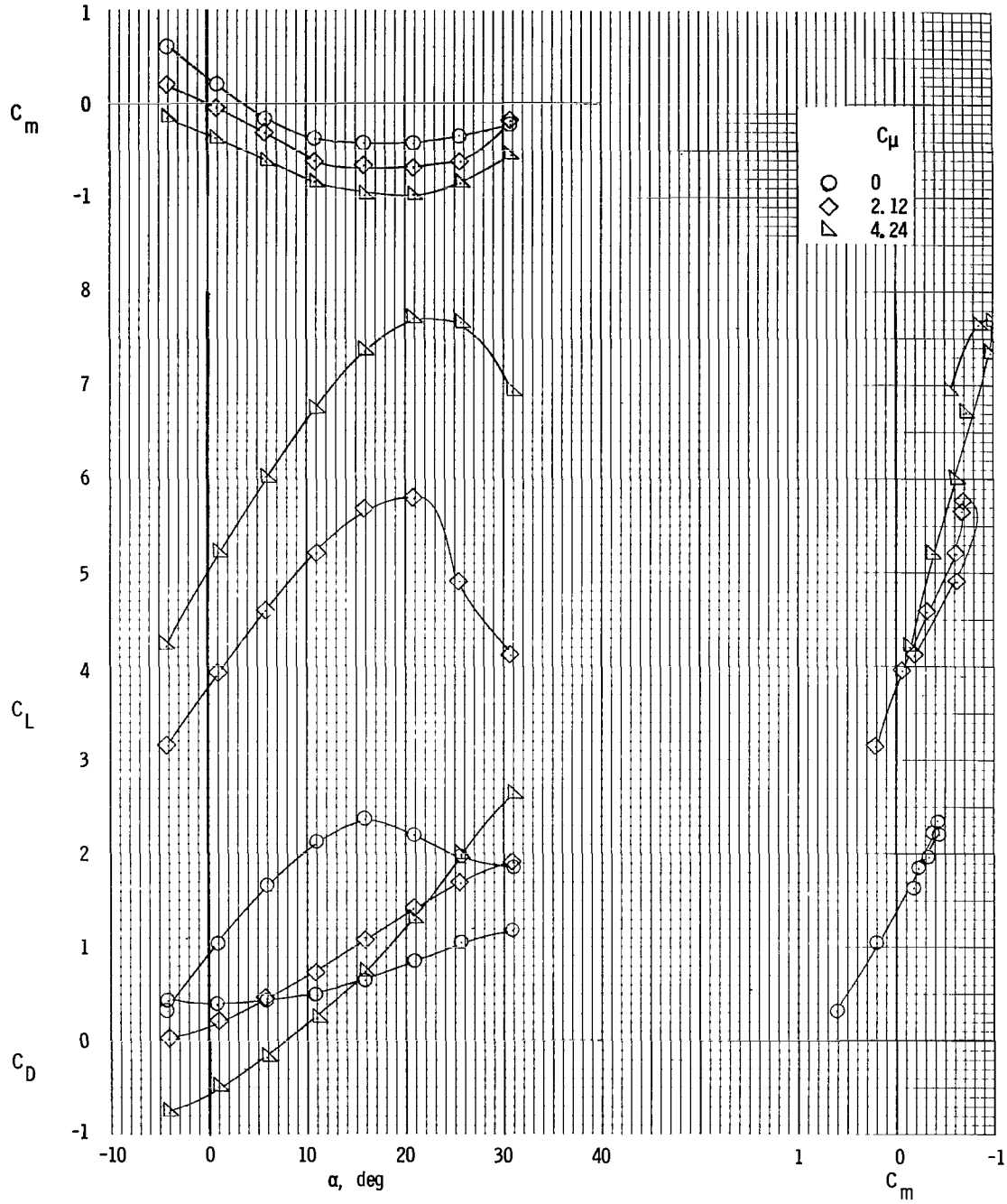

(a) $i_t = 0^o$; $\delta_a = 50^o$; $C_{\mu,a} = 0$.

Figure 11.- Longitudinal characteristics. Tail on; $\delta_{f1}/\delta_{f2} = 25^o/50^o$; $\delta_e = -50^o$.

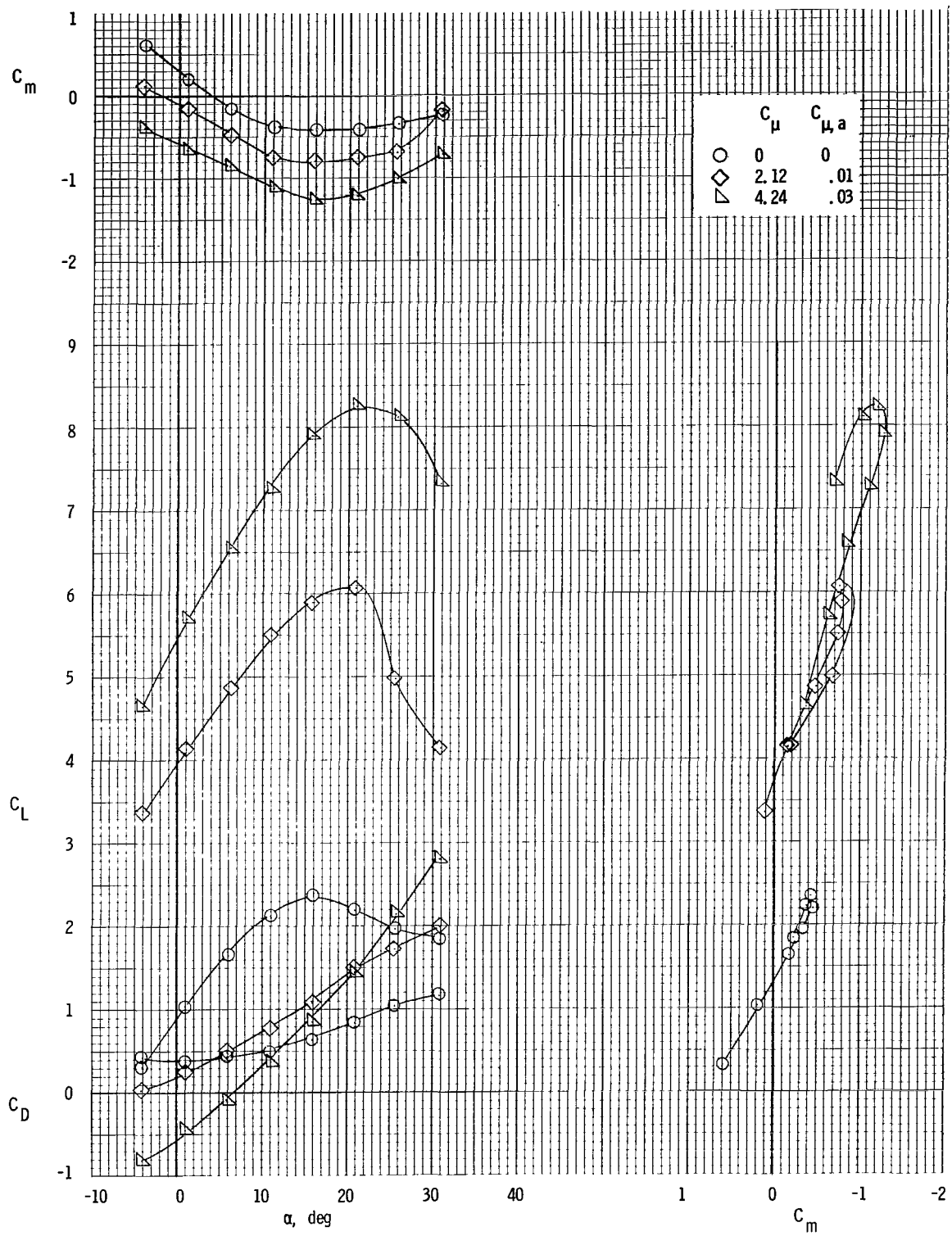

(b) $i_t = 0^o$; $\delta_a = 50^o$.

Figure 11.- Continued.

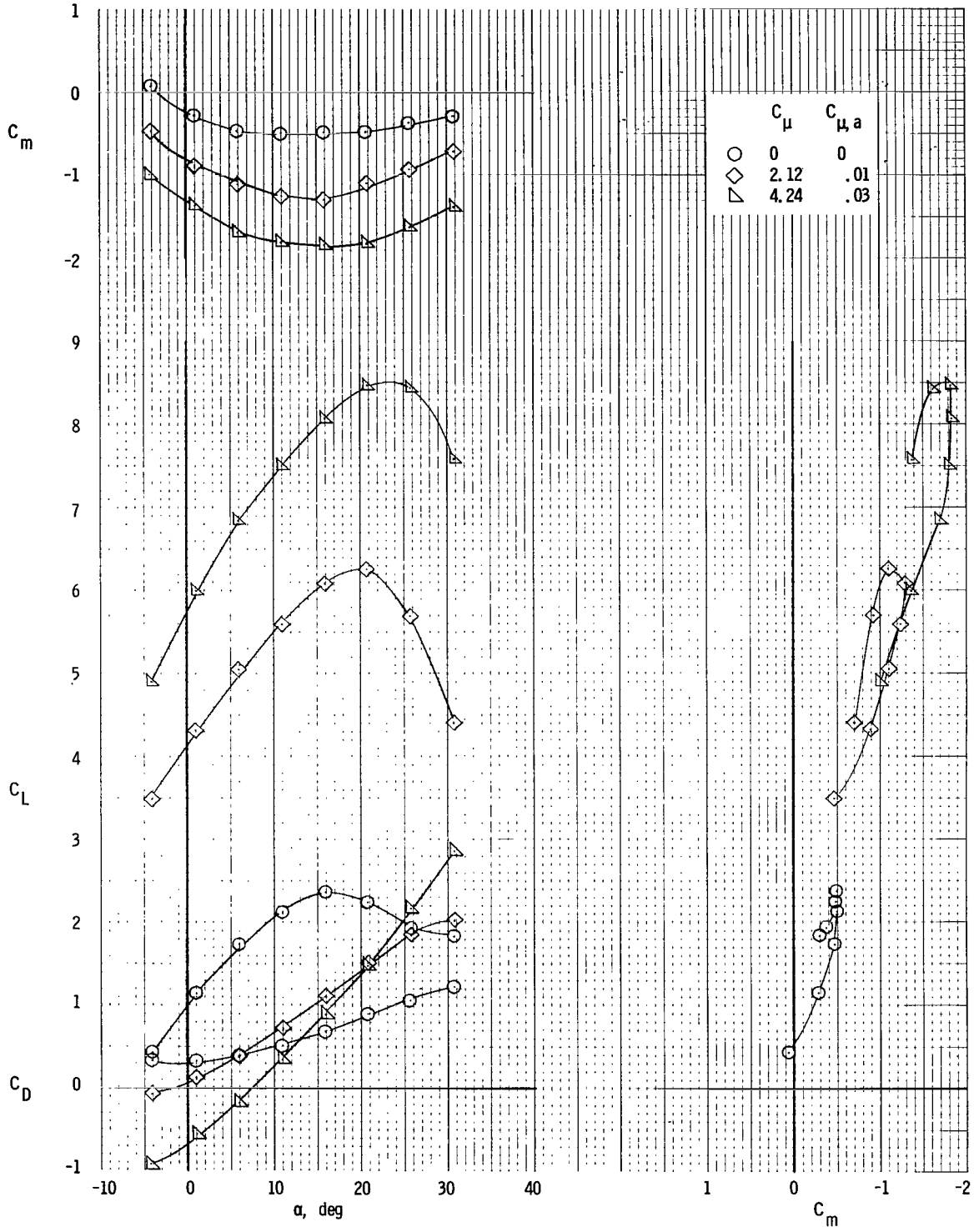

(c) $i_t = 5^o$; $\delta_a = 50^o$.

Figure 11.- Continued.

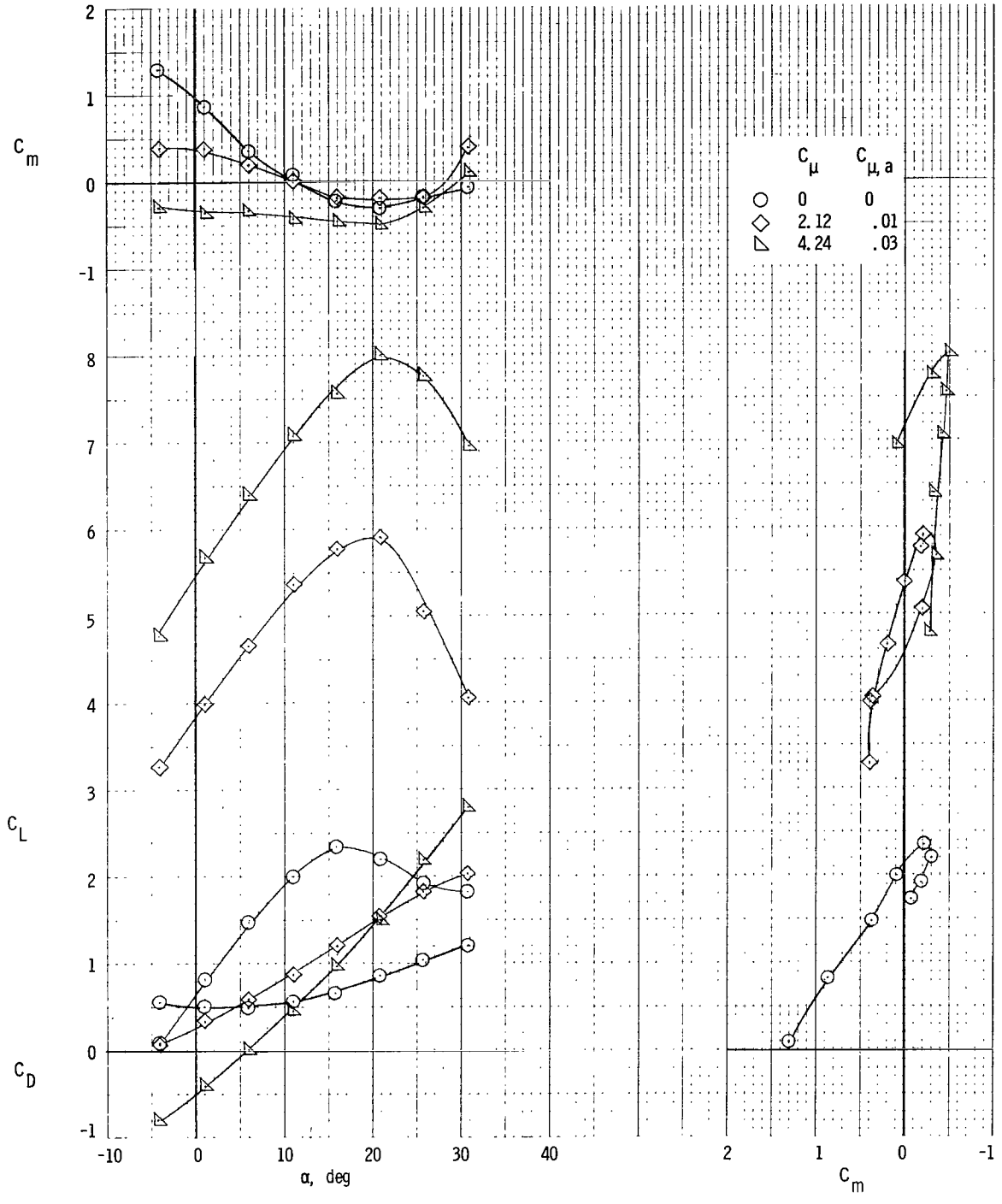

(d) $i_t = -5^o$; $\delta_a = 50^o$.

Figure 11.- Concluded.

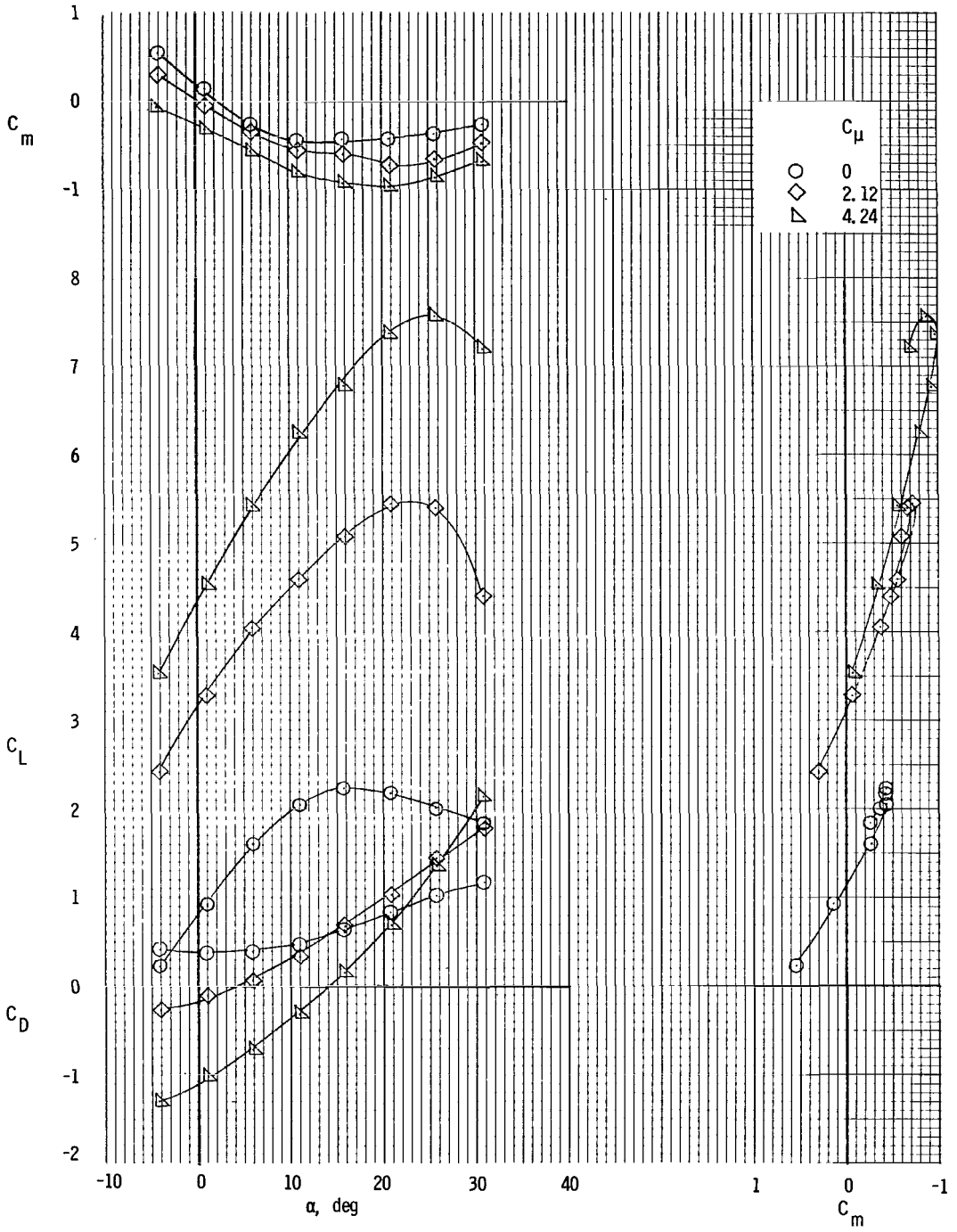

(a) $i_t = 0^o$; $\delta_a = 40^o$; $C_{\mu,a} = 0$.

Figure 12.- Longitudinal characteristics. Tail on; $\delta_{f1}/\delta_{f2} = 20^o/40^o$; $\delta_e = -50^o$.

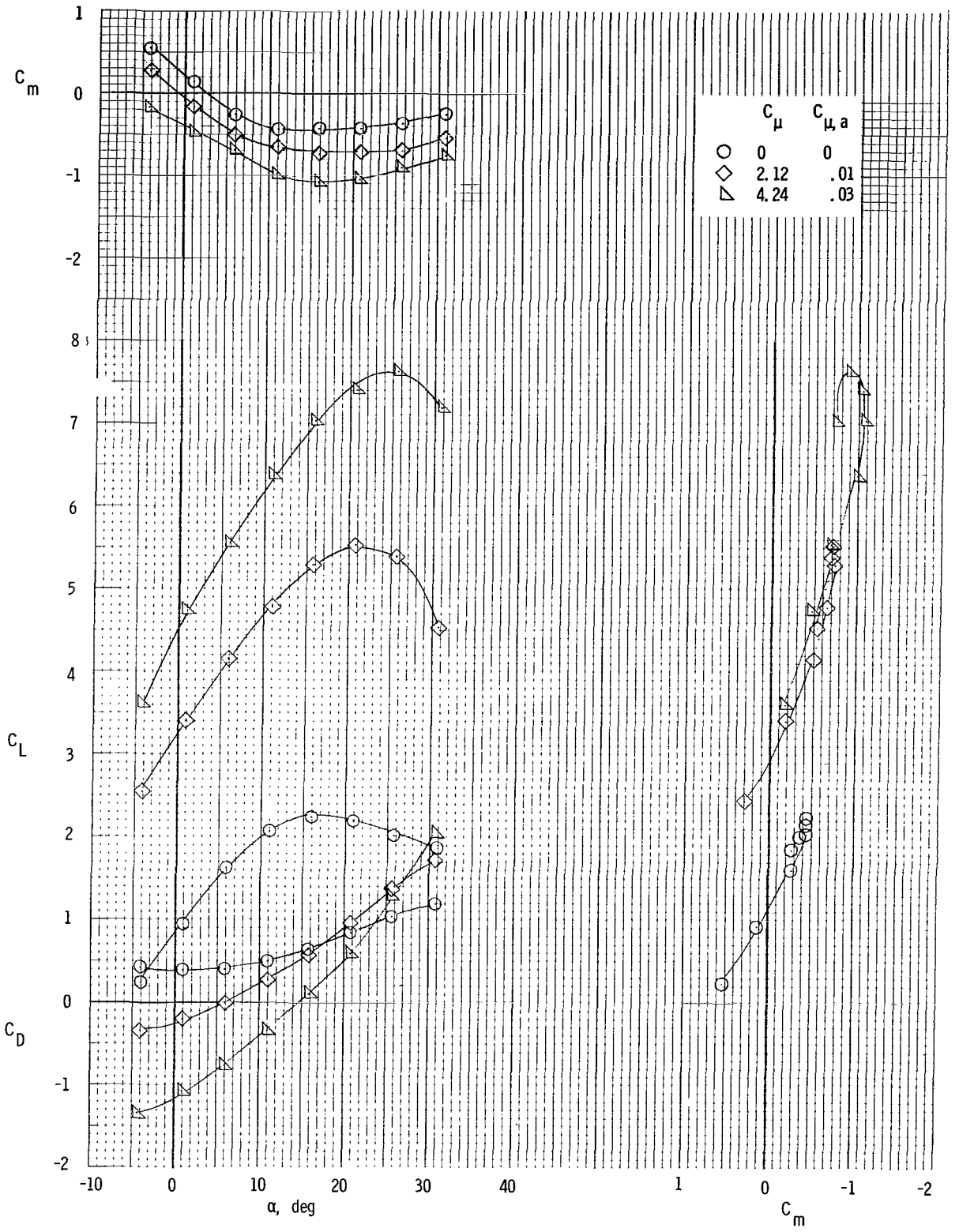

(b) $i_t = 0^o$; $\delta_a = 40^o$.

Figure 12.- Continued.

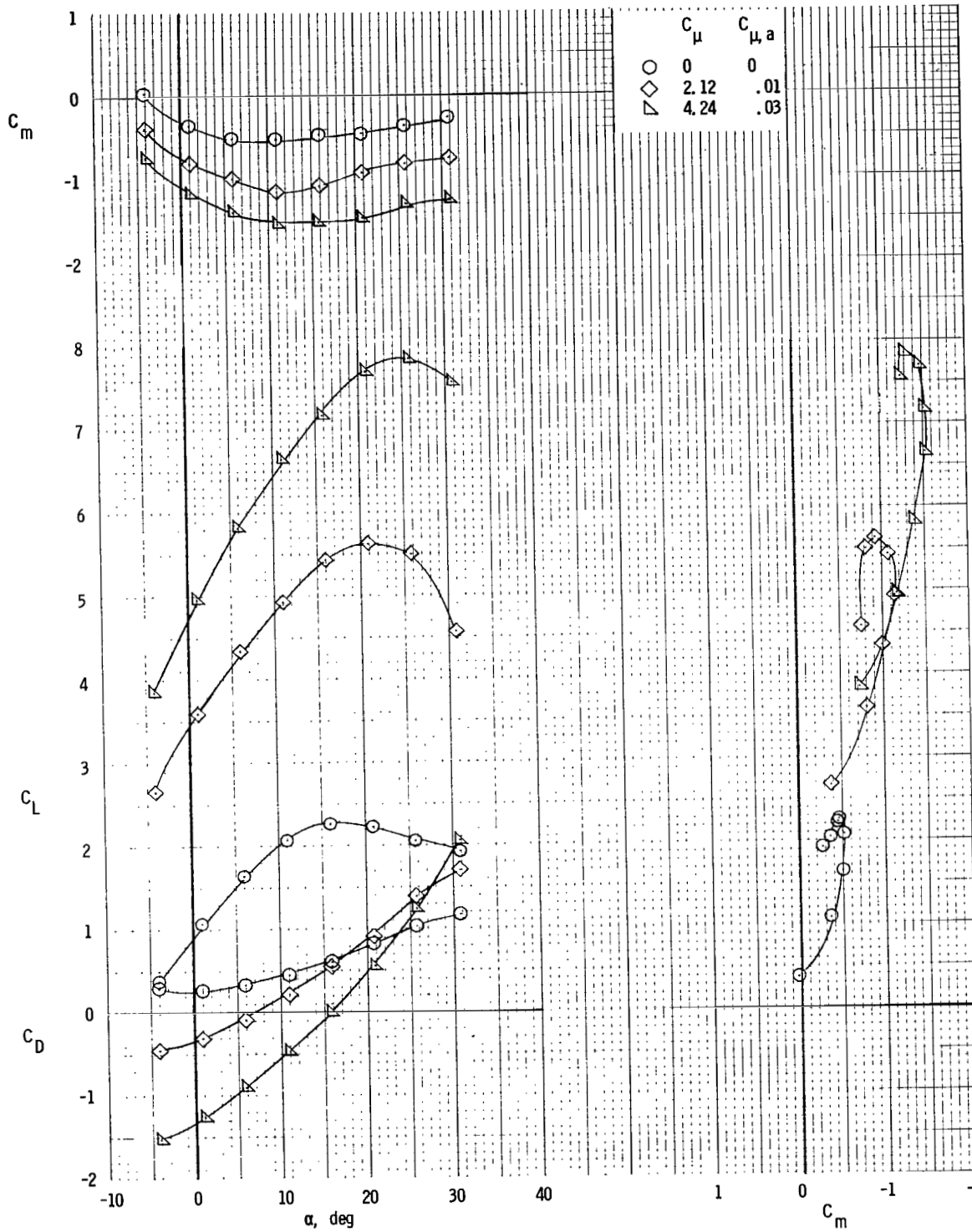

(c) $i_t = 5^o$; $\delta_a = 40^o$.

Figure 12.- Continued.

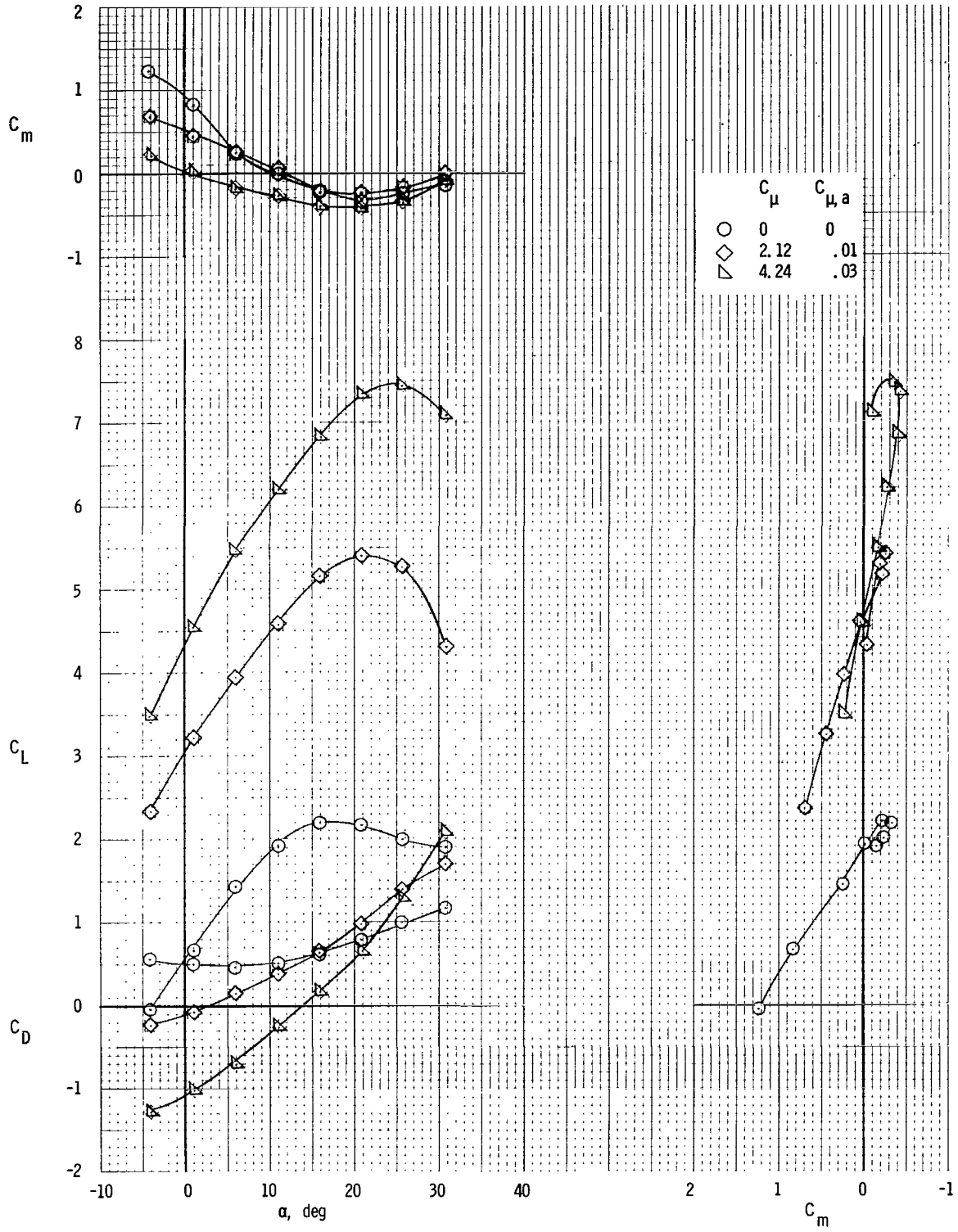

(d) $i_t = -5^o$; $\delta_a = 40^o$.

Figure 12.- Concluded.

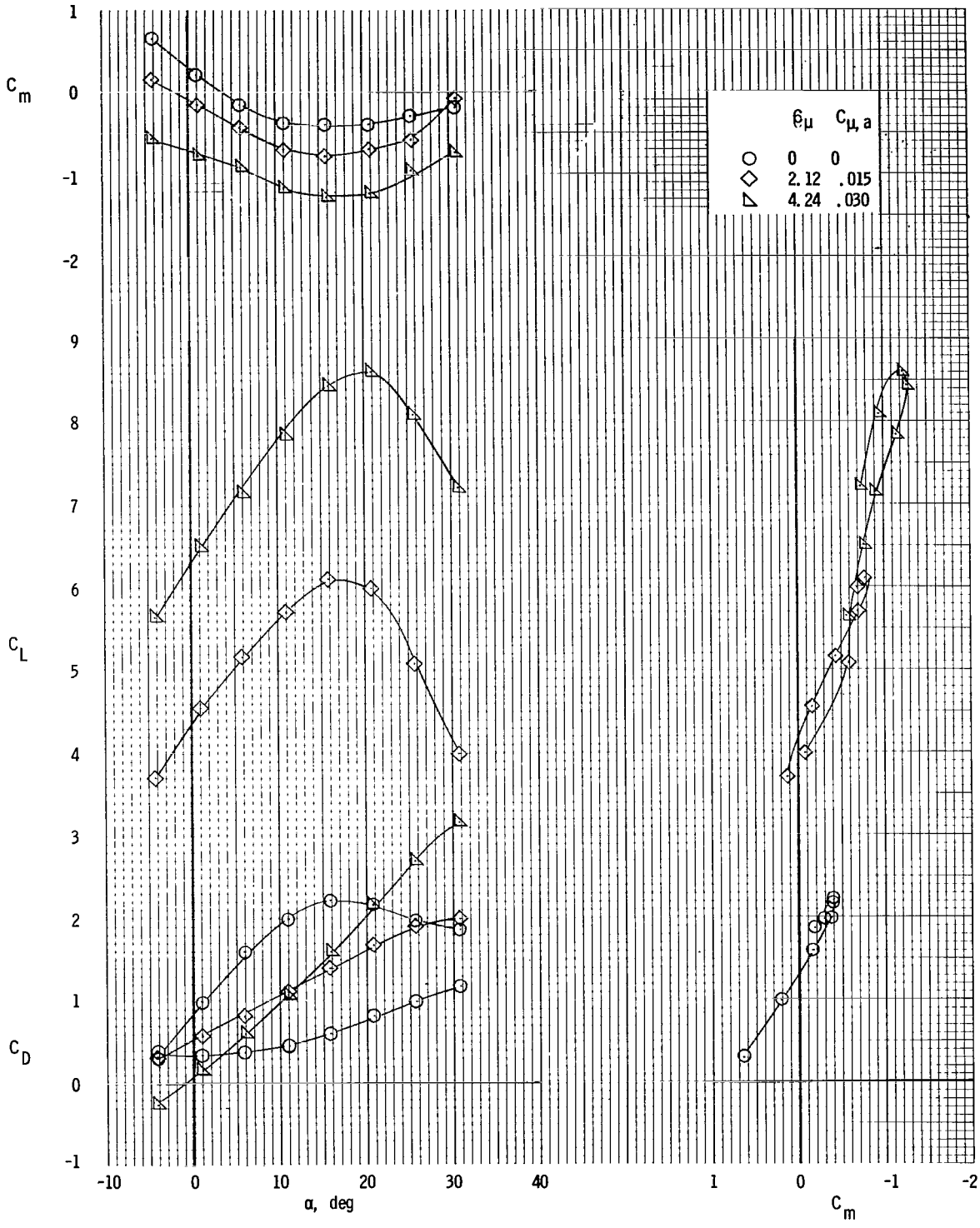

(a) $\delta_s = 10^o$.

Figure 13.- Longitudinal characteristics with symmetrical spoiler deflection. $\delta_{f1}/\delta_{f2} = 30^o/60^o$; $\delta_e = -50^o$; $i_t = 0^o$.

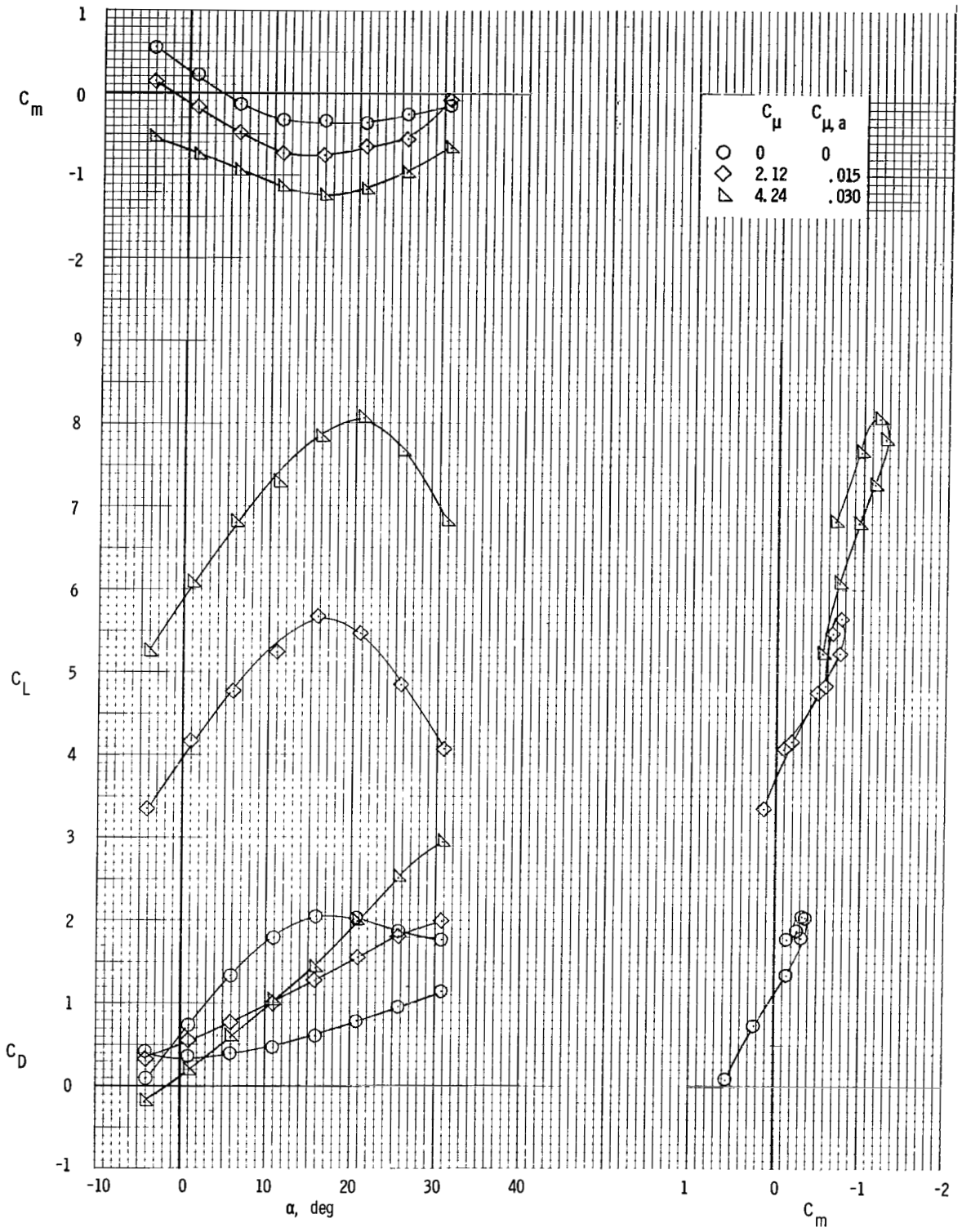

(b) $\delta_S = 20^O$.

Figure 13.- Continued.

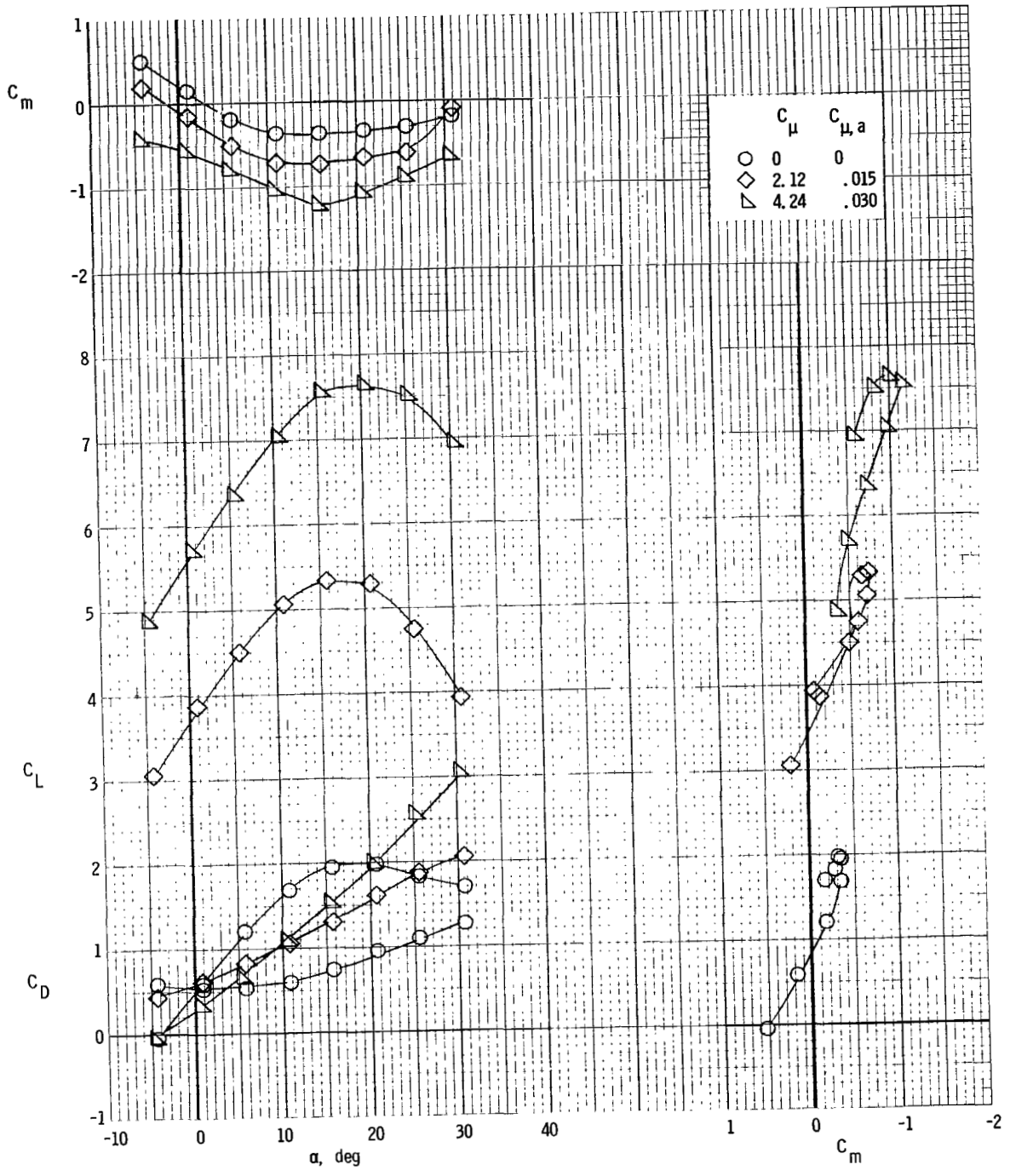

(c) $\delta_S = 30^O$.

Figure 13.- Concluded.

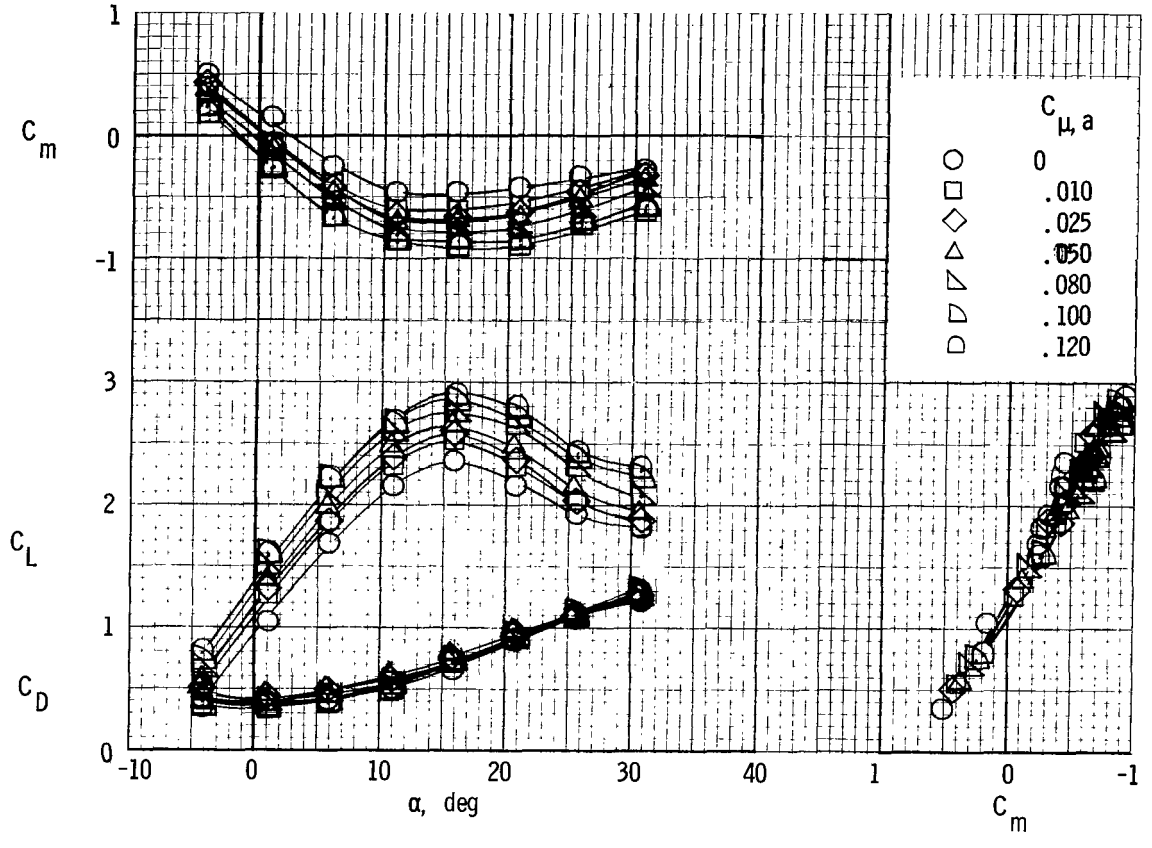

(a) $C_\mu = 0$.

Figure 14.- Longitudinal characteristics with aileron blowing. $\delta_{f1}/\delta_{f2} = 25^o/50^o$; $\delta_e = -50^o$; $i_t = 0^o$.

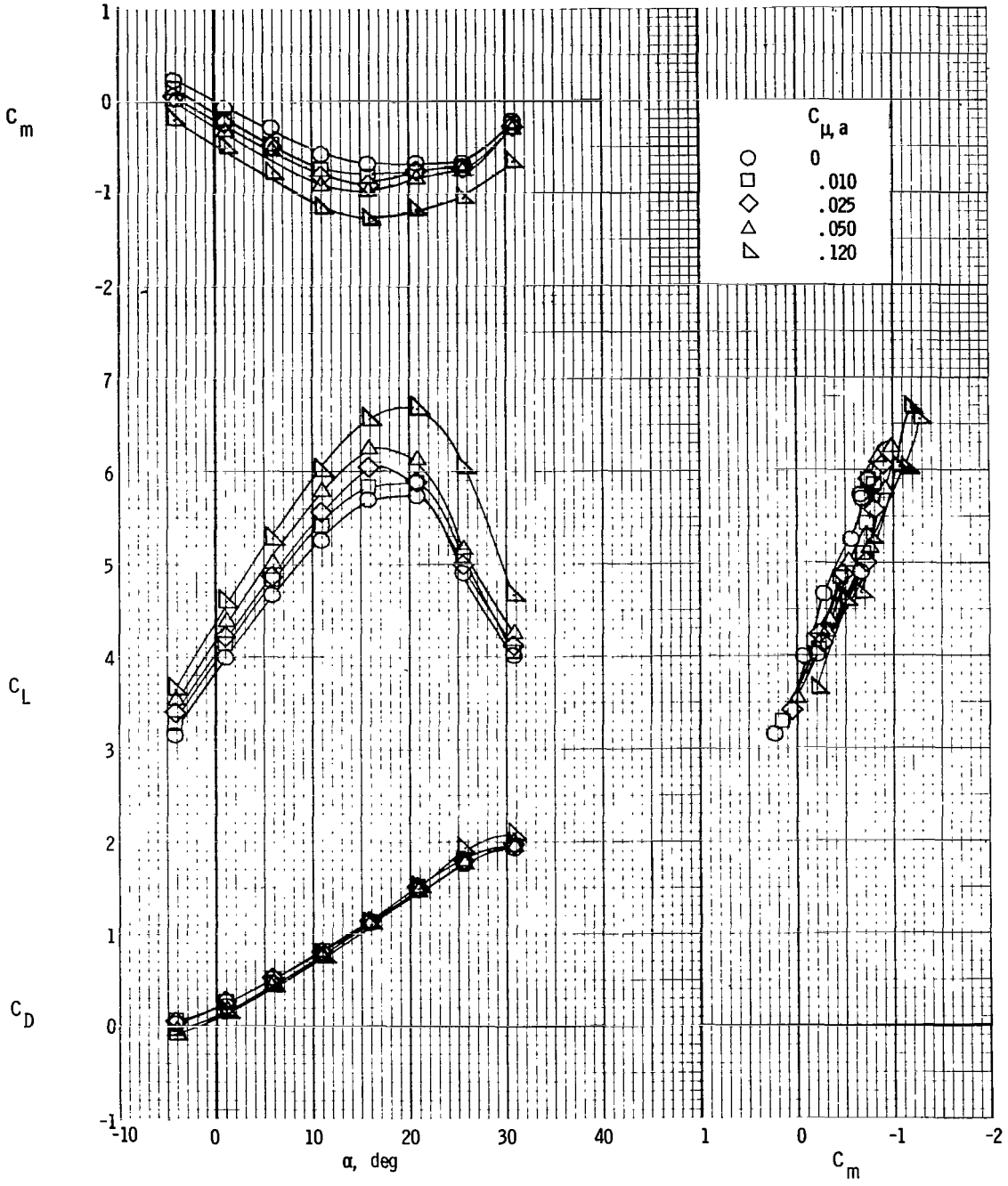

(b) $C_\mu = 2.12$.

Figure 14.- Continued.

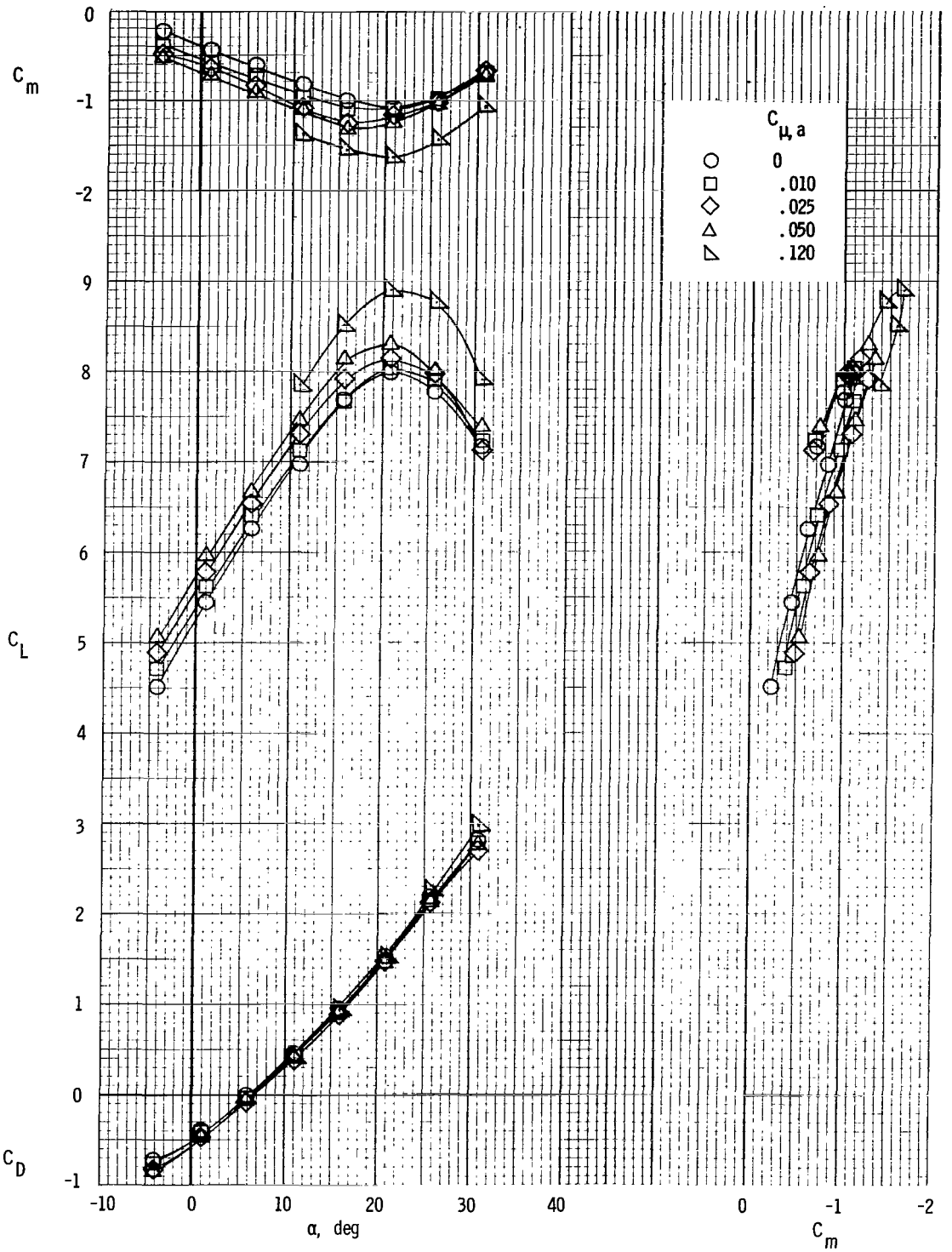

(c) $C_\mu = 4.24$.

Figure 14.- Concluded.

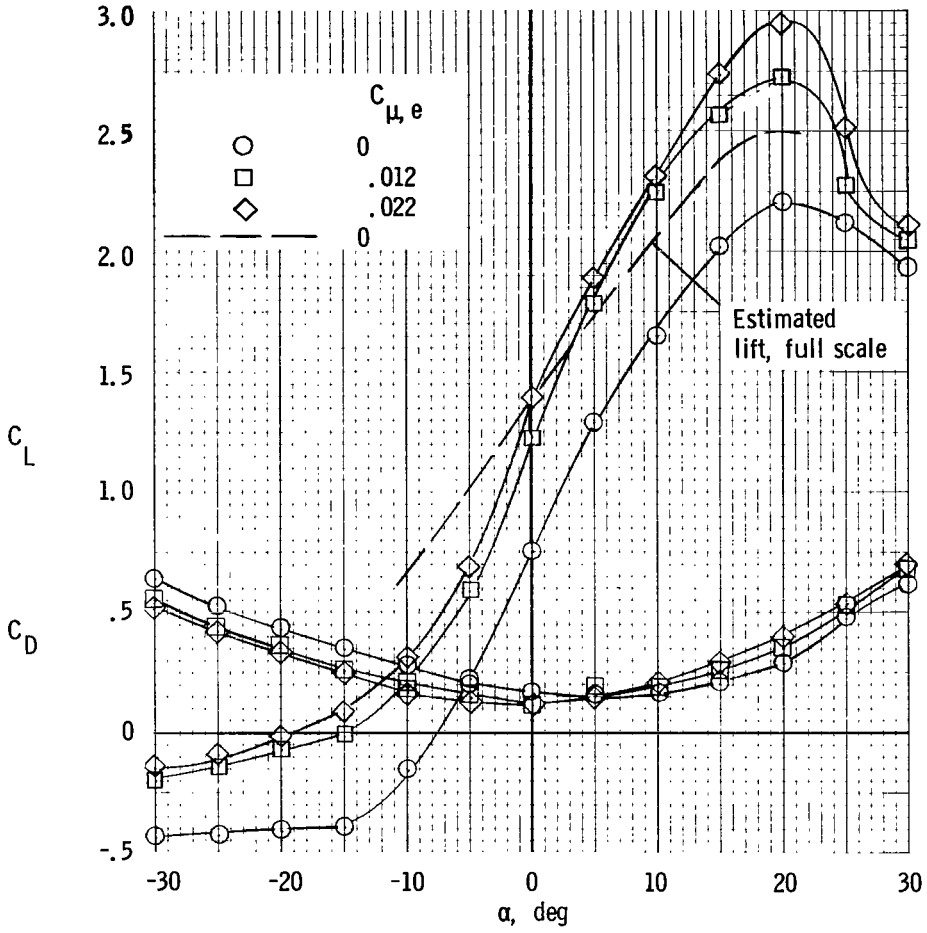

Figure 15.- Lift characteristics of horizontal tail. Leading- and trailing-edge flaps deflected. (Coefficients based on horizontal-tail area for this plot.)

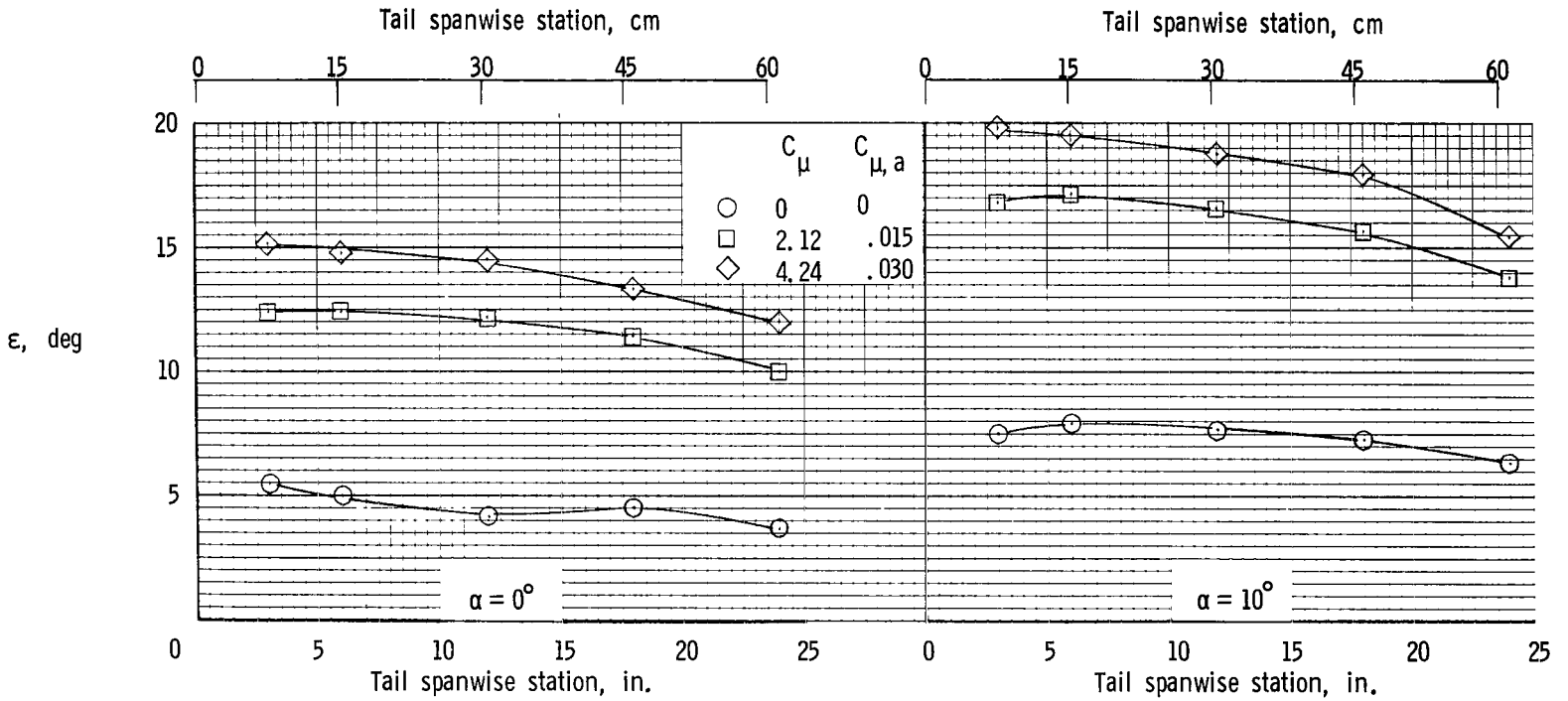

(a) z/c = 1.5.

Figure 16.- Variation of downwash angle with tail spanwise station. $\delta_{f1}/\delta_{f2} = 30^o/60^o$.

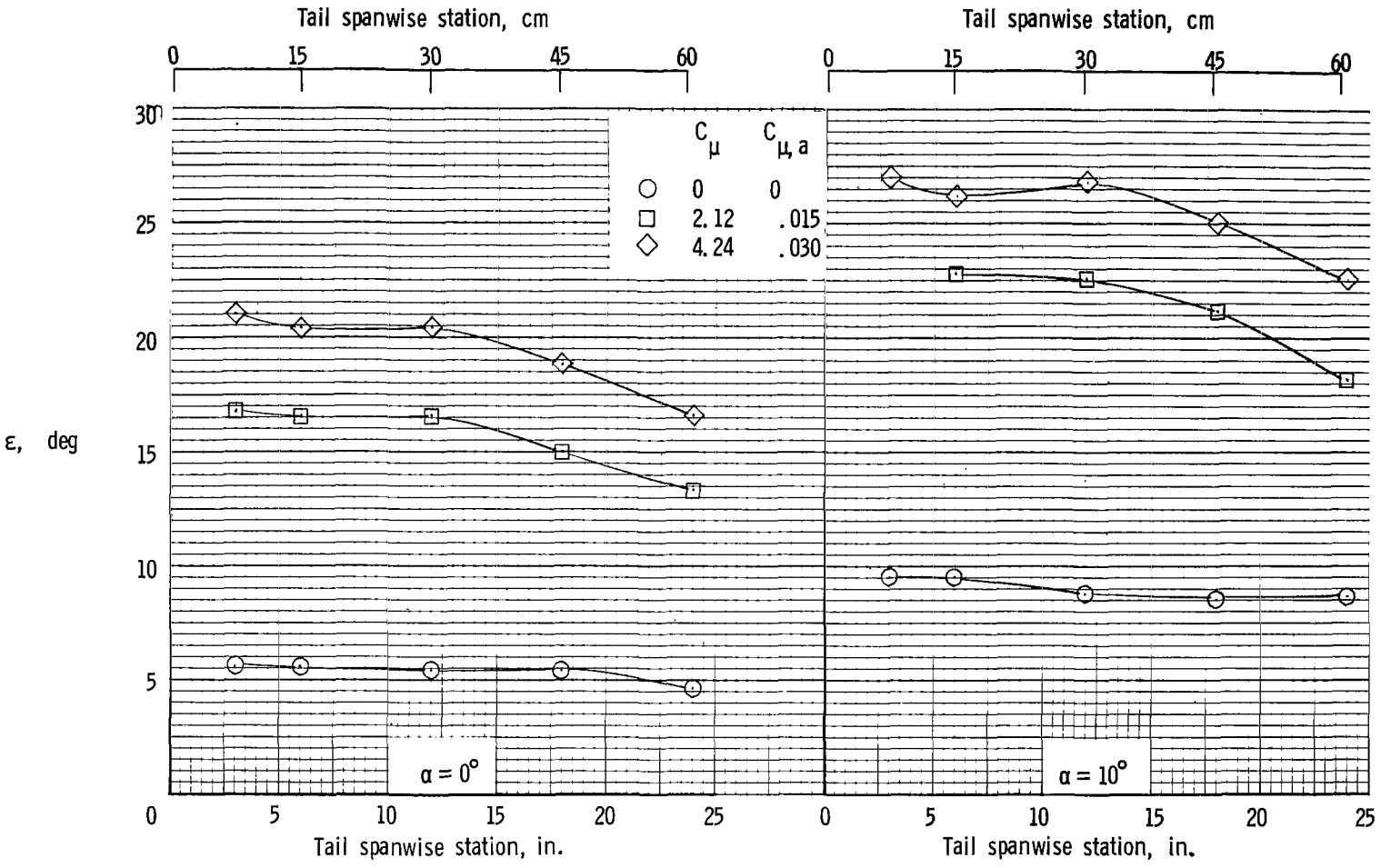

(b) z/c = 0.75.

Figure 16.- Continued.

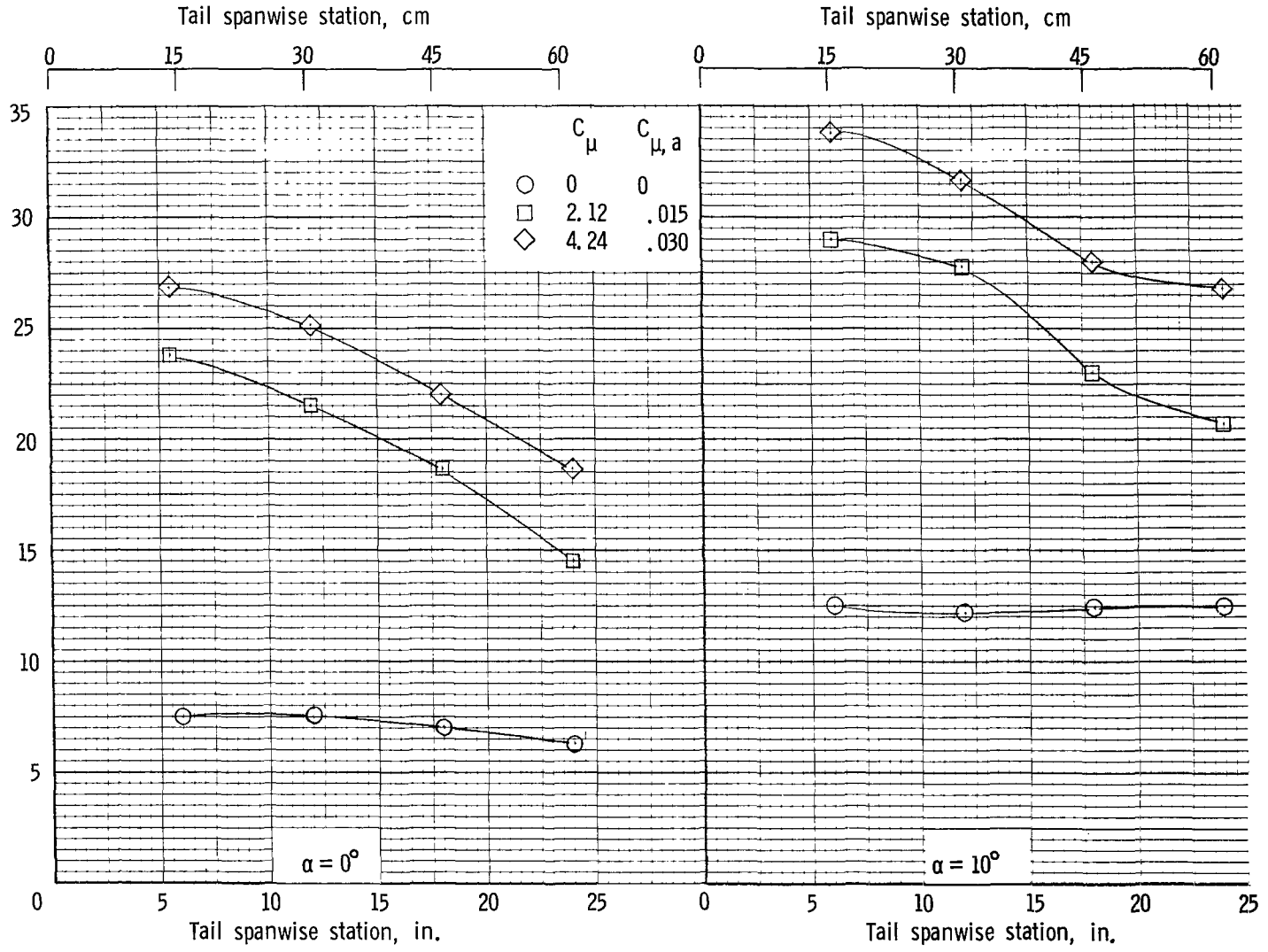

(c) z/c = 0.

Figure 16.- Concluded.

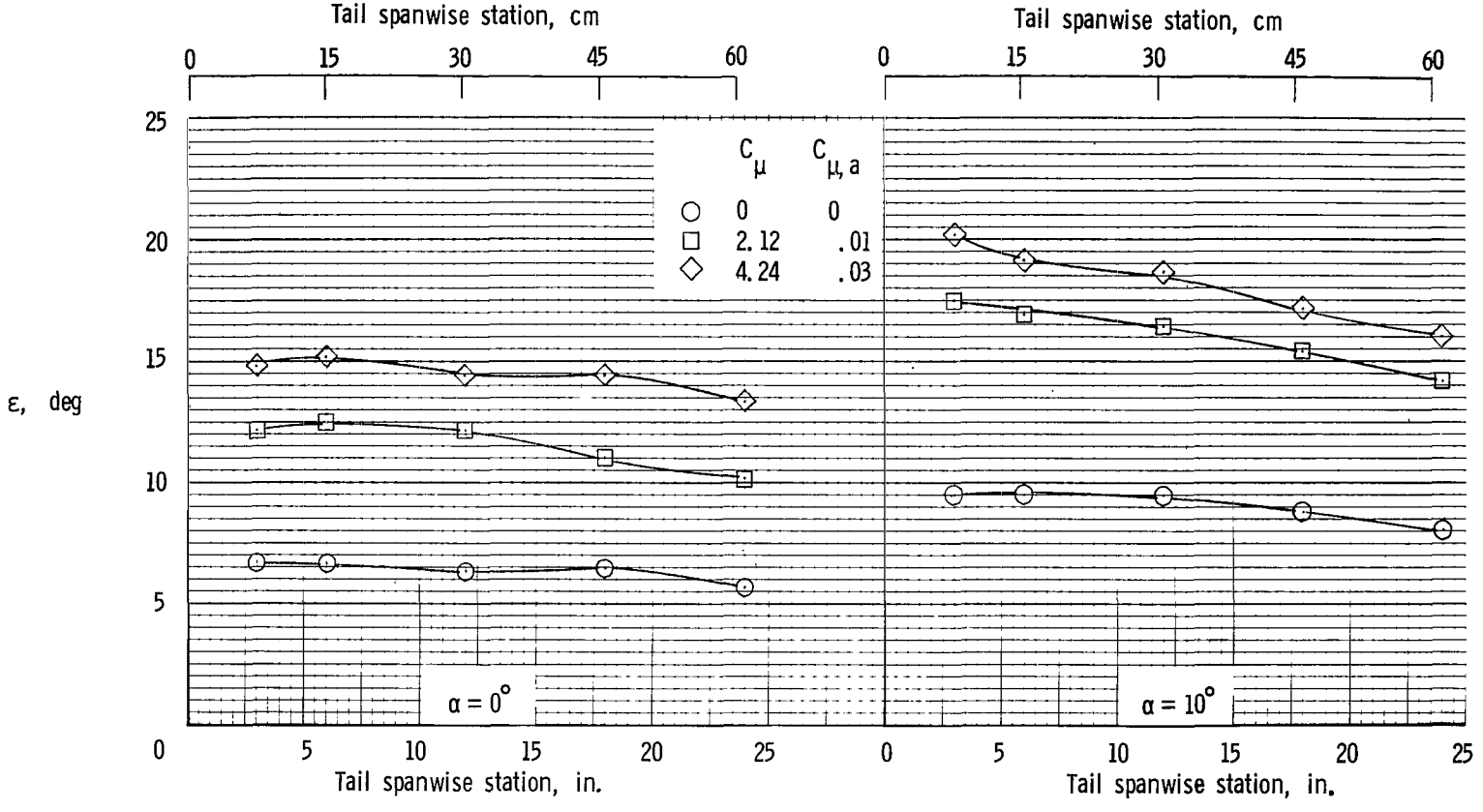

(a) z/c = 1.5.

Figure 17.- Variation of downwash angle with tail spanwise station. $\delta_{f1}/\delta_{f2} = 20^o/40^o$.

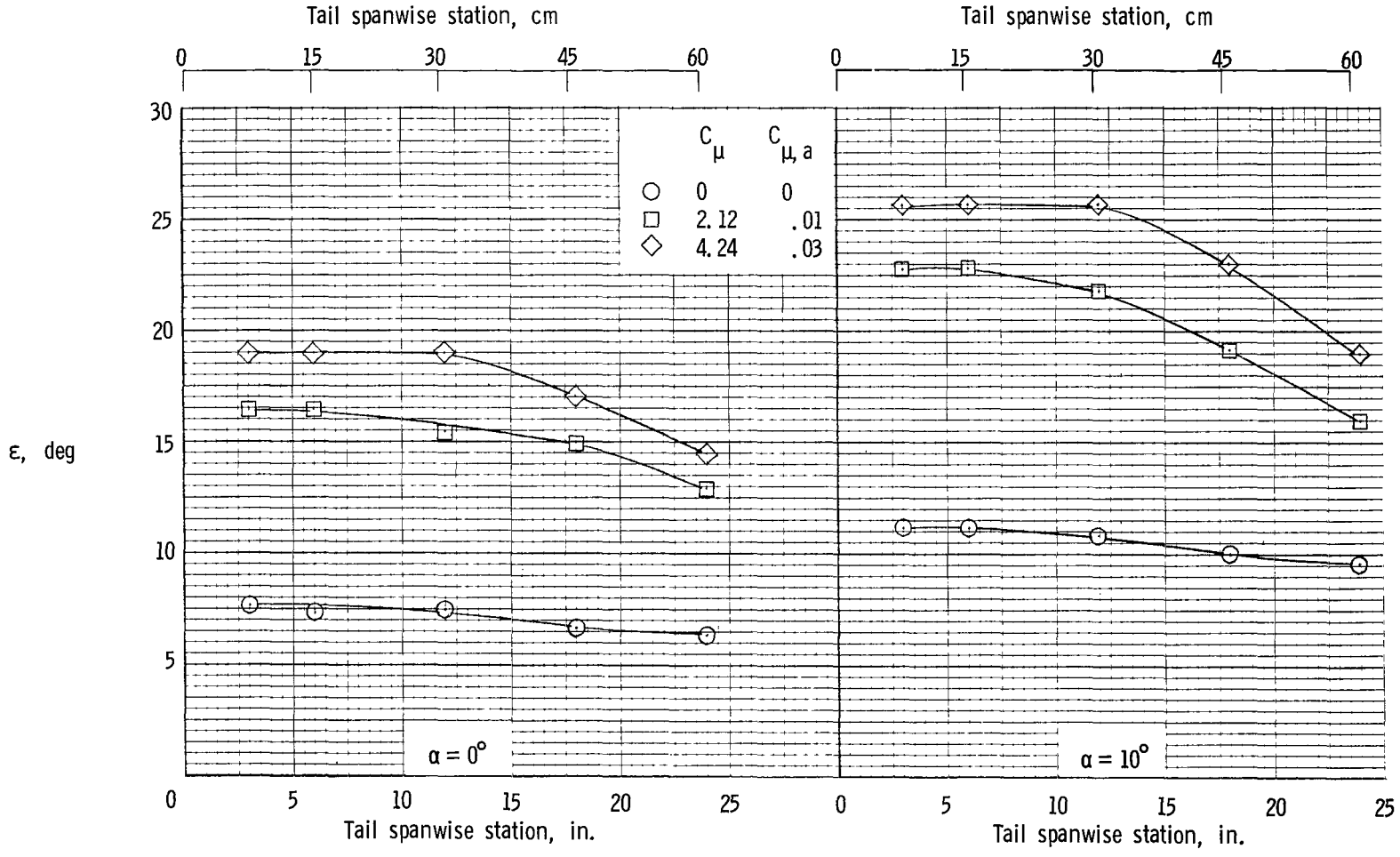

(b) z/c = 0.75.

Figure 17.- Continued.

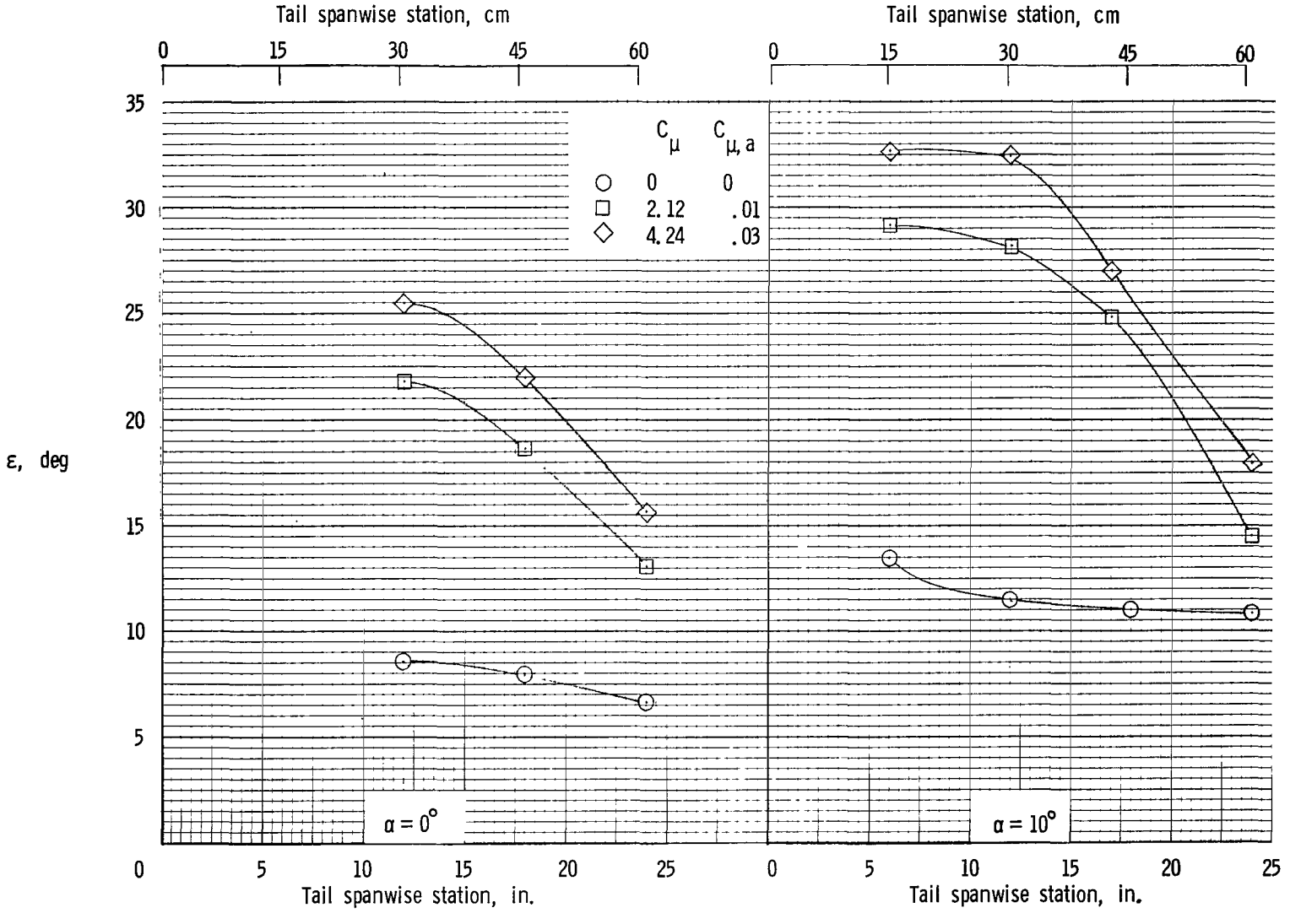

(c) z/c = 0.

Figure 17.- Concluded.

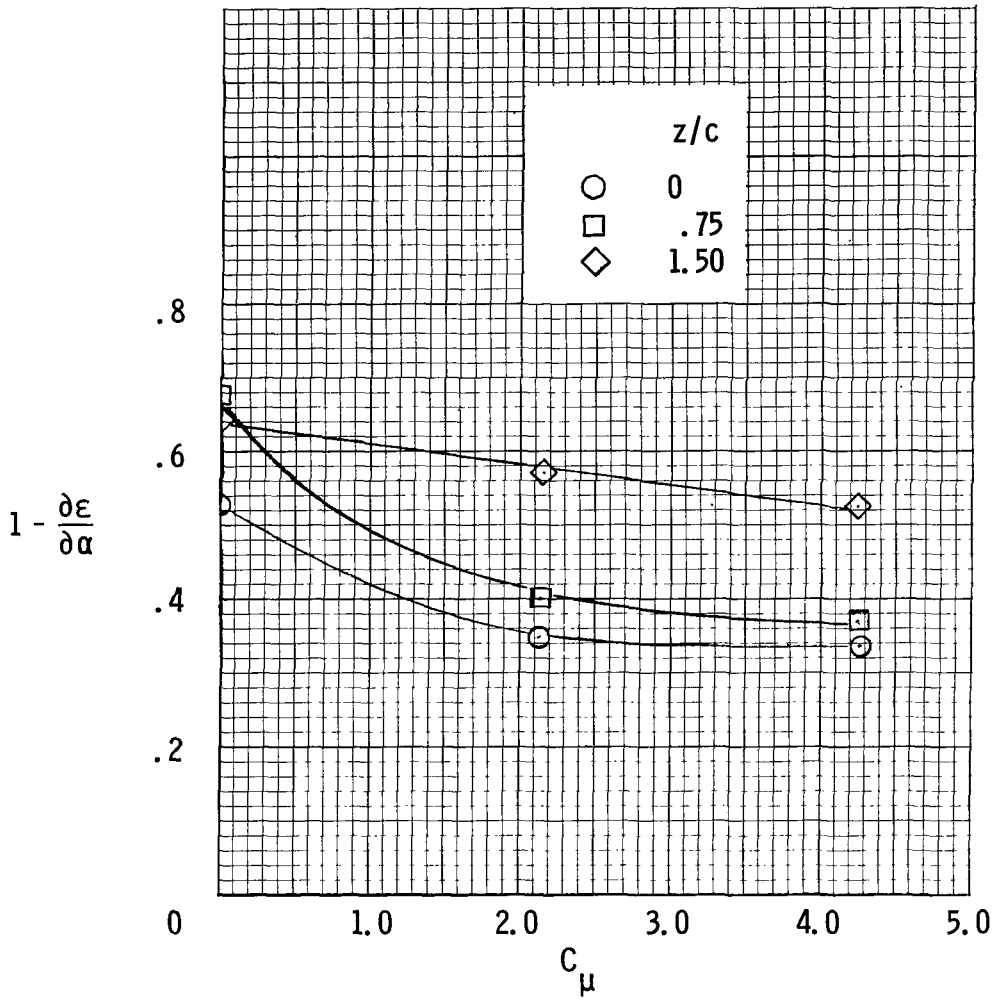

(a) $\delta_{f1}/\delta_{f2} = 30^o/60^o$.

Figure 18.- Summary of downwash flow studies. Spanwise station 12 in. (30.48 cm) from model center line.

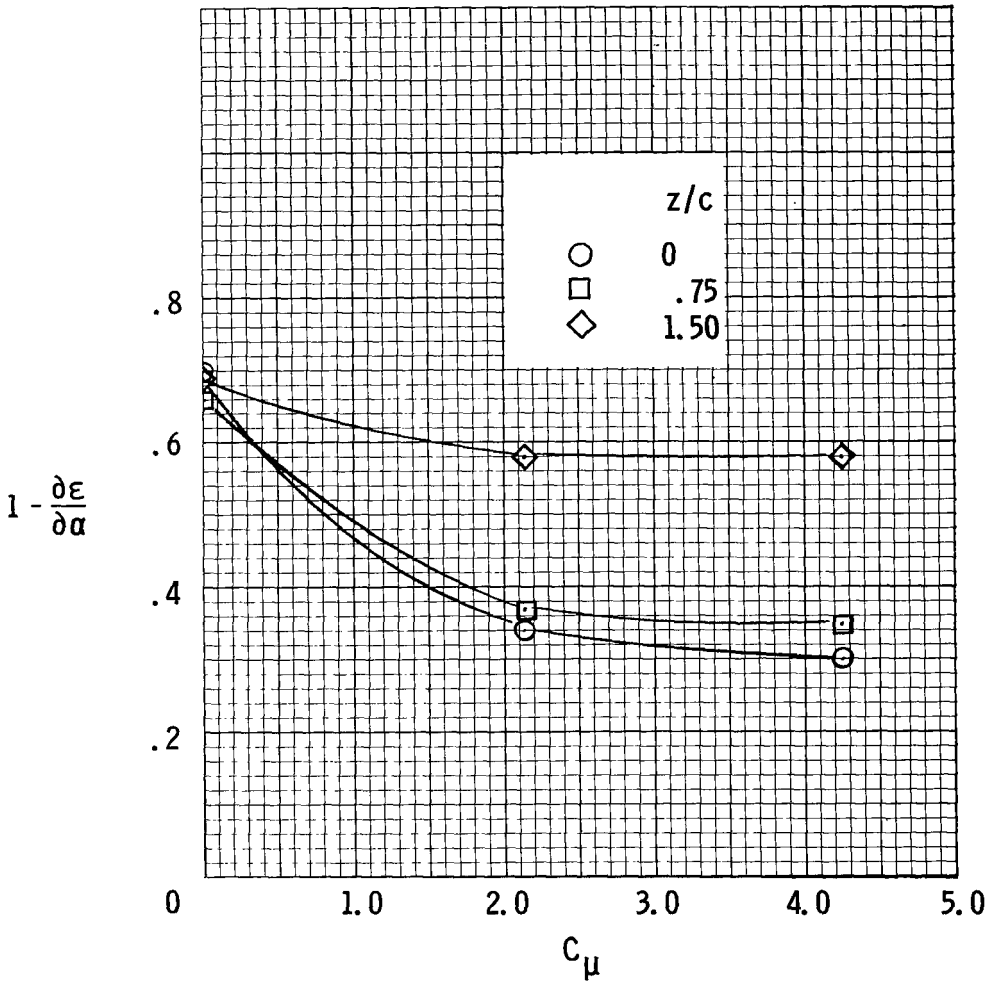

(b) $\delta_{f1}/\delta_{f2} = 20^o/40^o$.

Figure 18.- Concluded.

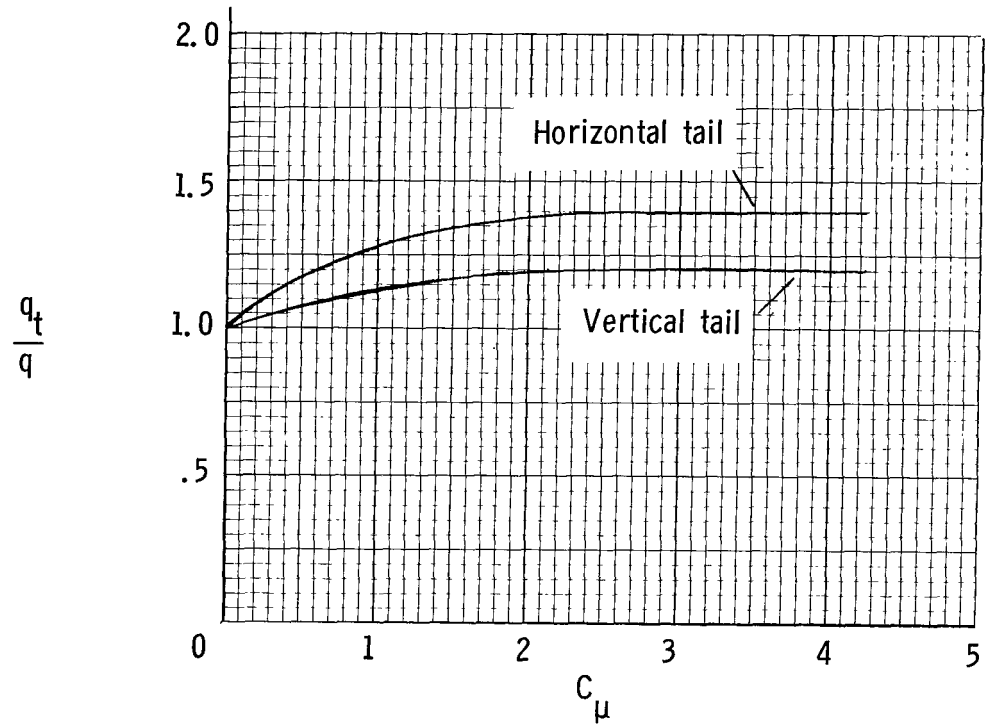

Figure 19.- Variation of dynamic pressure at horizontal- and vertical-tail locations with C_μ. $\alpha = 5^o$; $\delta_{f1}/\delta_{f2} = 30^o/60^o$.

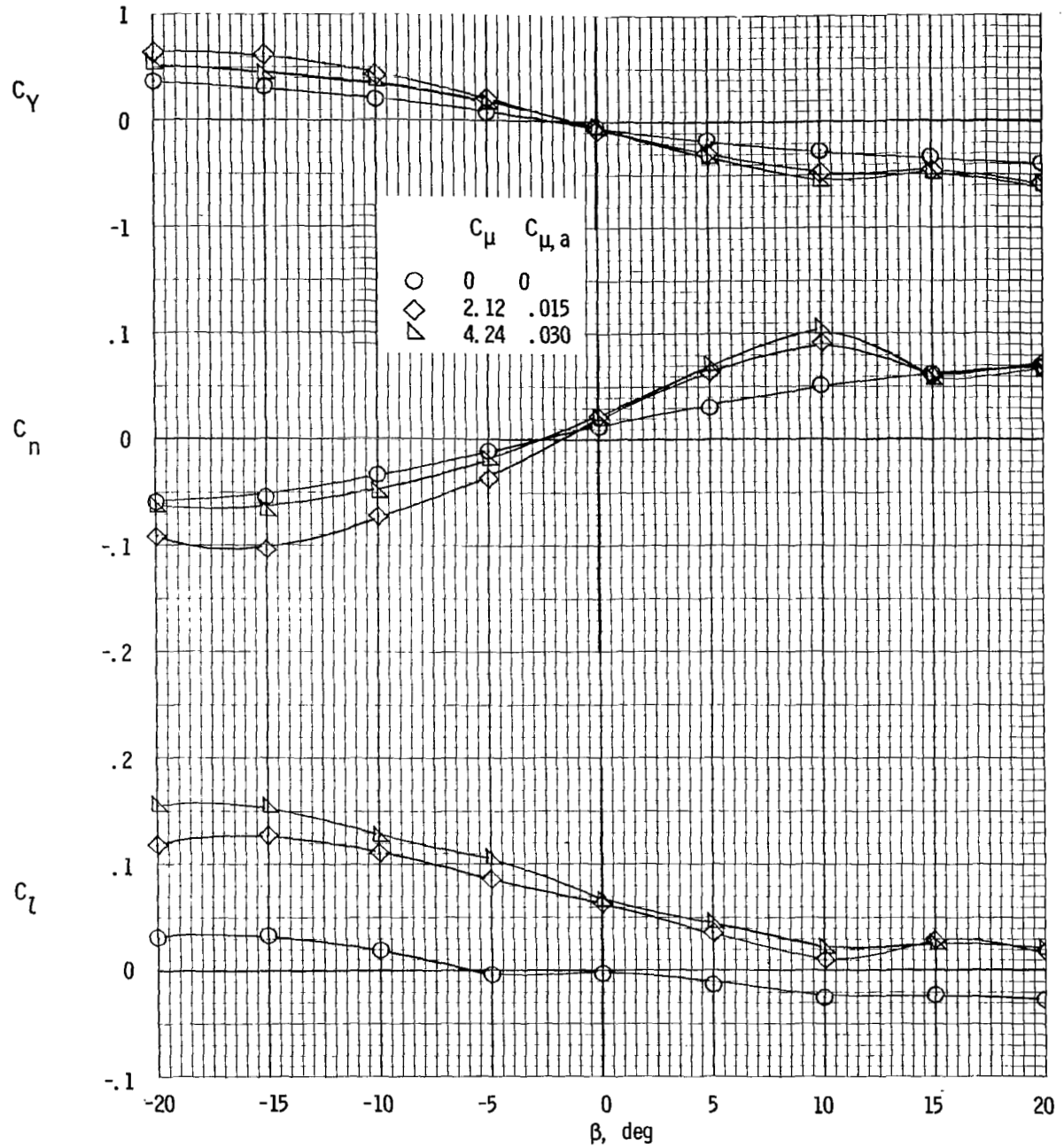

Figure 20.- Variation of lateral stability characteristics with sideslip angle. $\delta_{f1}/\delta_{f2} = 30^o/60^o$; $\alpha = 1^o$.

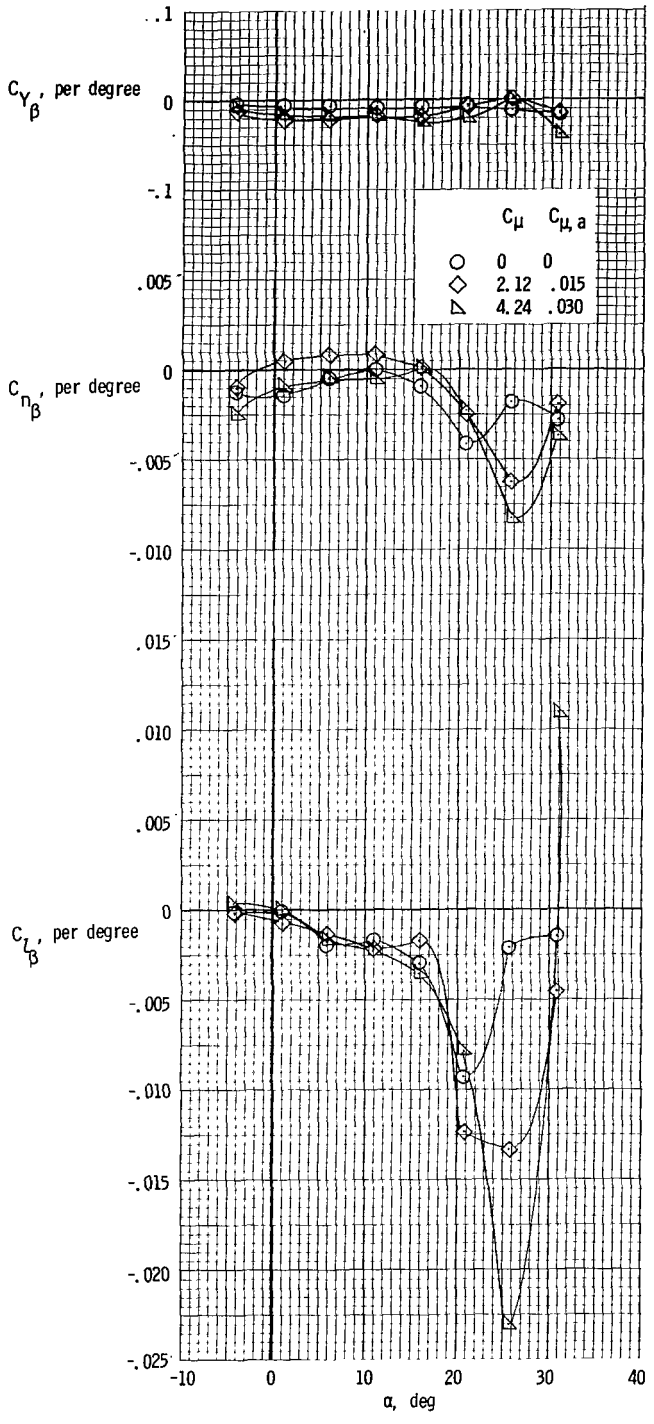

(a) Vertical tail off.

Figure 21.- Lateral stability characteristics. $\delta_{f1}/\delta_{f2} = 30^o/60^o$.

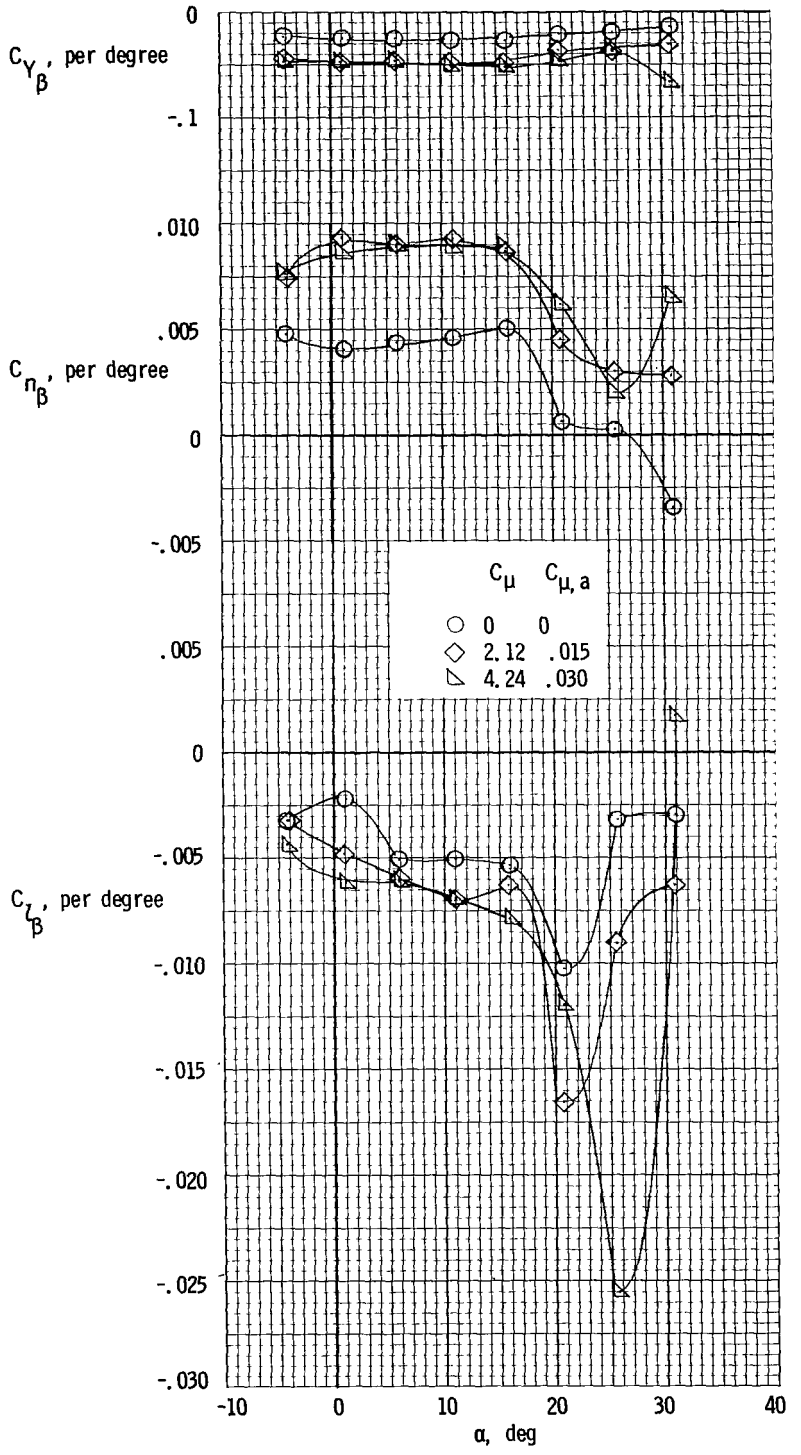

(b) Vertical tail on.

Figure 21.- Concluded.

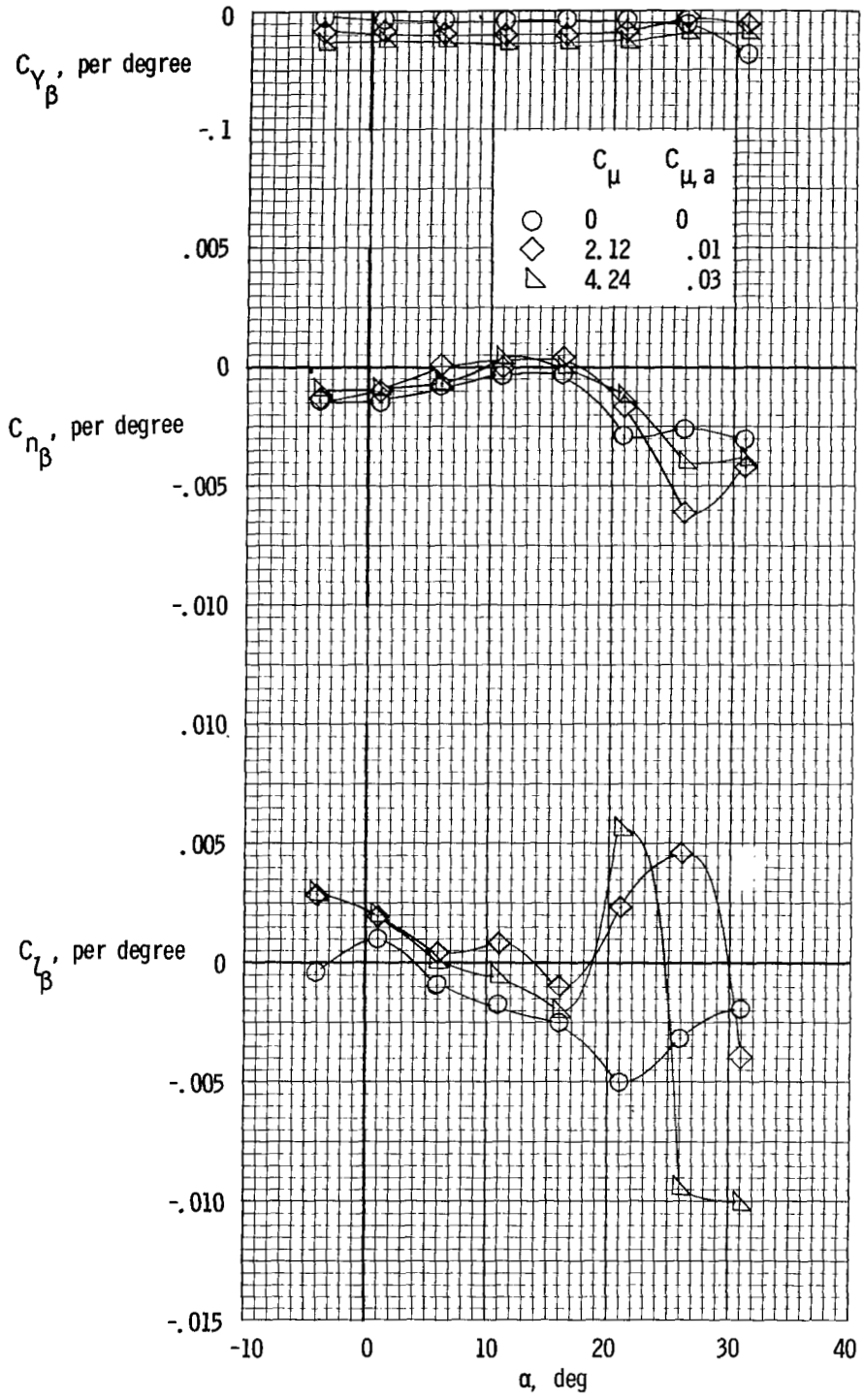

(a) Vertical tail off.

Figure 22.- Lateral stability characteristics. $\delta_{f1}/\delta_{f2} = 20^o/40^o$.

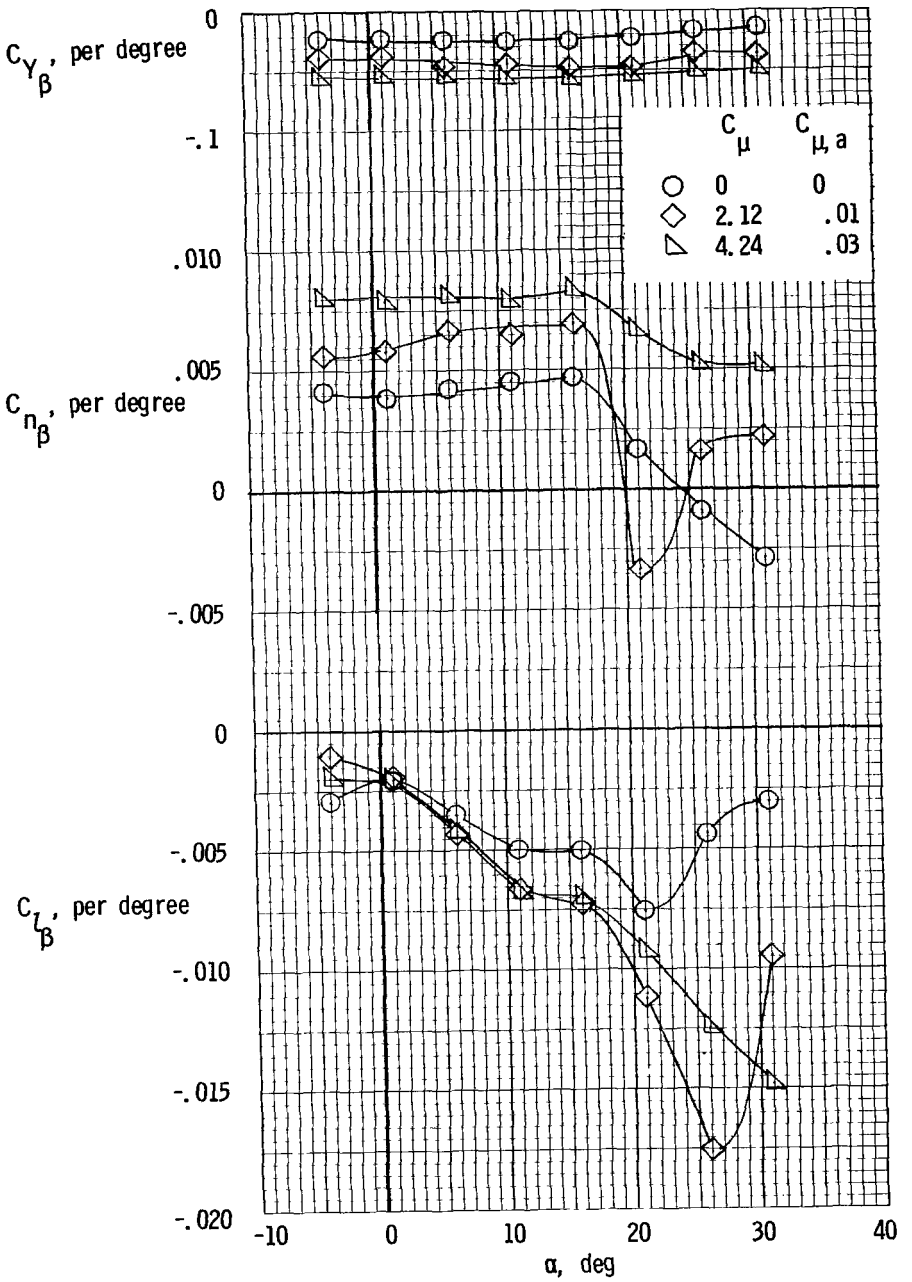

(b) Vertical tail on.

Figure 22.- Concluded.

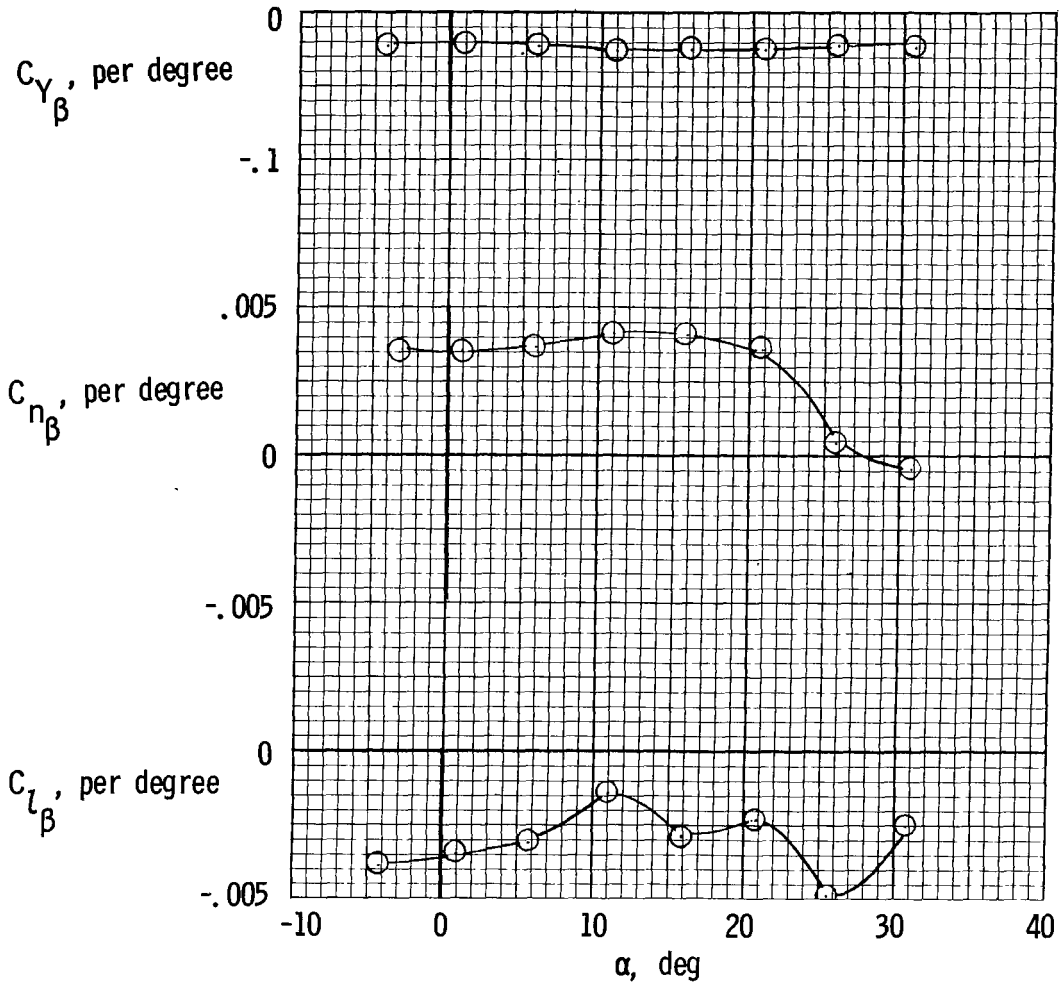

Figure 23.- Lateral stability characteristics. $\delta_{f1}/\delta_{f2} = 0^o$; $C_\mu = 0$; $C_{\mu,a} = 0$.

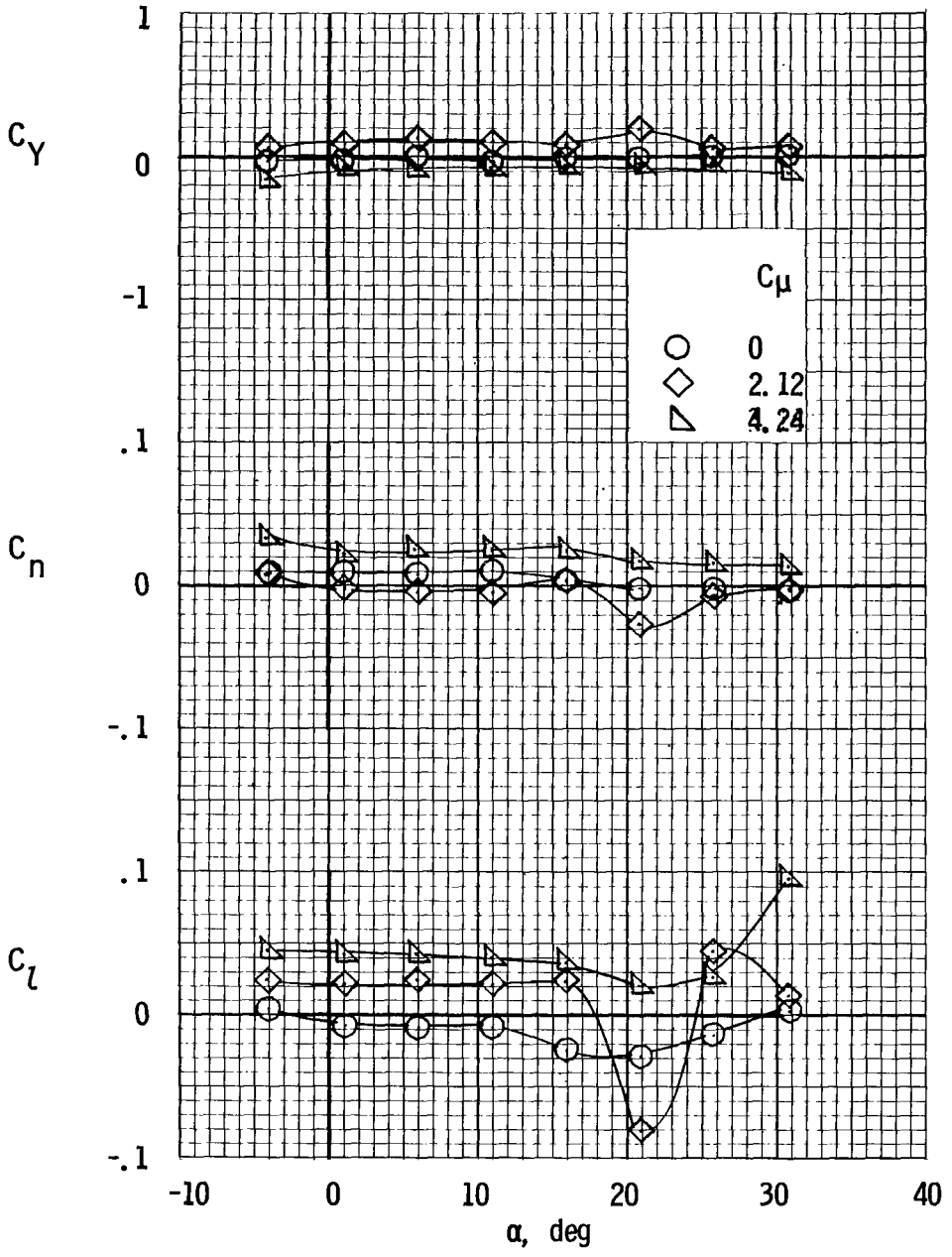

(a) Lateral characteristics, all engines operating.

Figure 24.- Lateral and longitudinal characteristics, left outboard engine not operating. $\delta_{f1}/\delta_{f2} = 30^o/60^o$; $\delta_e = -50^o$; $i_t = 0^o$; $\delta_a = 60^o$; $C_{\mu,a} = 0$.

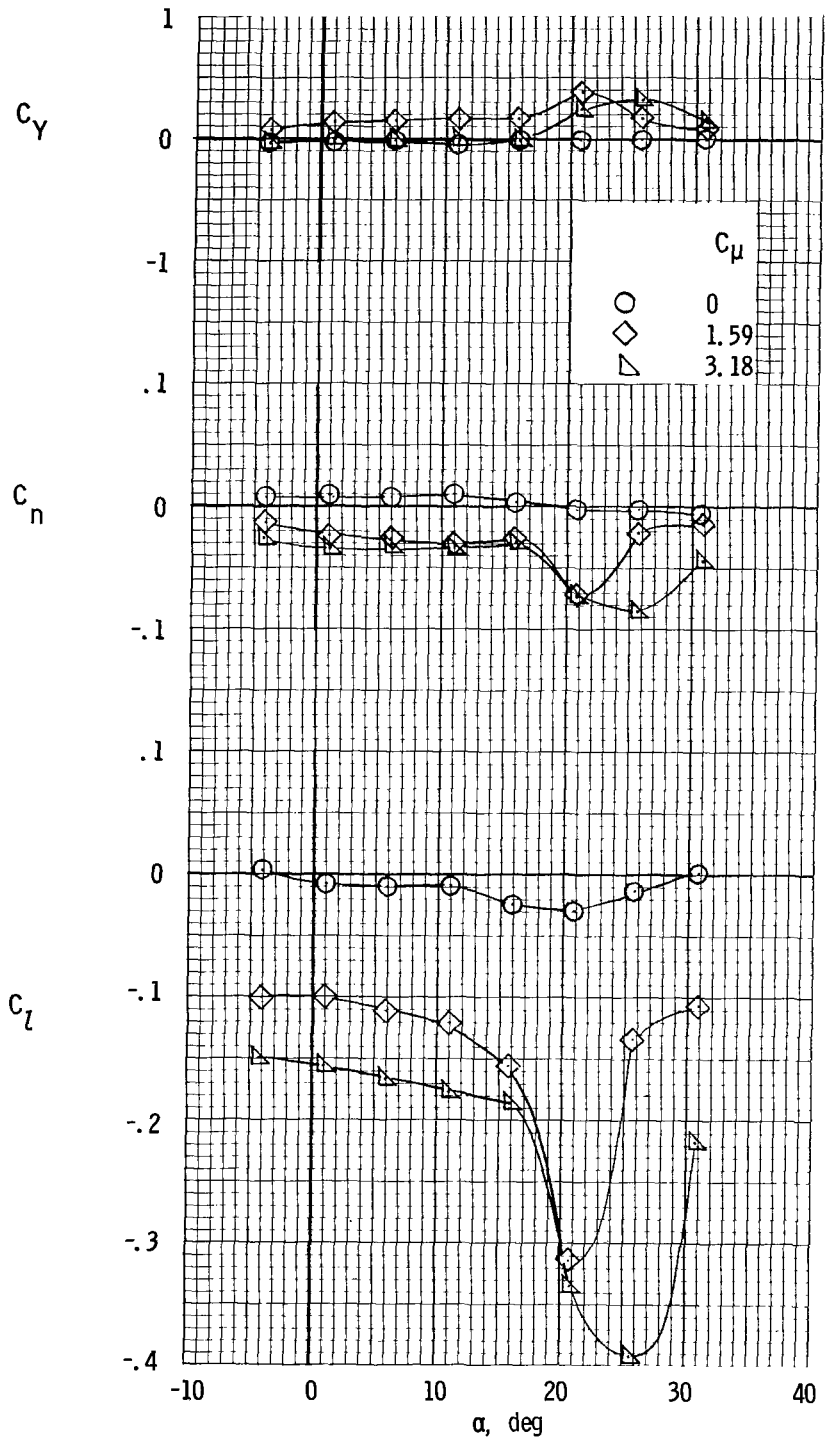

(b) Lateral characteristics, left outboard engine not operating.

Figure 24.- Continued.

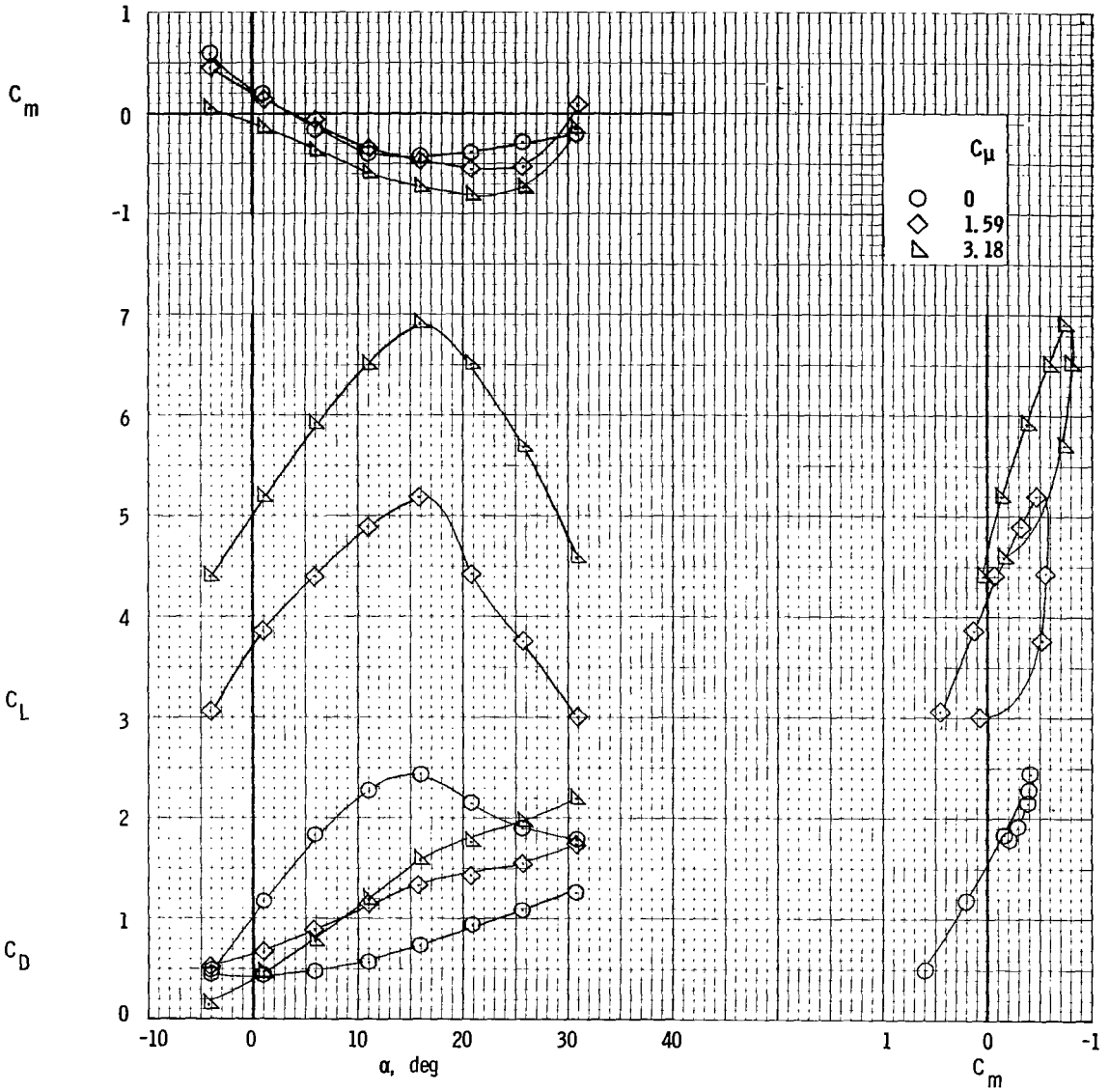

(c) Longitudinal characteristics, left outboard engine not operating.

Figure 24.- Concluded.

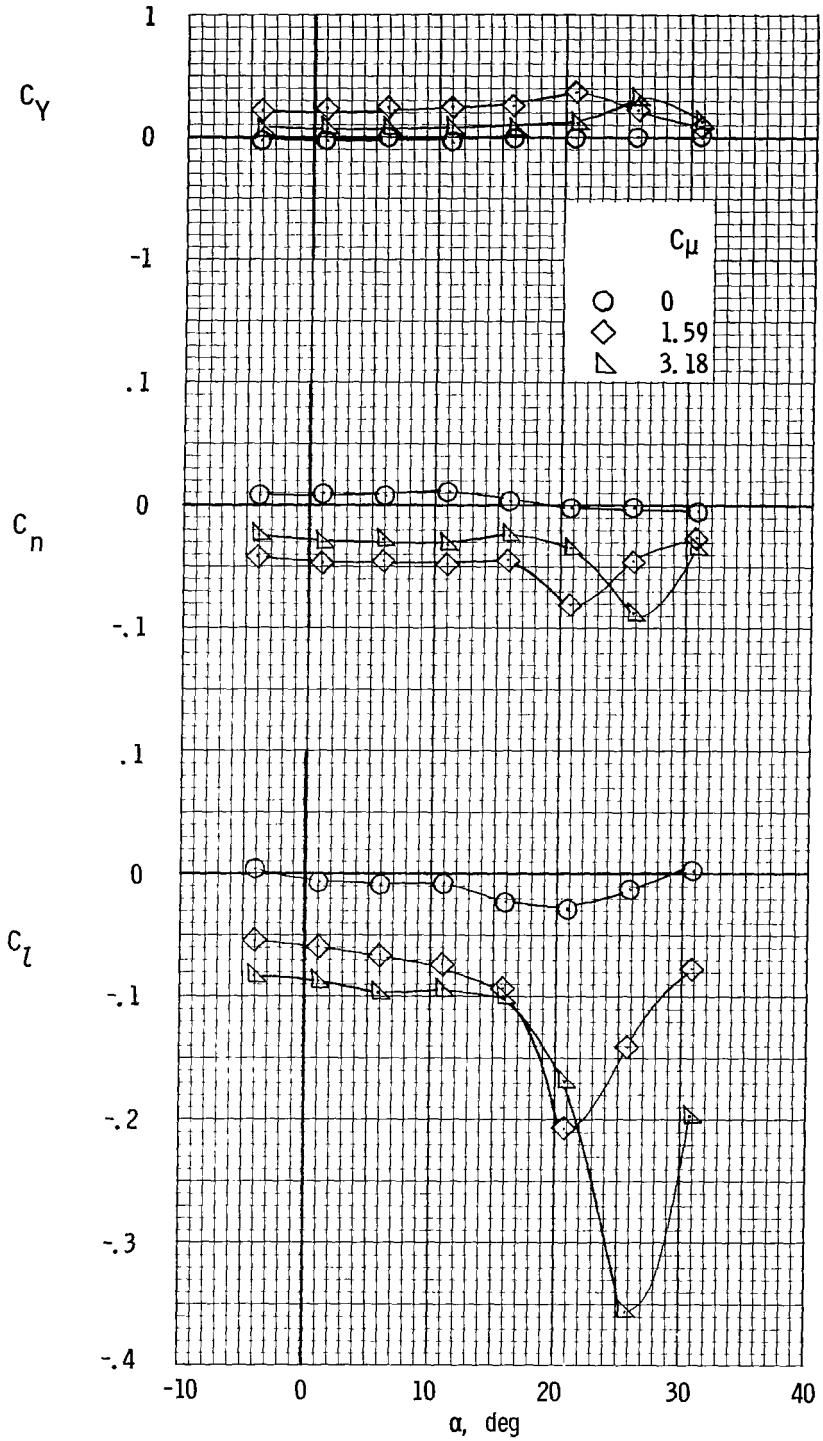

(a) Lateral characteristics.

Figure 25.- Lateral and longitudinal characteristics, left inboard engine not operating. $\delta_{f1}/\delta_{f2} = 30^o/60^o$; $\delta_e = -50^o$; $i_t = 0^o$; $\delta_a = 60^o$; $C_{\mu,a} = 0$.

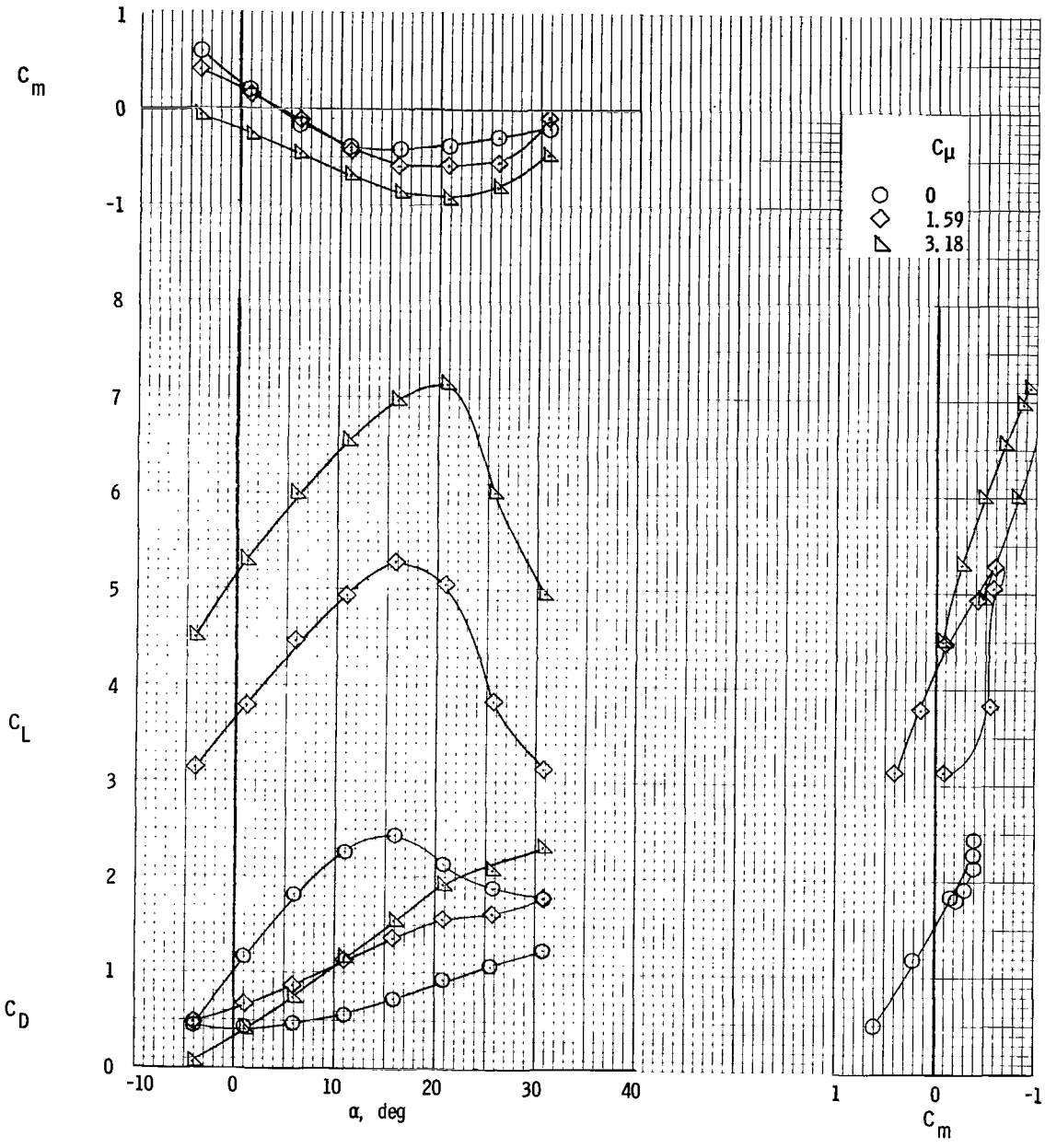

(b) Longitudinal characteristics.

Figure 25.- Concluded.

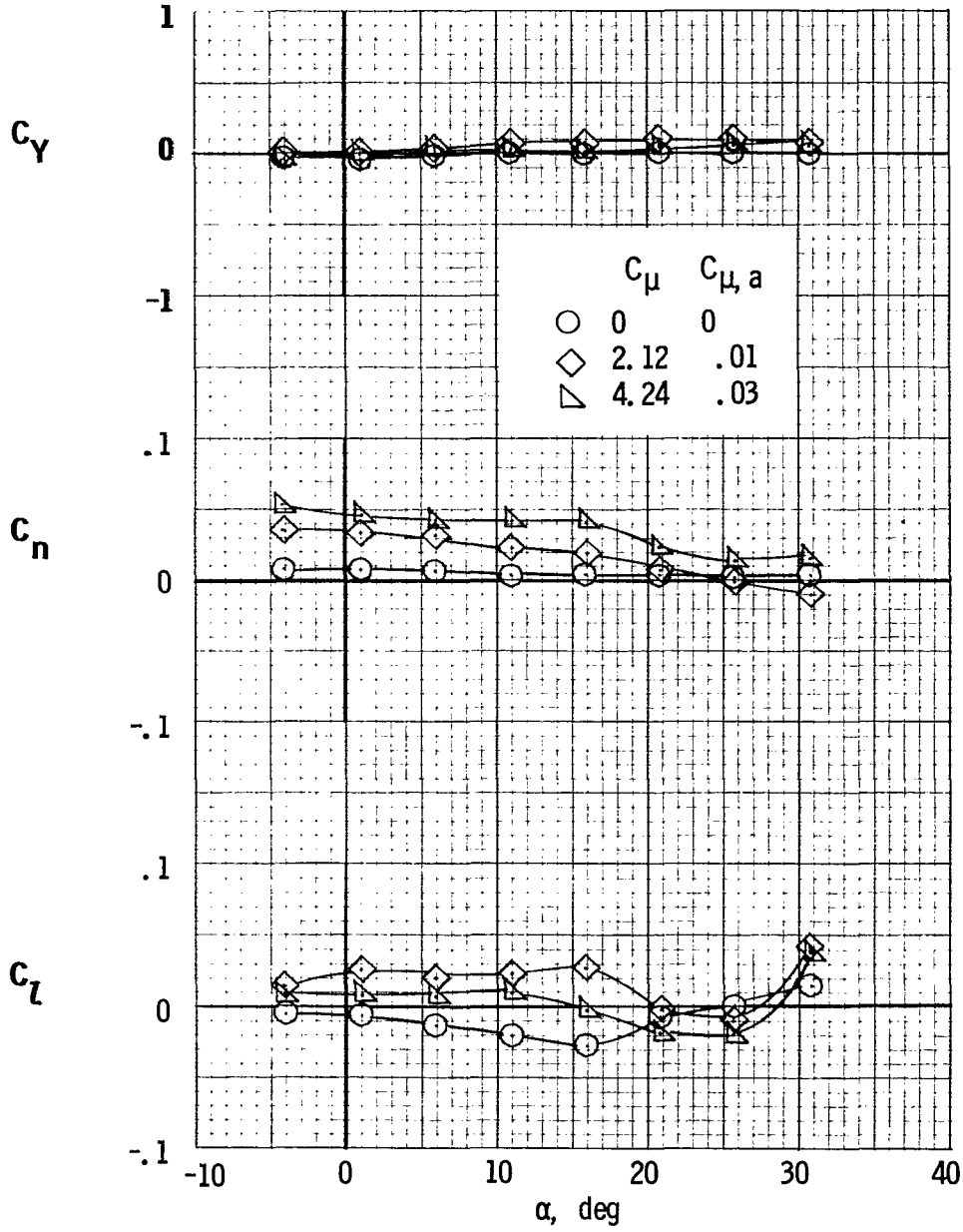

(a) Lateral characteristics, all engines operating.

Figure 26.- Lateral and longitudinal characteristics, left outboard engine not operating. $\delta_{f1}/\delta_{f2} = 25^o/50^o$; $i_t = 0^o$; $\delta_e = -50^o$; $\delta_a = 50^o$.

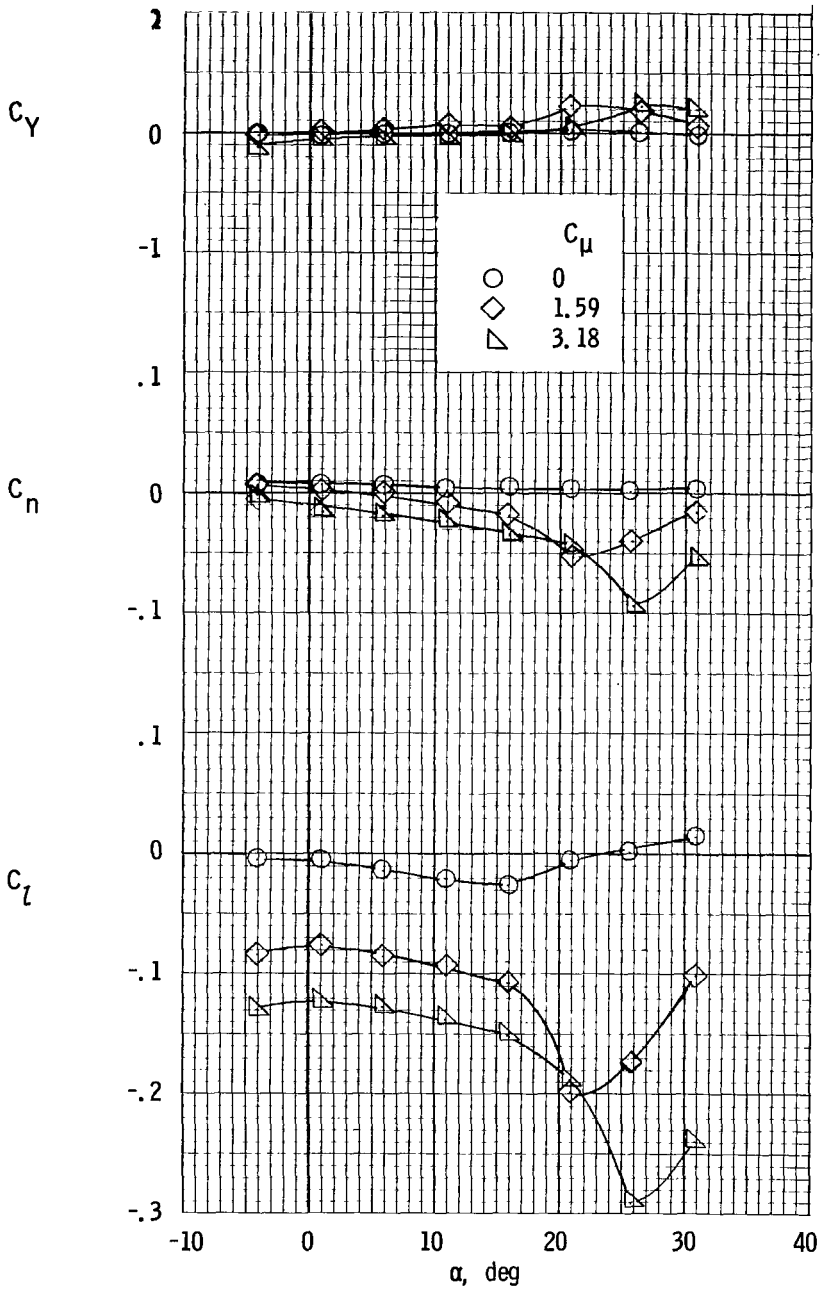

(b) Lateral characteristics, left outboard engine not operating. $C_{\mu,a} = 0$.

Figure 26.- Continued.

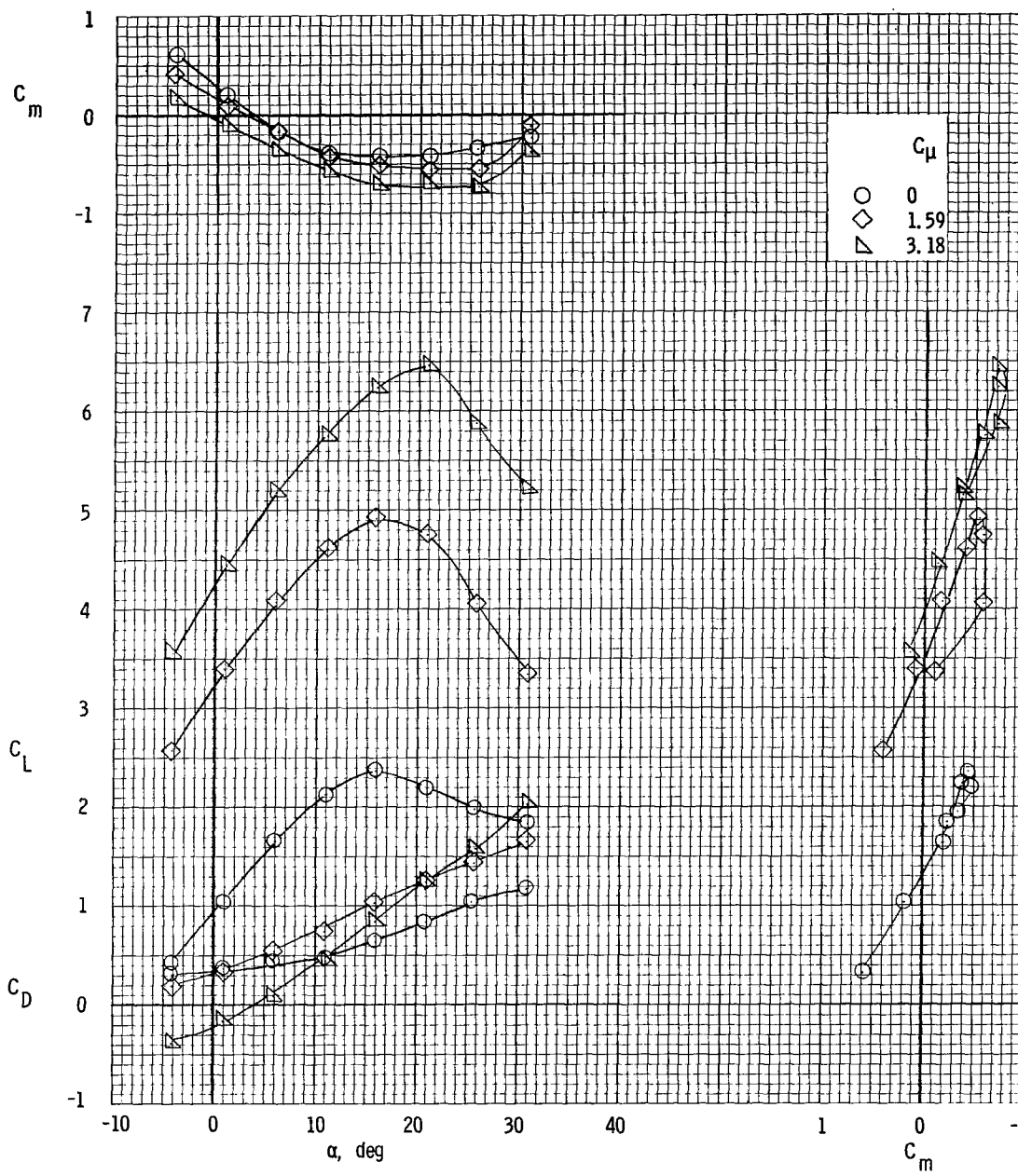

(c) Longitudinal characteristics. $C_{\mu,a} = 0$.

Figure 26.- Concluded.

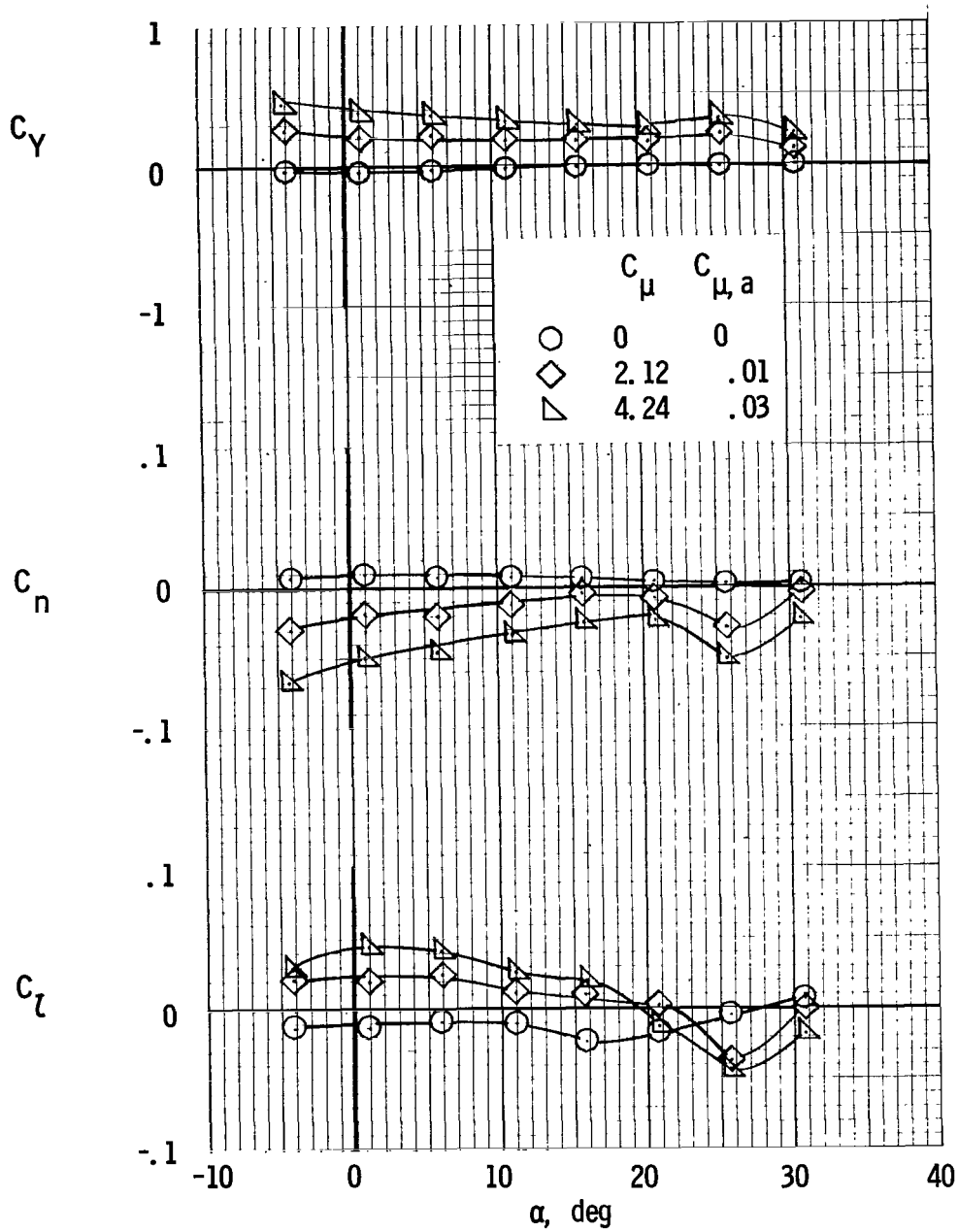

(a) Lateral characteristics, all engines operating.

Figure 27.- Lateral and longitudinal characteristics, left outboard engine not operating. $\delta_{f1}/\delta_{f2} = 20^o/40^o$; $i_t = 0^o$; $\delta_e = -50^o$; $\delta_a = 40^o$.

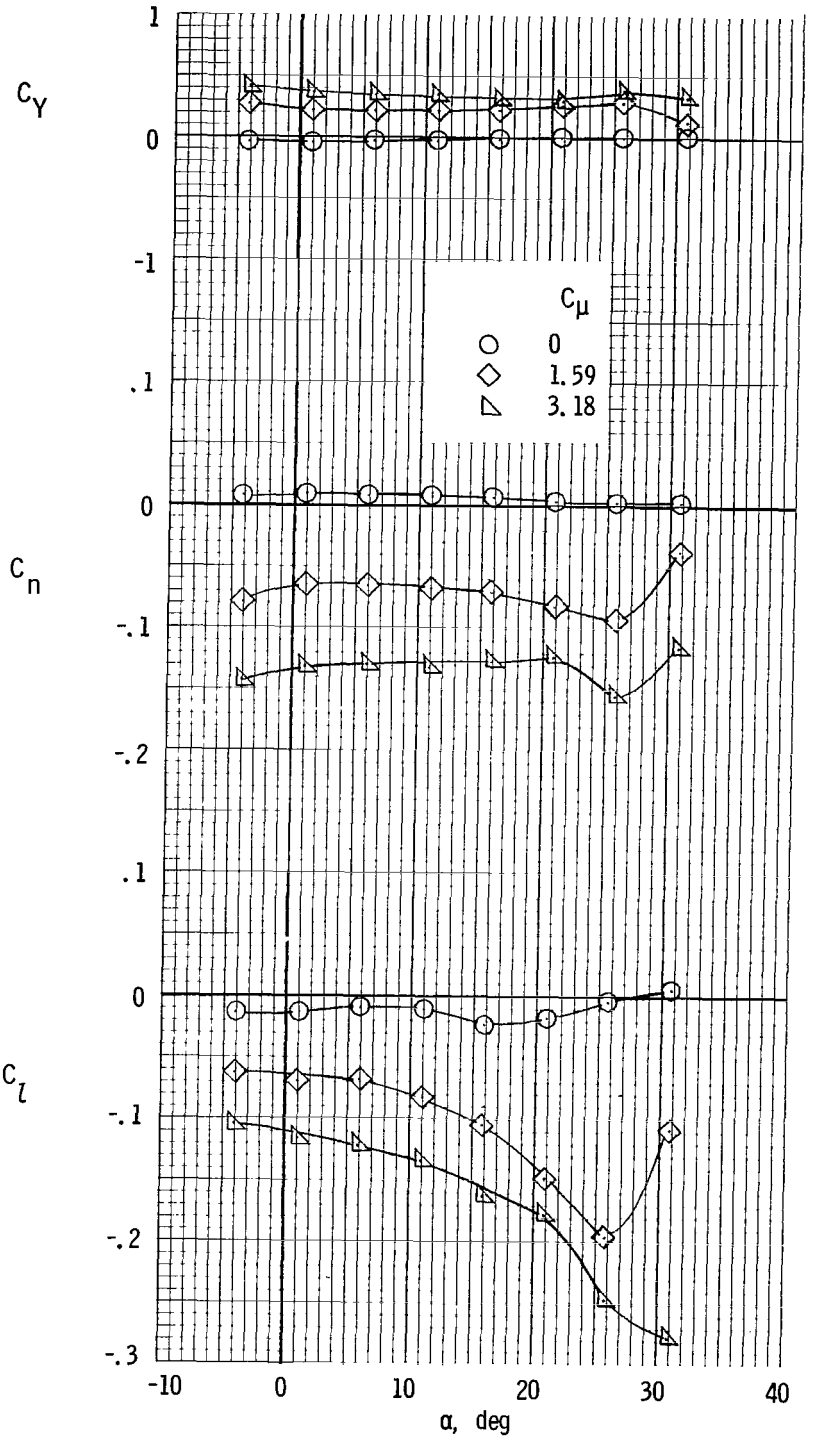

(b) Lateral characteristics, left outboard engine not operating. $C_{\mu,a} = 0$.

Figure 27.- Continued.

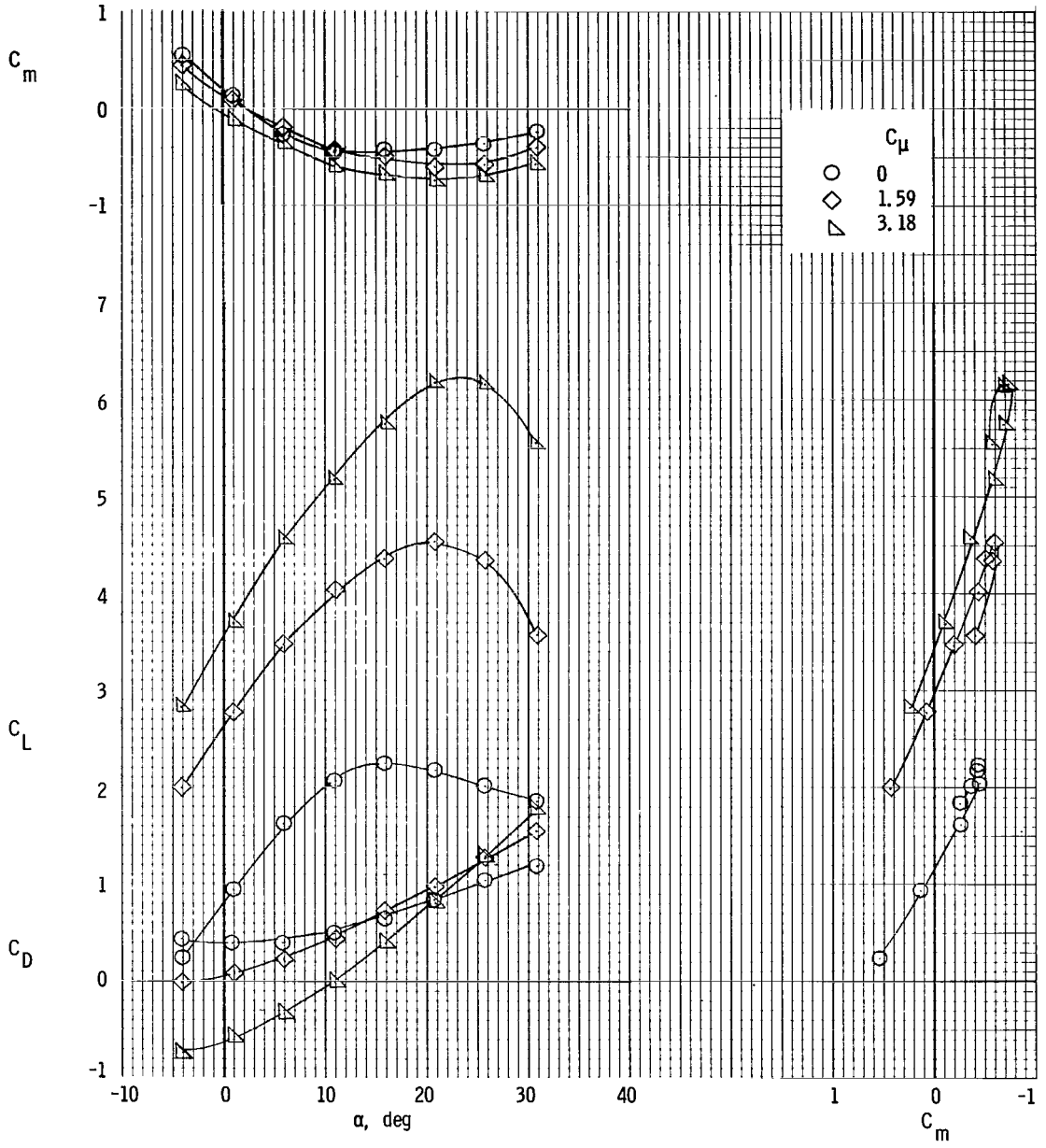

(c) Longitudinal characteristics, left outboard engine not operating. $C_{\mu,a} = 0$.

Figure 27.- Concluded.

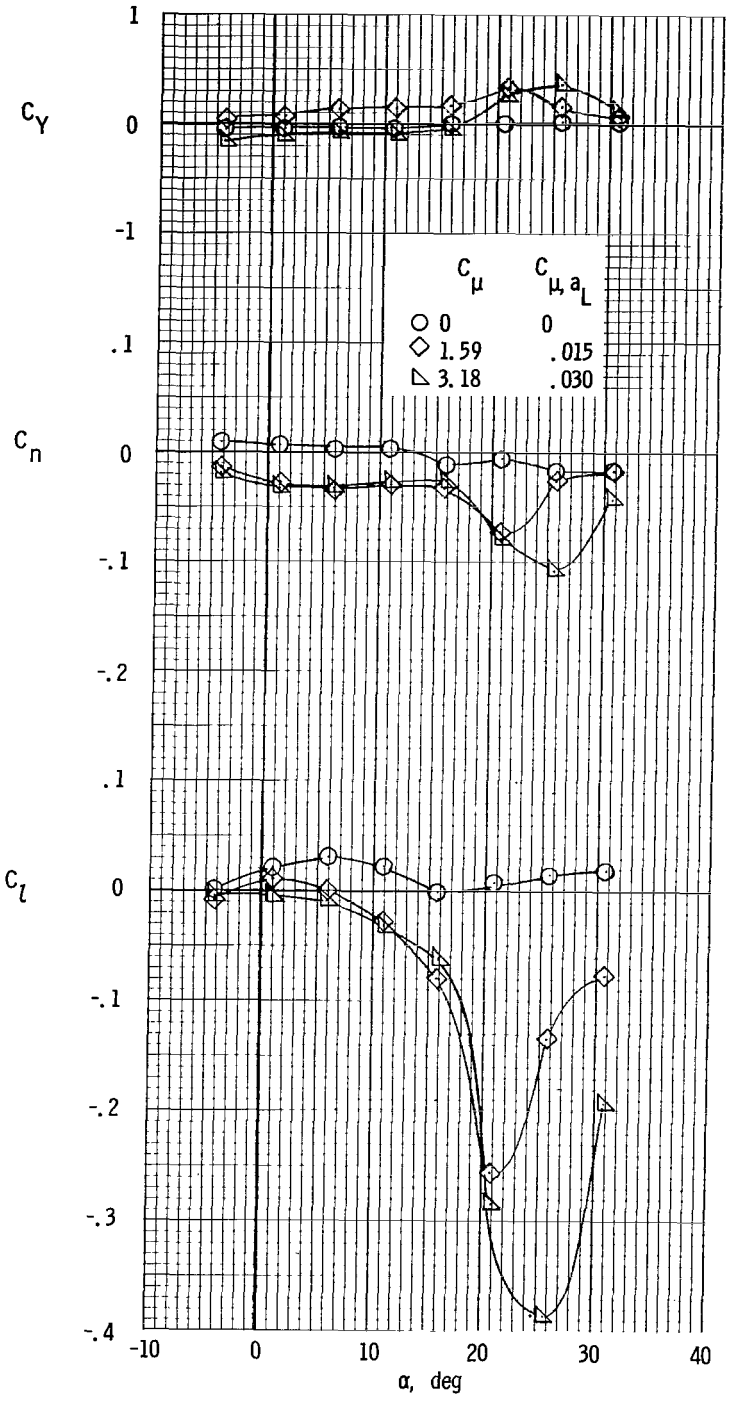

(a) Lateral characteristics.

Figure 28.- Lateral and longitudinal characteristics, left outboard engine not operating. Asymmetric aileron blowing; $\delta_{f1}/\delta_{f2} = 30^o/60^o$; $i_t = 0^o$; $\delta_e = -50^o$; $\delta a_L = 60^o$; $\delta a_R = 0^o$; $C_{\mu,a_R} = 0$.

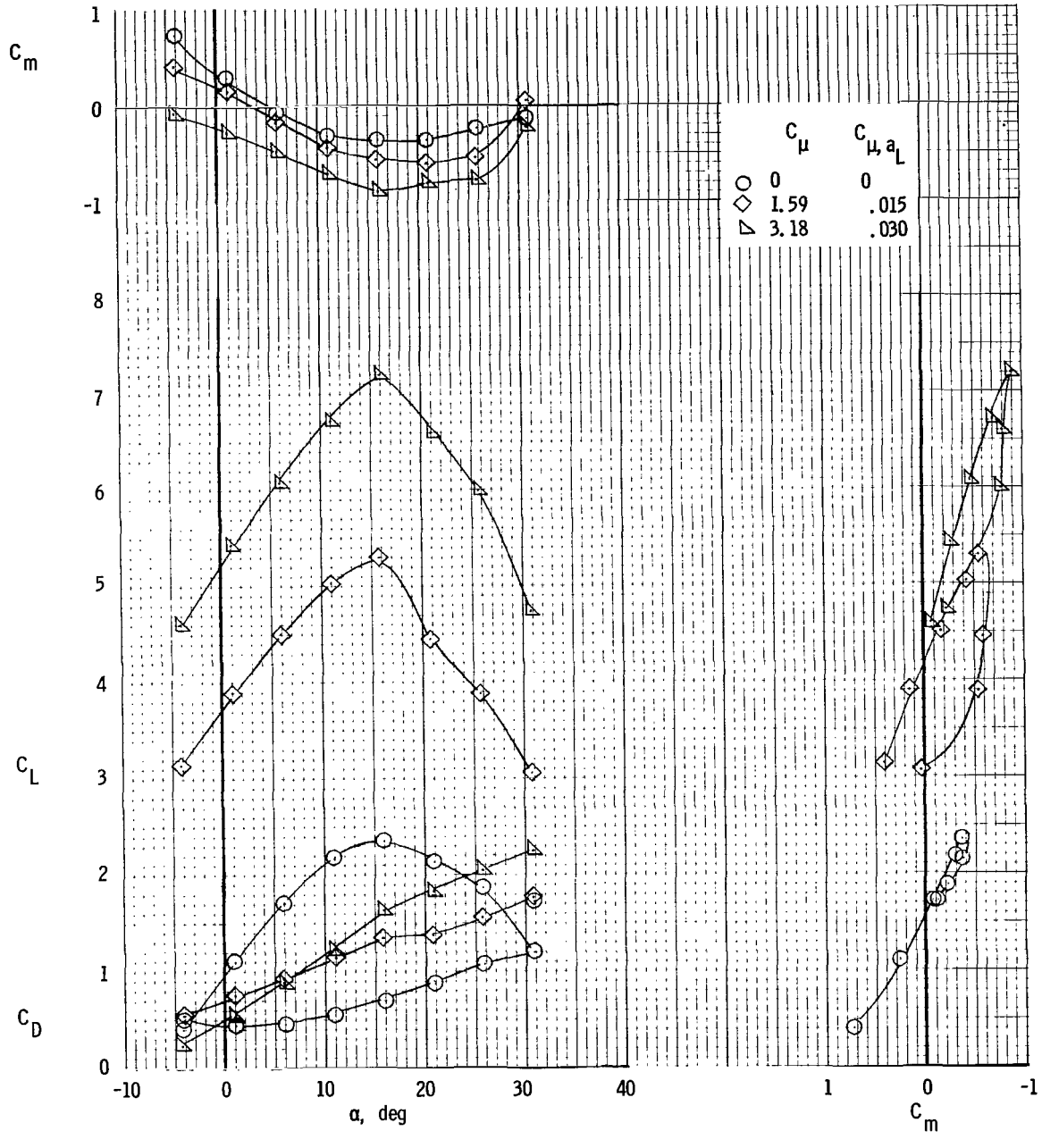

(b) Longitudinal characteristics.

Figure 28.- Concluded.

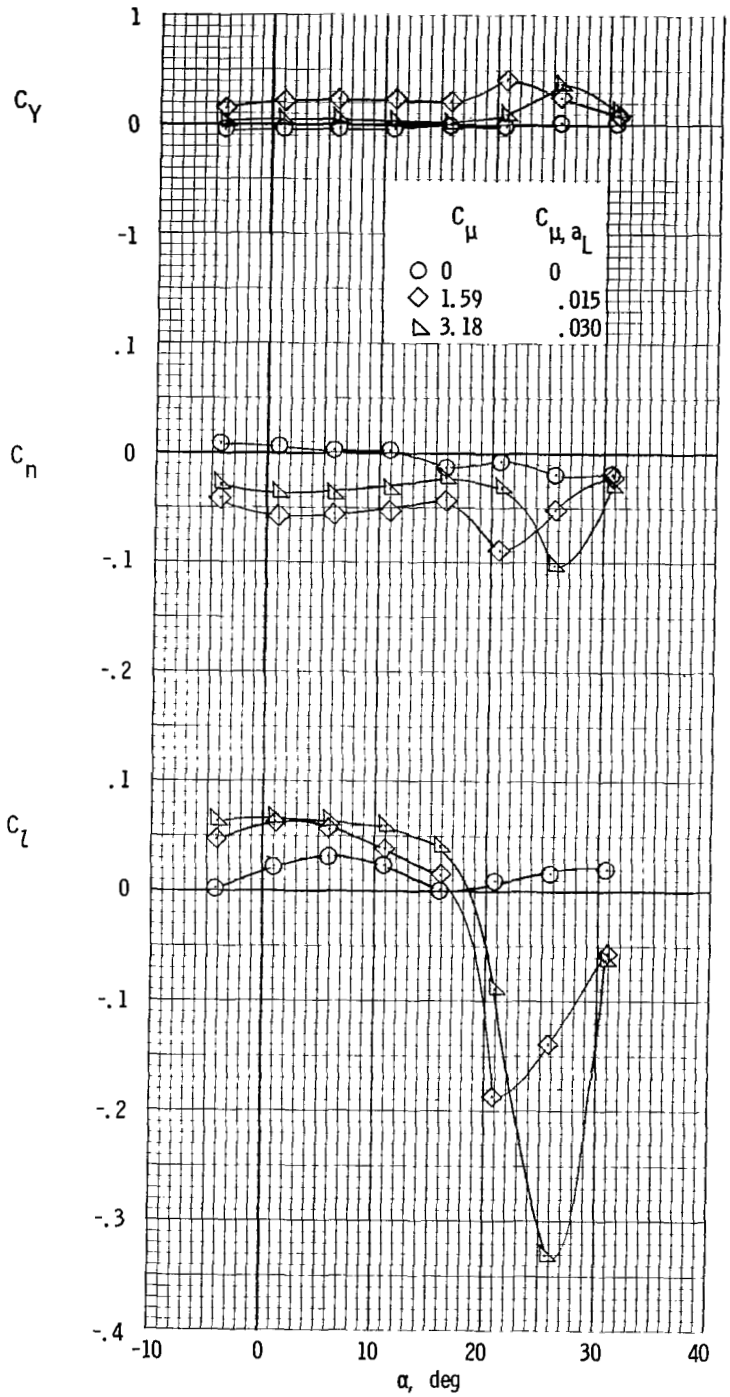

(a) Lateral characteristics.

Figure 29.- Longitudinal and lateral characteristics, left inboard engine not operating. Asymmetric aileron blowing; $\delta_{f1}/\delta_{f2} = 30^o/60^o$; $i_t = 0^o$; $\delta_e = -50^o$; $\delta_{a_L} = 60^o$; $\delta_{a_R} = 0^o$; $C_{\mu,a_R} = 0$.

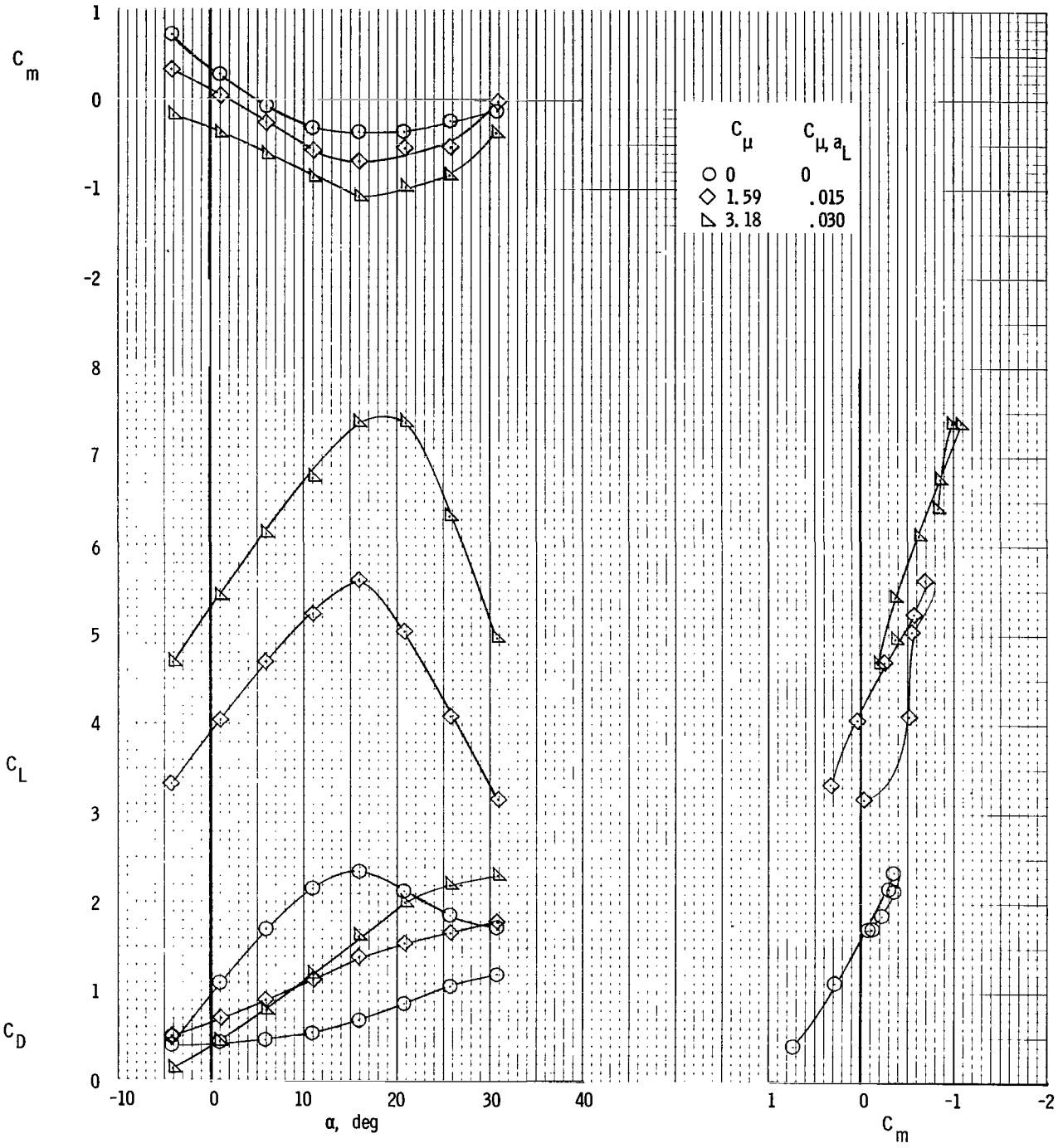

(b) Longitudinal characteristics.

Figure 29.- Concluded.

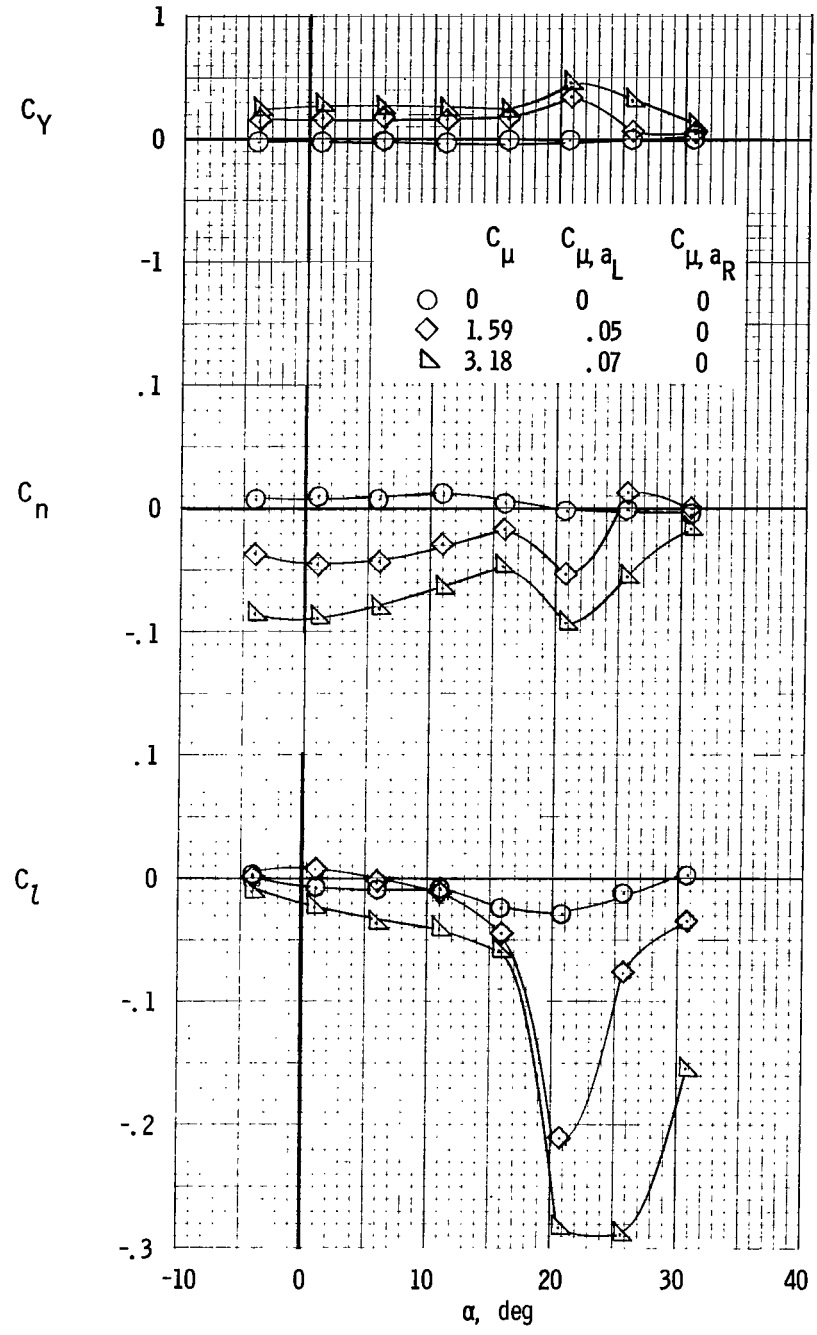

(a) Lateral characteristics.

Figure 30.- Lateral and longitudinal characteristics, left outboard engine not operating. Asymmetric aileron blowing; $\delta_{f1}/\delta_{f2} = 30^o/60^o$; $i_t = 0^o$; $\delta_e = -50^o$; $\delta_{a_L} = 60^o$; $\delta_{a_R} = 60^o$.

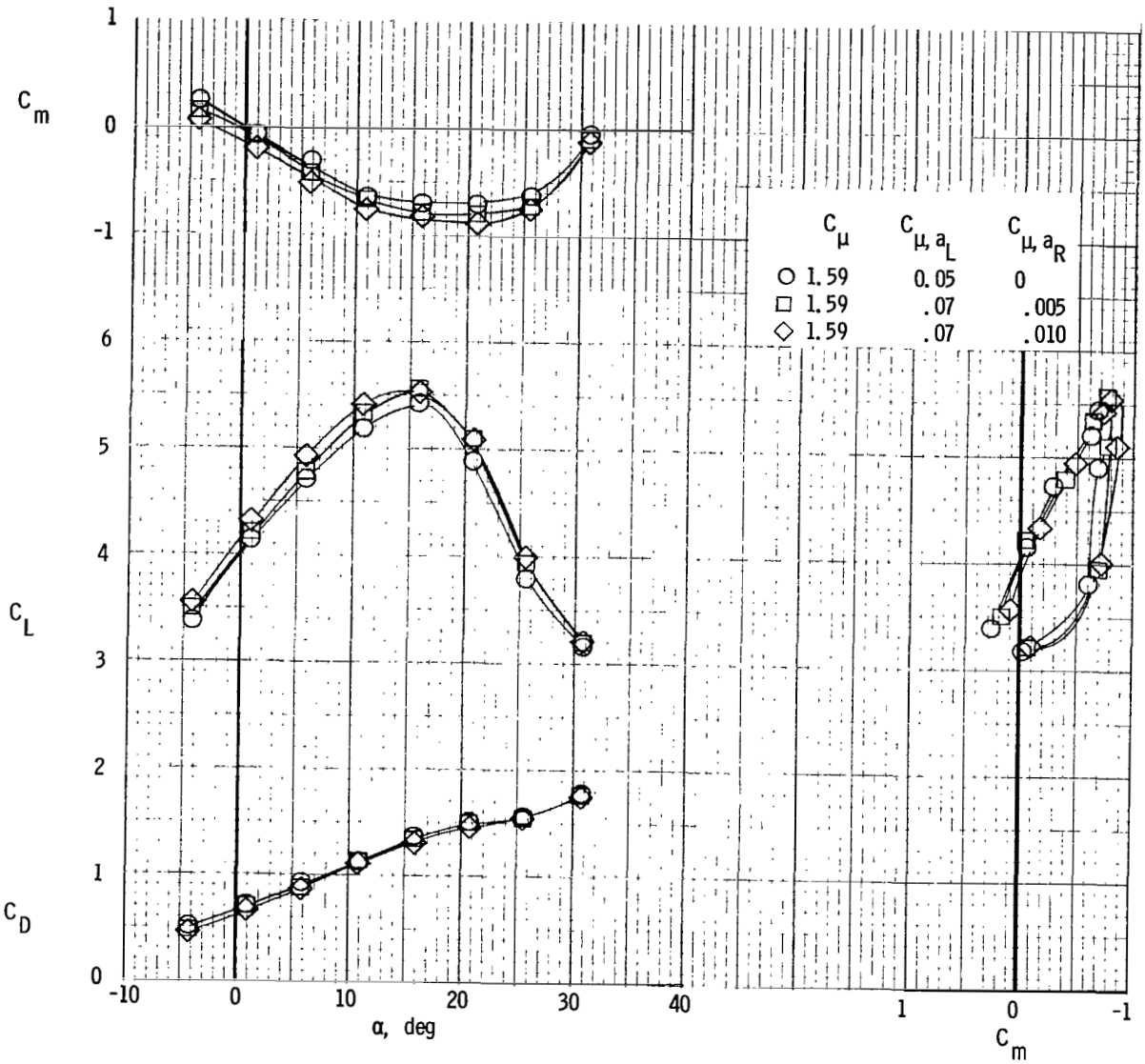

(b) Longitudinal characteristics.

Figure 30.- Continued.

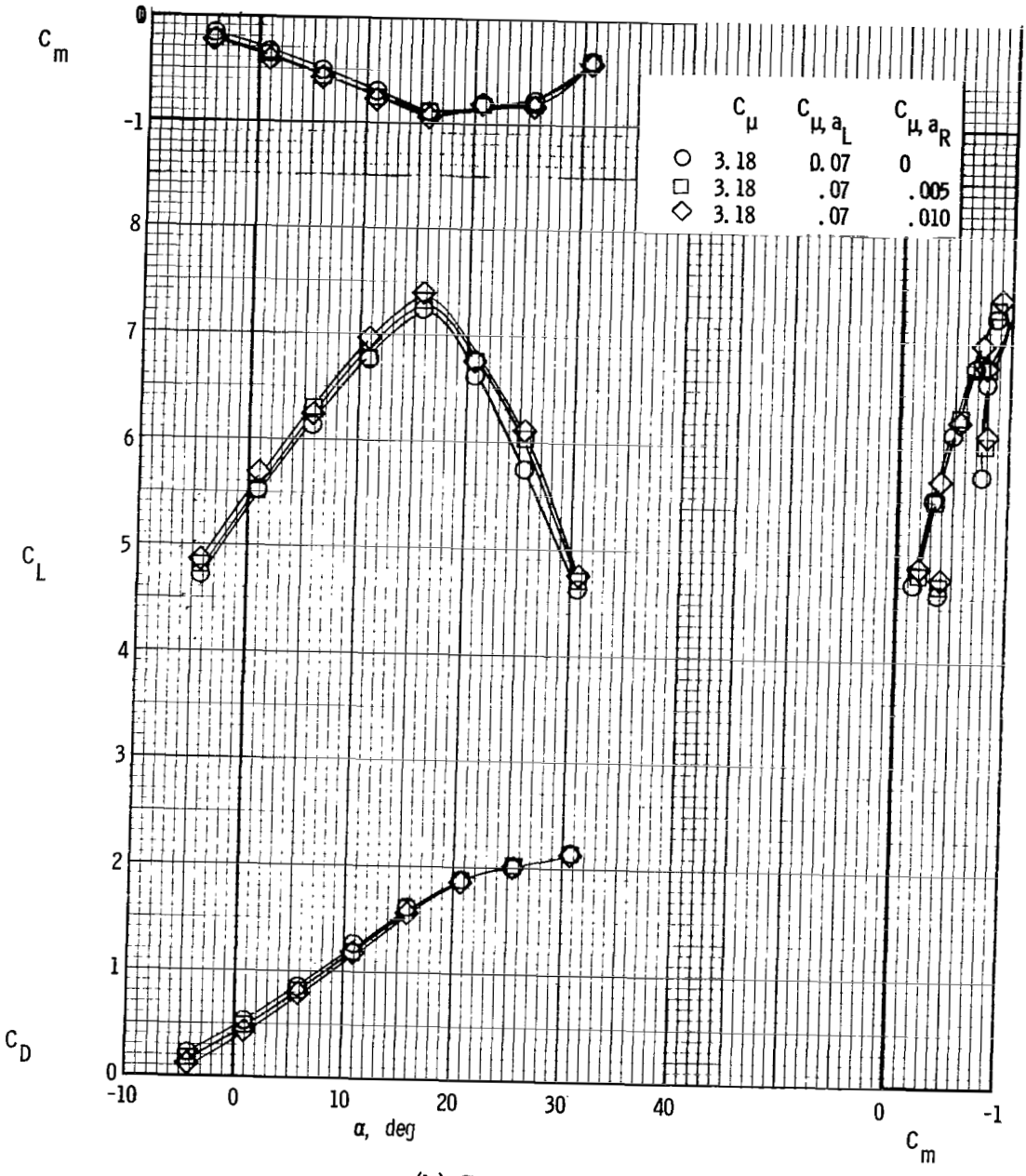

(b) Concluded.

Figure 30.- Concluded.

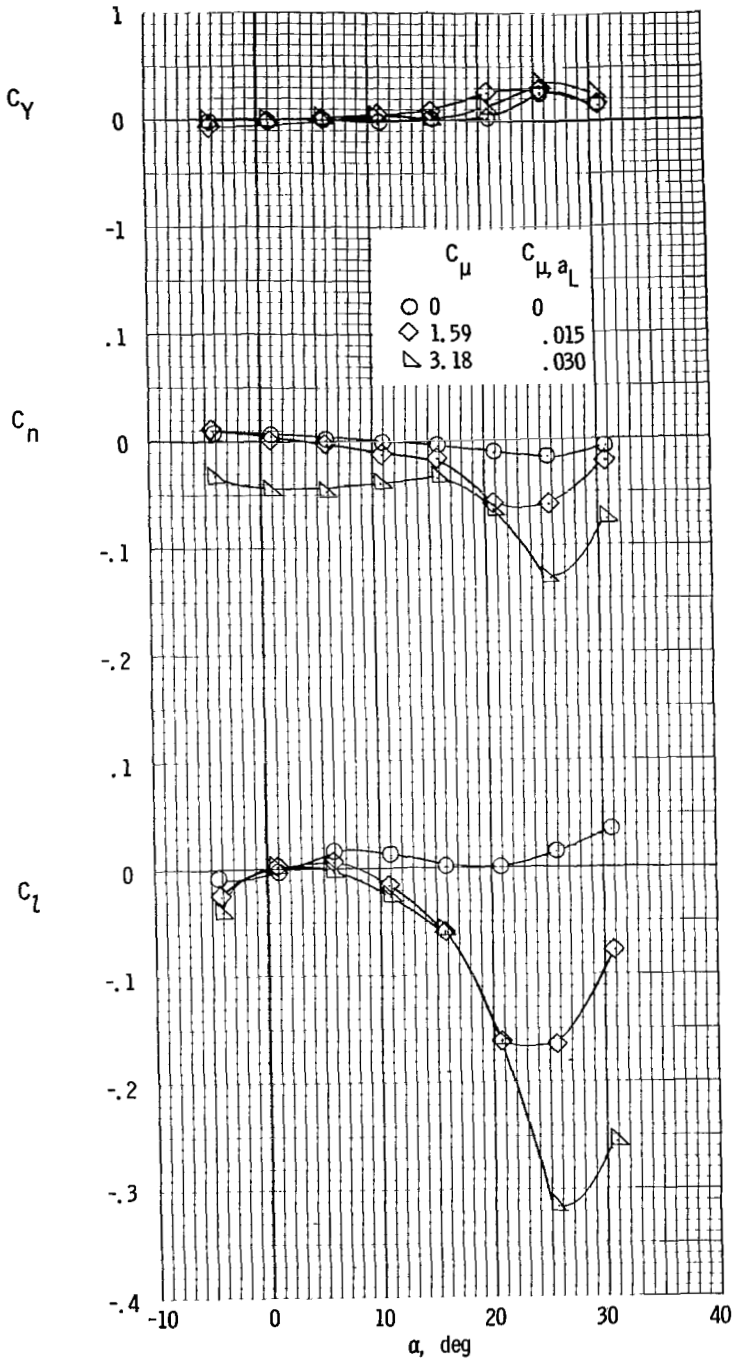

(a) Lateral characteristics.

Figure 31.- Lateral and longitudinal characteristics, left outboard engine not operating. Asymmetric aileron blowing; $\delta_{f1}/\delta_{f2} = 25^o/50^o$; $i_t = 0^o$; $\delta_e = -50^o$; $\delta_{a_L} = 50^o$; $\delta_{a_R} = 0^o$; $C_{\mu,a_R} = 0$.

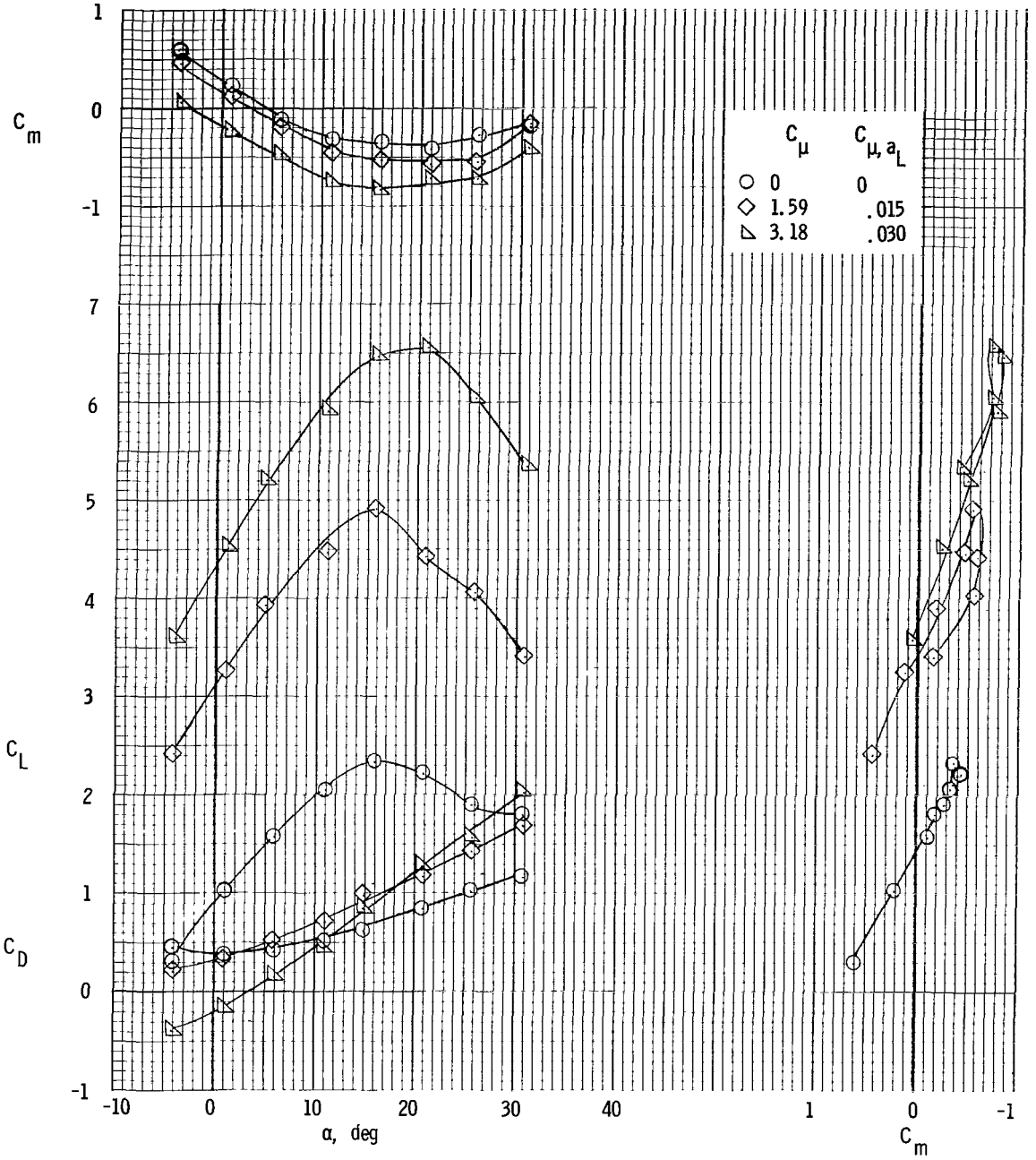

(b) Longitudinal characteristics.

Figure 31.- Concluded.

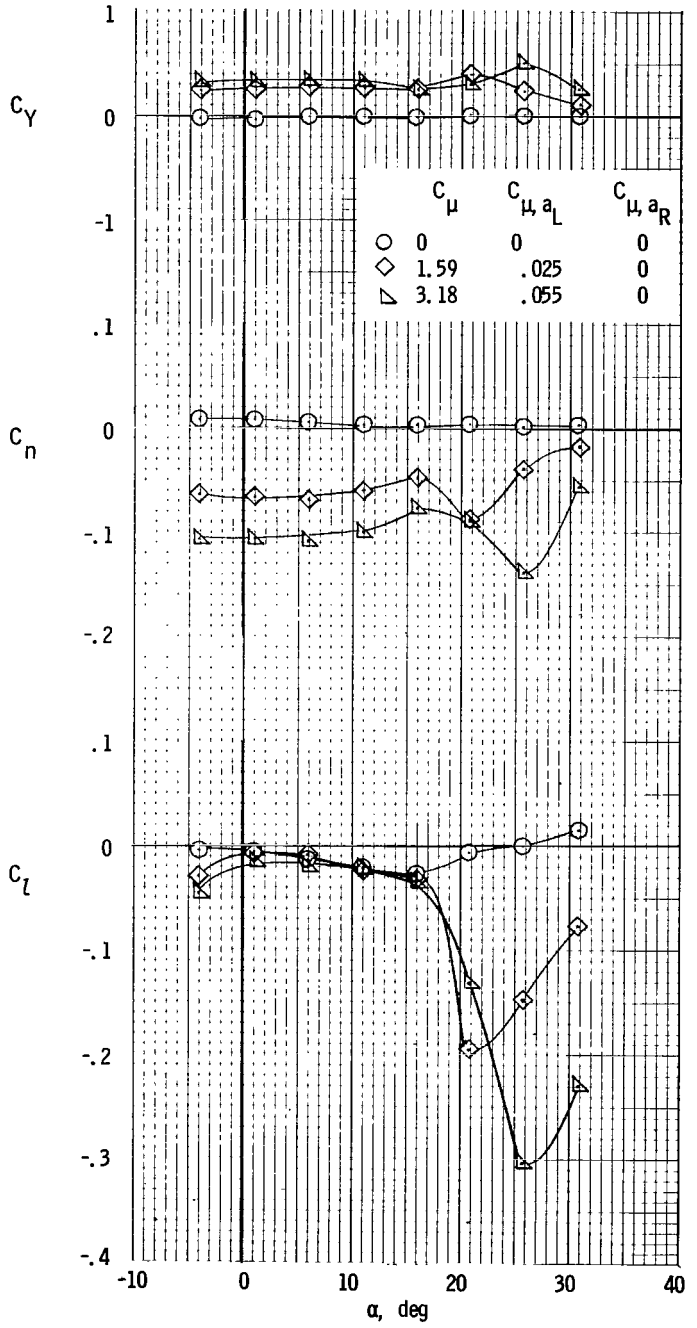

(a) Lateral characteristics.

Figure 32.- Lateral and longitudinal characteristics, left outboard engine not operating. Asymmetric aileron blowing; $\delta_{f1}/\delta_{f2} = 25^o/50^o$; $i_t = 0^o$; $\delta_e = -50^o$; $\delta_{a_L} = 50^o$; $\delta_{a_R} = 50^o$.

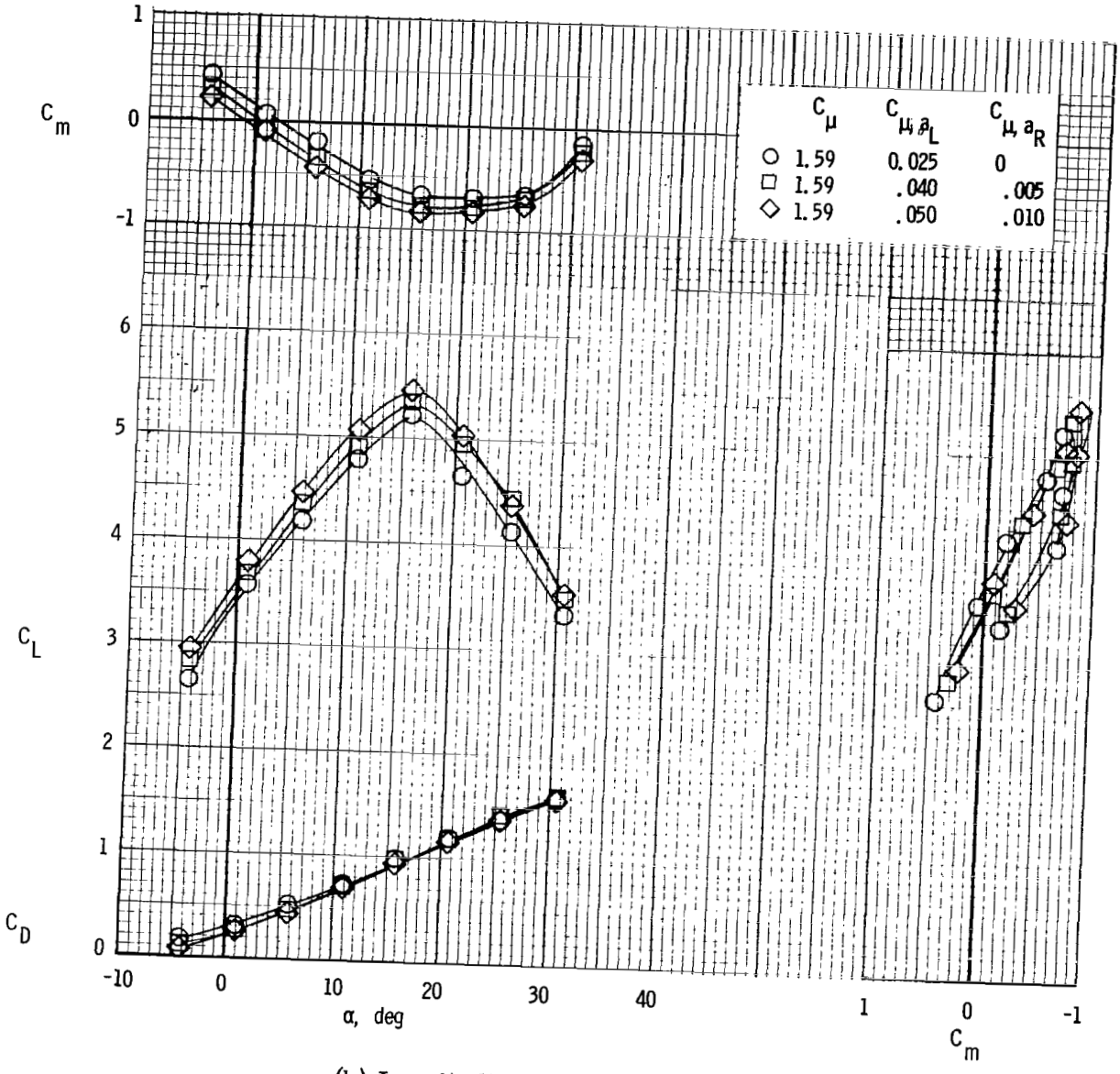

(b) Longitudinal characteristics.

Figure 32.- Continued.

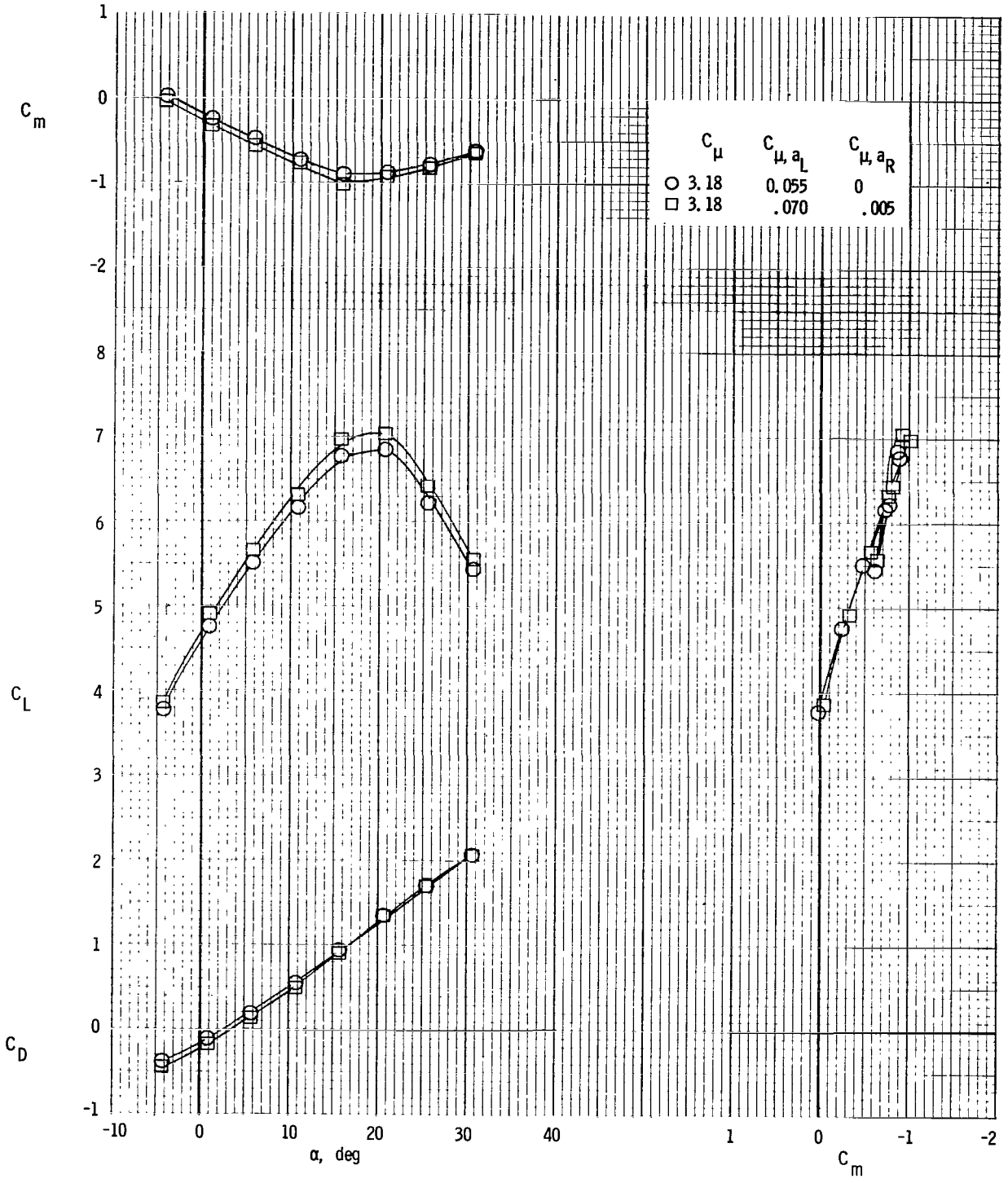

(b) Concluded.

Figure 32.- Concluded.

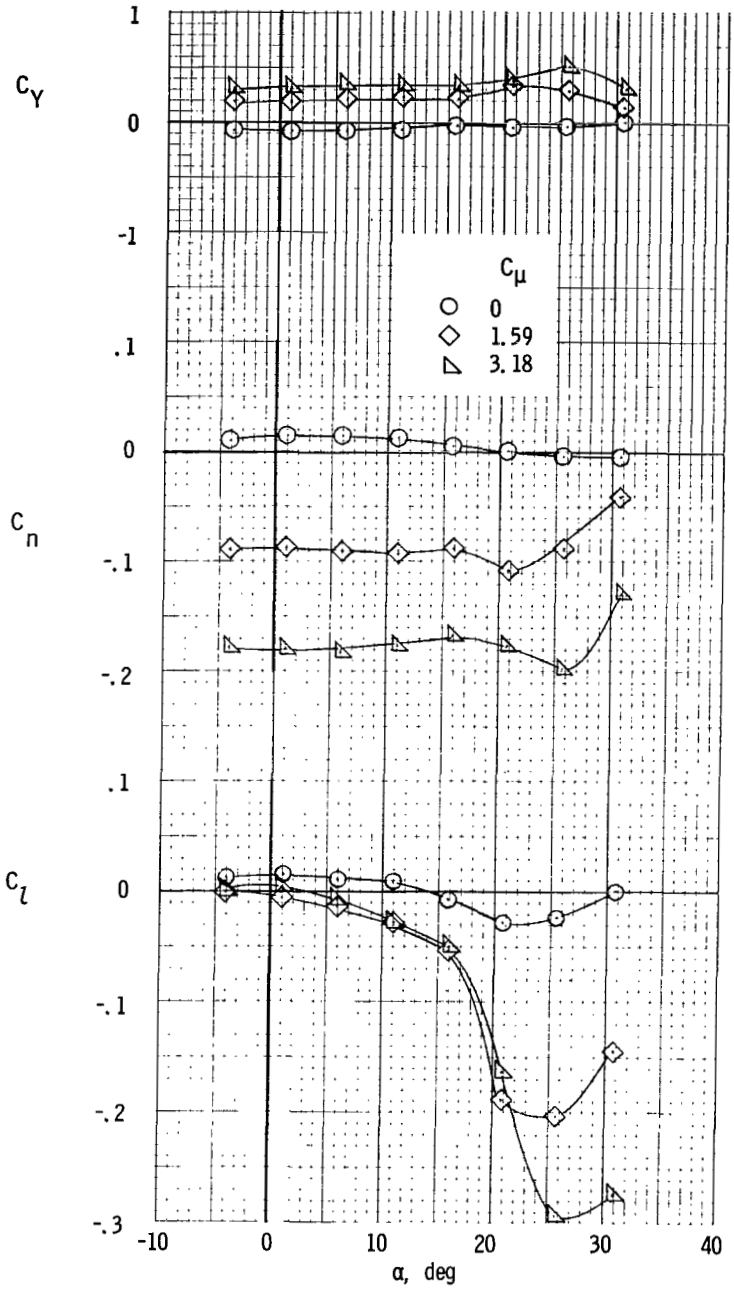

(a) Lateral characteristics.

Figure 33.- Lateral and longitudinal characteristics, left outboard engine not operating. Differential flap deflection; $(\delta_{f1}/\delta_{f2})_L = 30^o/60^o$; $(\delta_{f1}/\delta_{f2})_R = 20^o/40^o$; $i_t = 0^o$; $\delta_e = -50^o$; $\delta a_L = 60^o$; $\delta a_R = 40^o$.

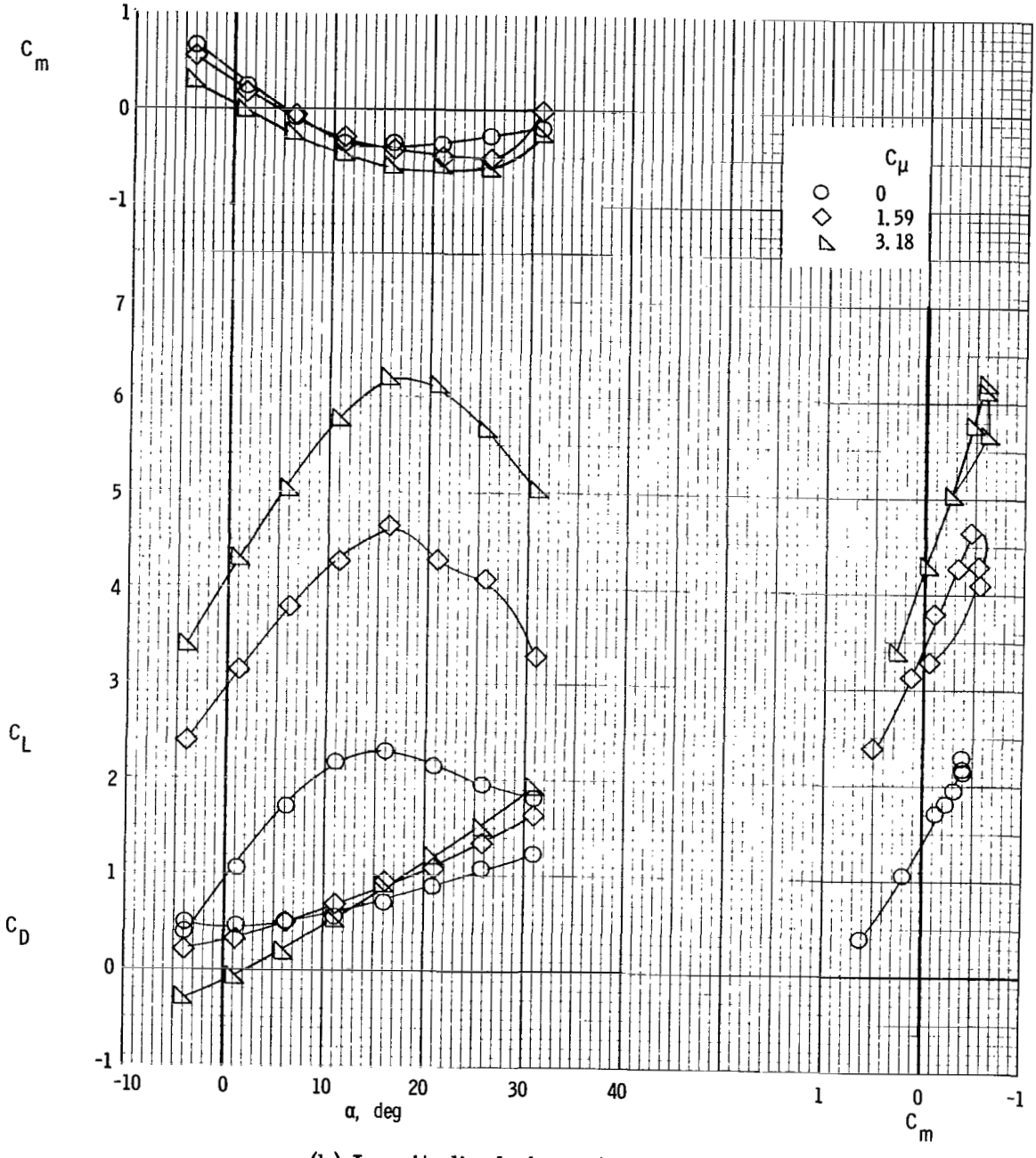

(b) Longitudinal characteristics.

Figure 33.- Continued.

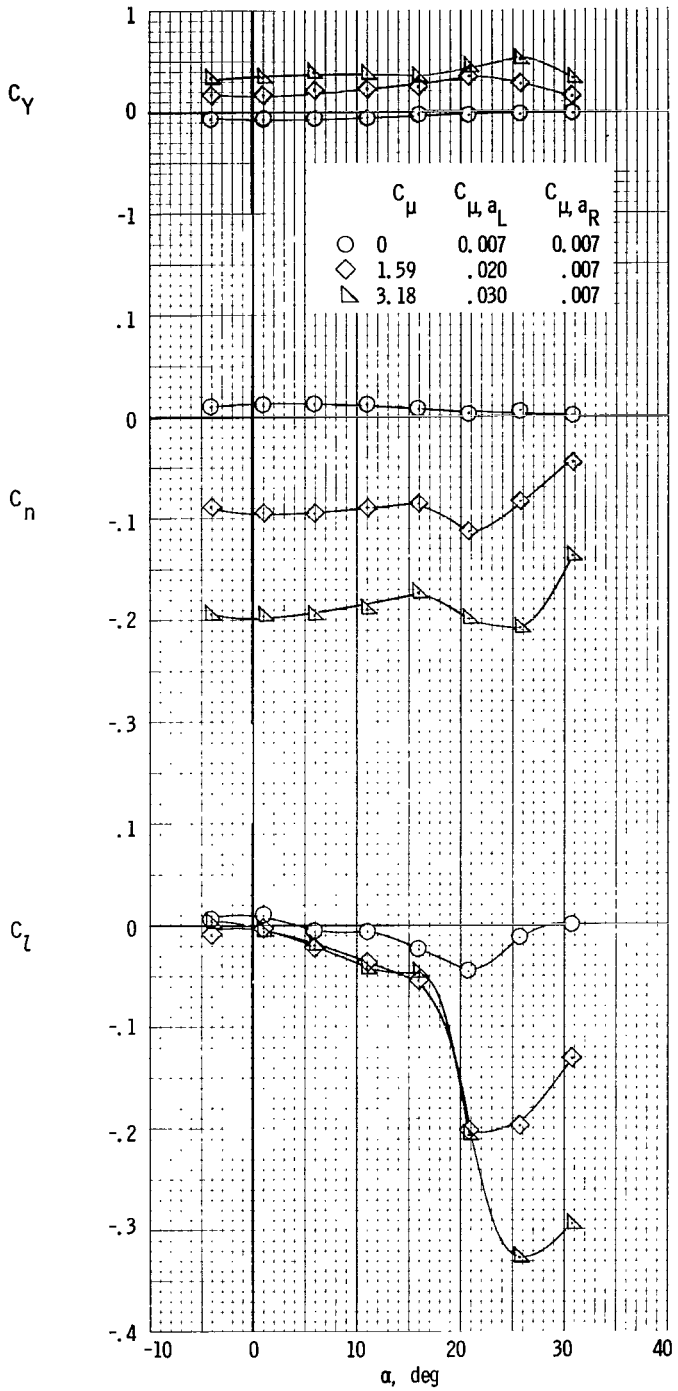

(c) Lateral characteristics, aileron blowing.

Figure 33.- Continued.

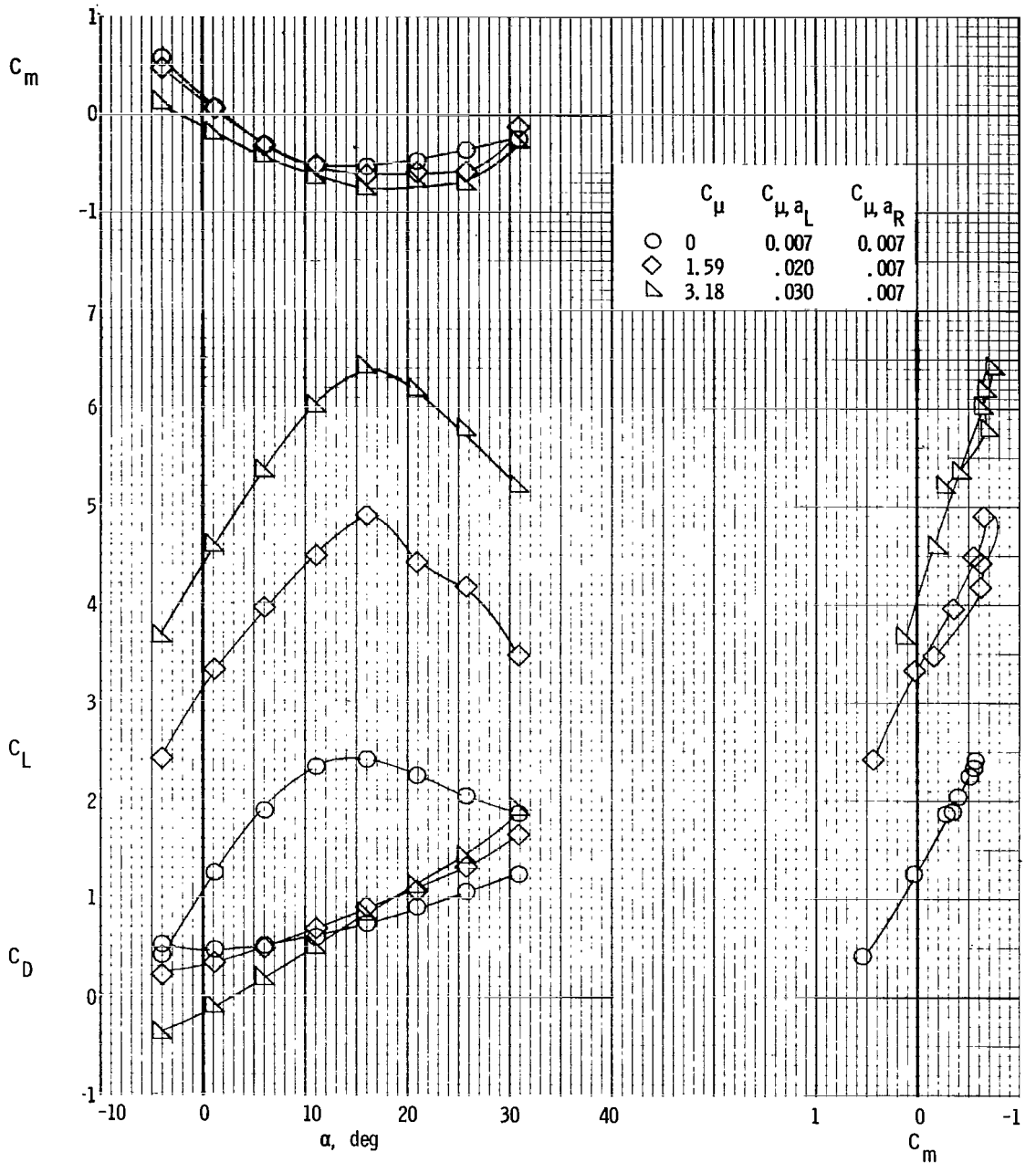

(d) Longitudinal characteristics, aileron blowing.

Figure 33.- Continued.

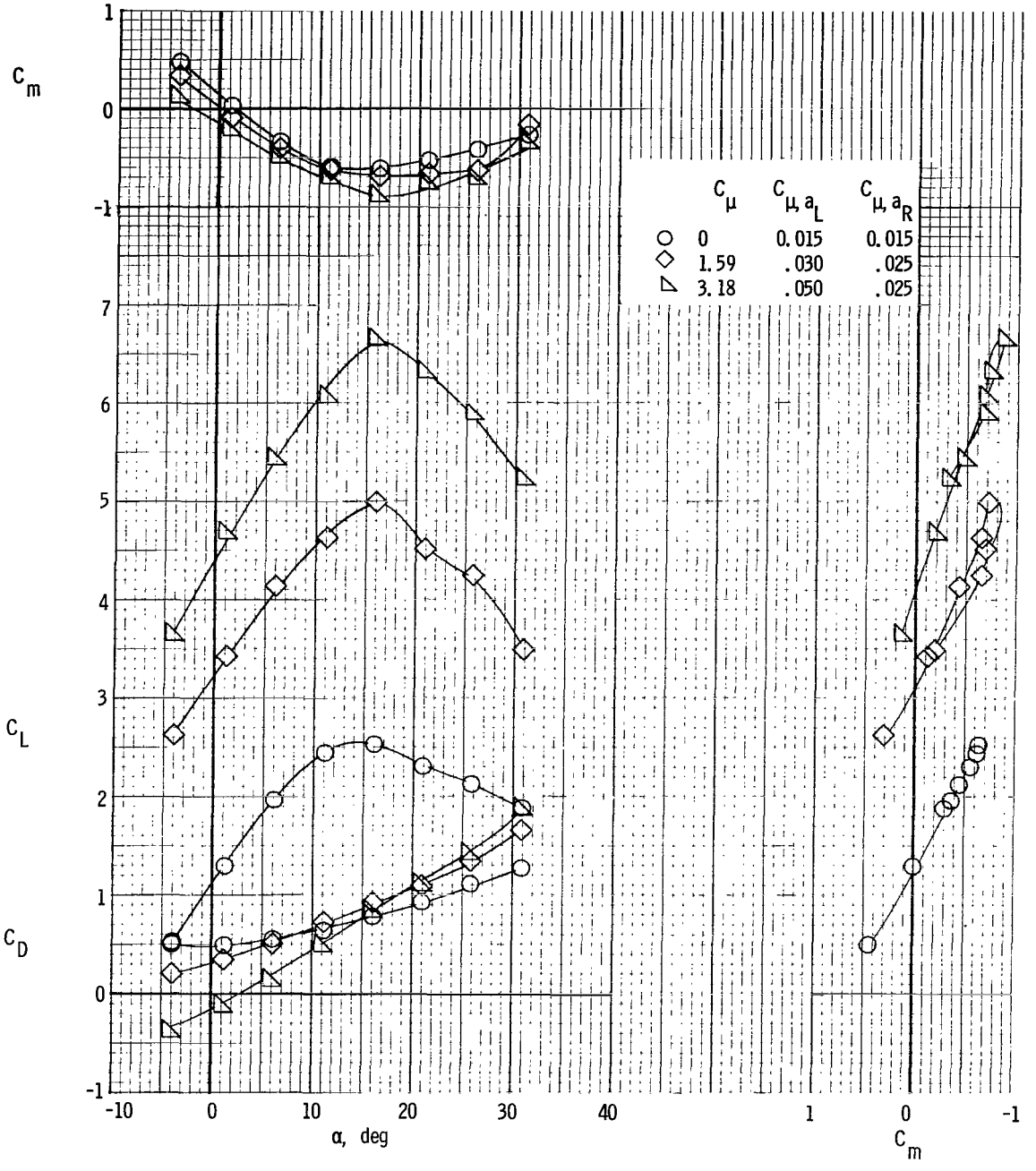

(d) Concluded.

Figure 33.- Concluded.

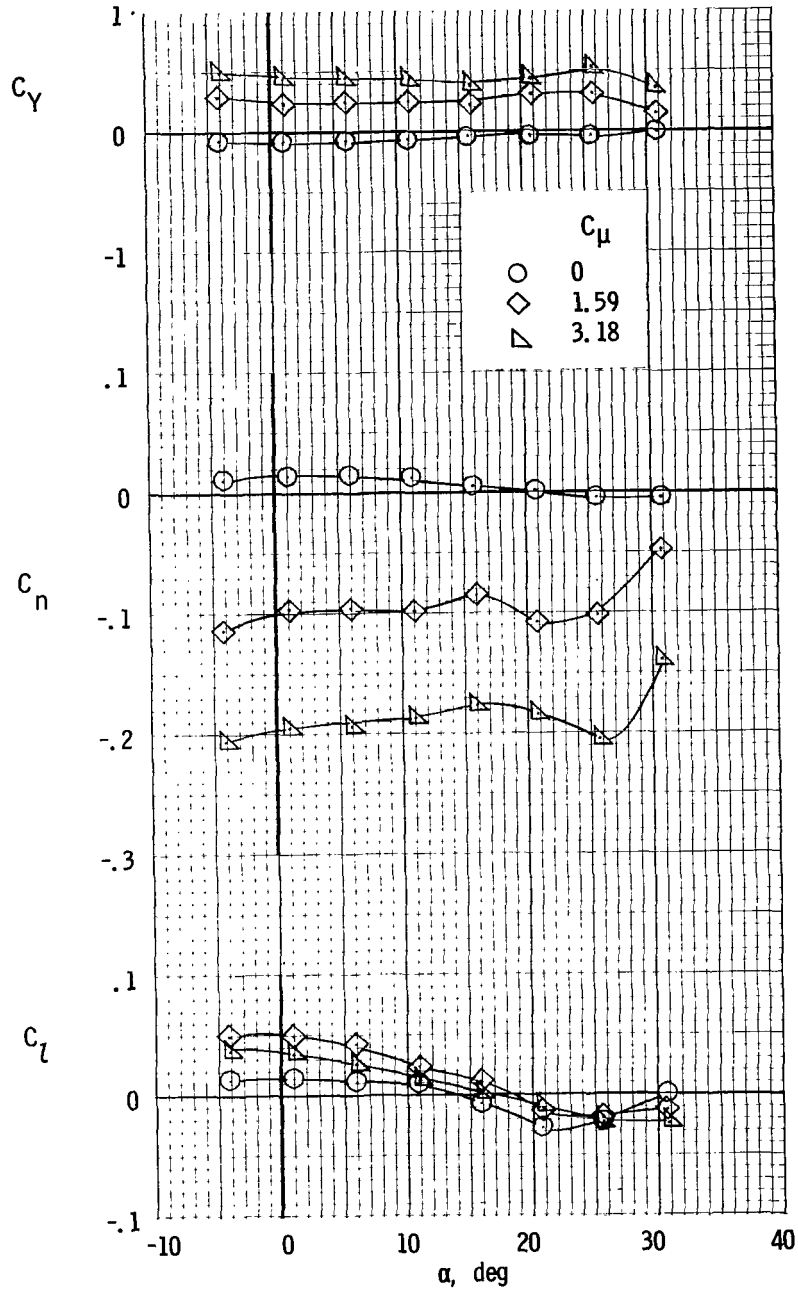

(a) Lateral characteristics.

Figure 34.- Lateral and longitudinal characteristics, left inboard engine not operating. Differential flap settings; $(\delta_{f1}/\delta_{f2})_L = 30^o/60^o$; $(\delta_{f1}/\delta_{f2})_R = 20^o/40^o$; $i_t = -50^o$; $\delta a_L = 60^o$; $\delta a_R = 40^o$.

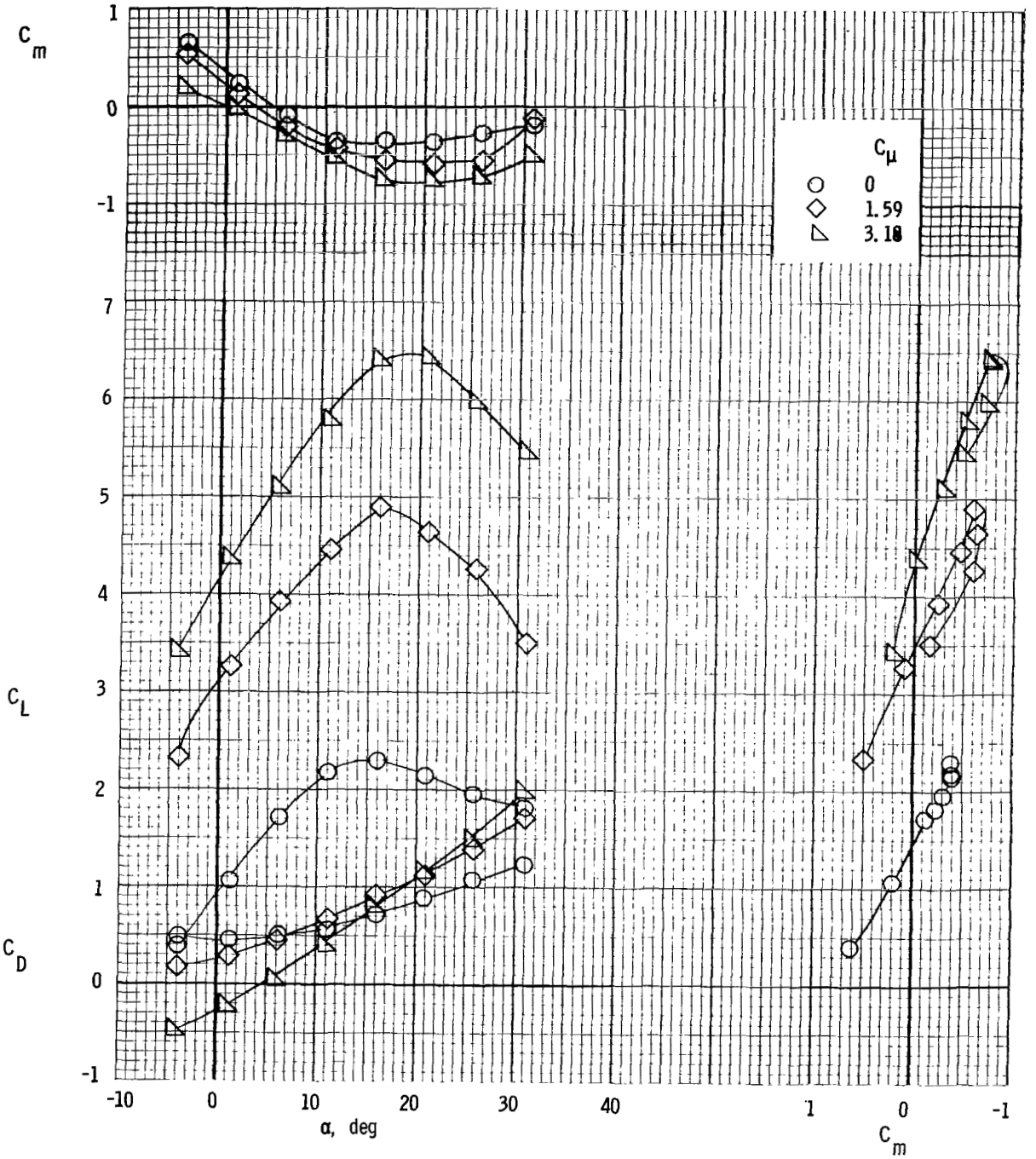

(b) Longitudinal characteristics.

Figure 34.- Concluded.

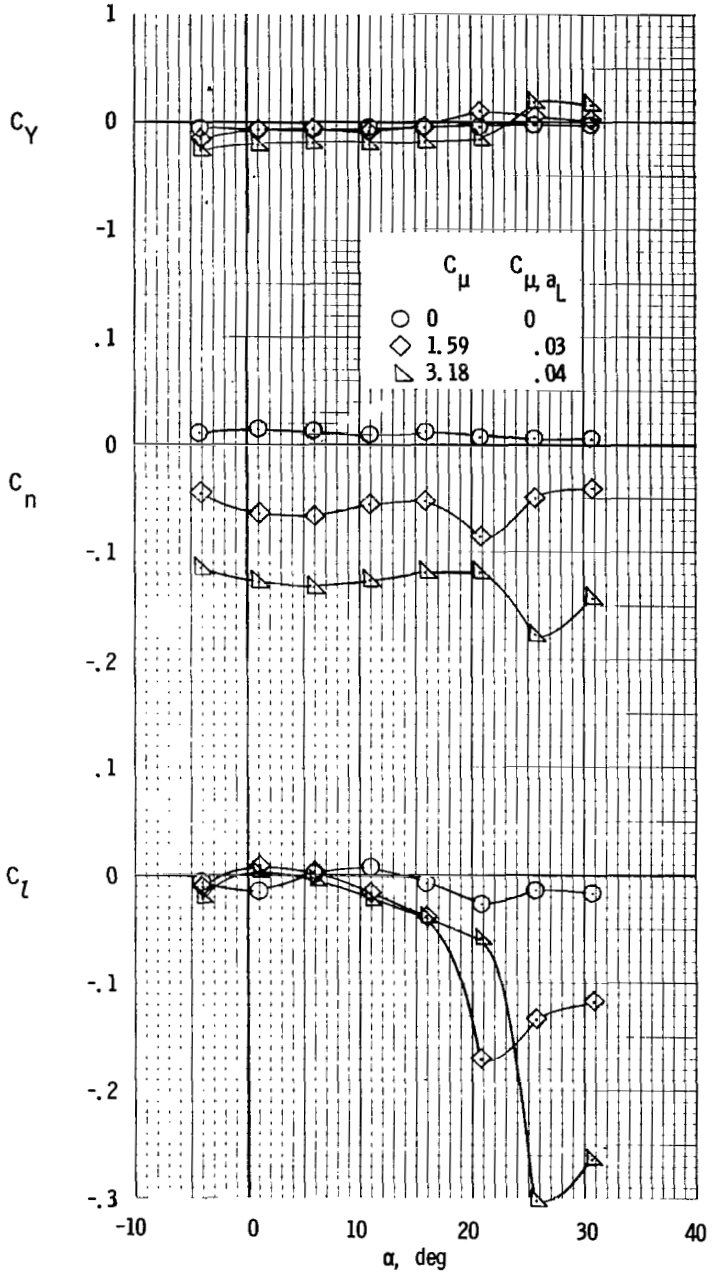

(a) Lateral characteristics.

Figure 35.- Lateral and longitudinal characteristics, left outboard engine not operating. Differential flap deflection; engines spread out; $(\delta_{f1}/\delta_{f2})_L = 30^o/60^o$; $(\delta_{f1}/\delta_{f2})_R = 20^o/40^o$; $i_t = 0^o$; $\delta_e = -50^o$; $\delta_{a_L} = 60^o$; $\delta_{a_R} = 40^o$; $C_{\mu,a_R} = 0$.

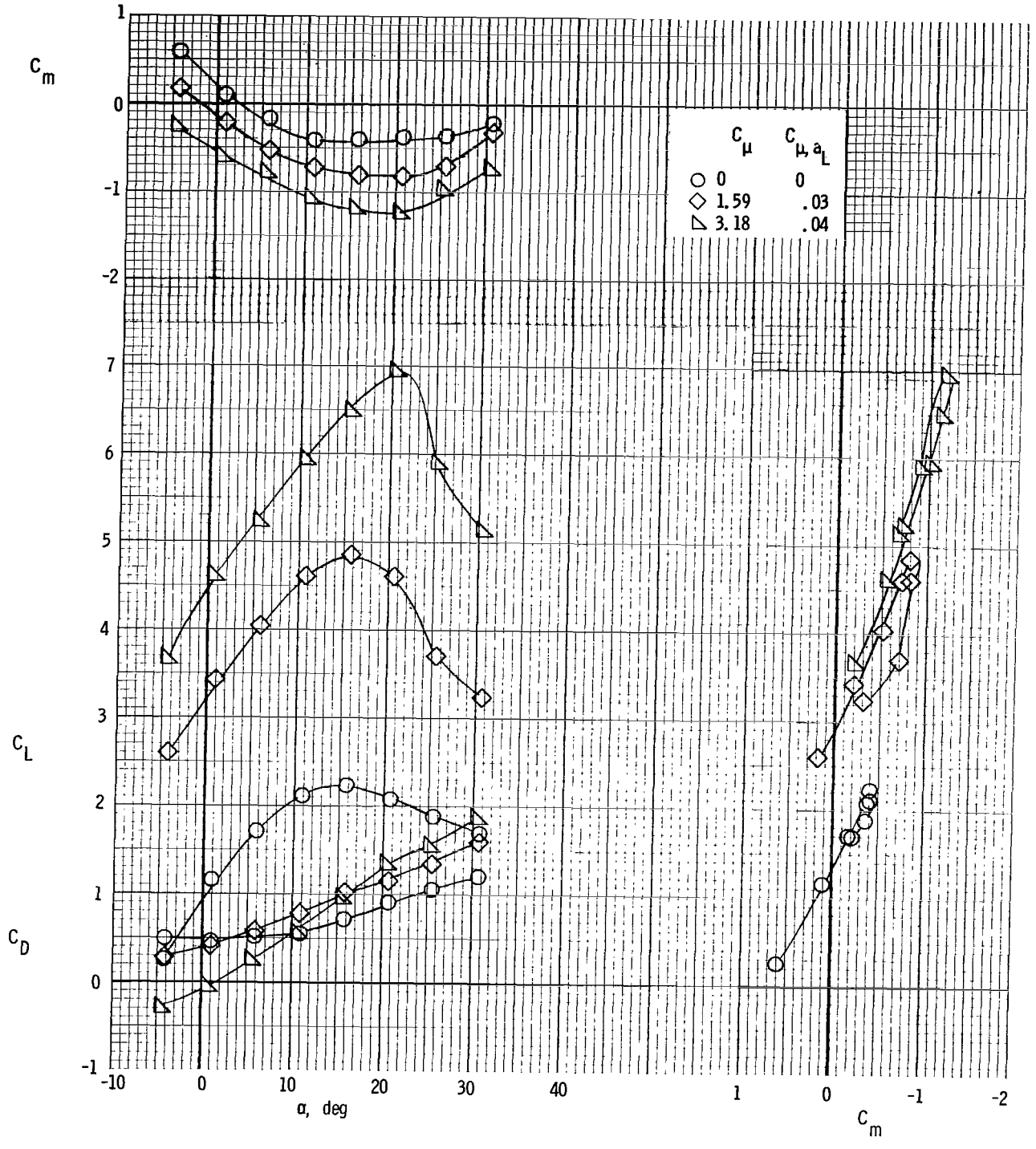

(b) Longitudinal characteristics.

Figure 35.- Concluded.

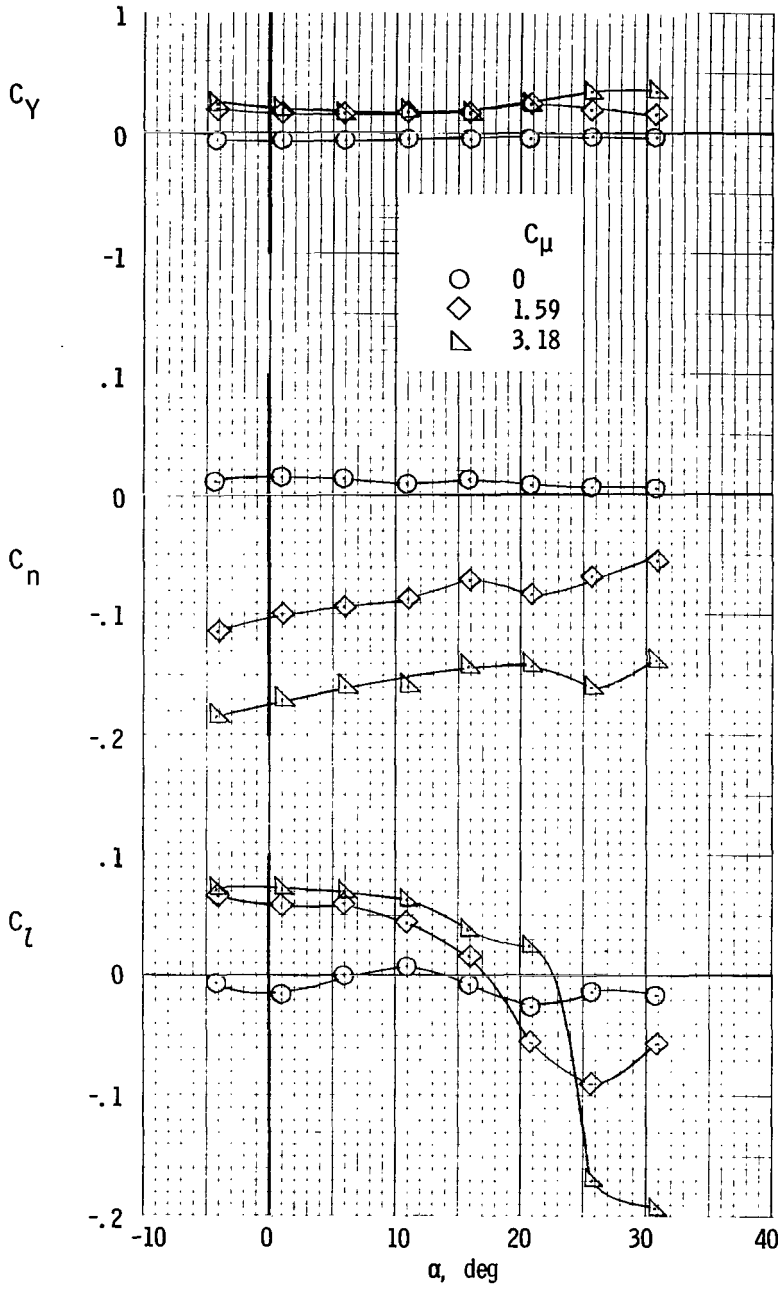

(a) Lateral characteristics.

Figure 36.- Lateral and longitudinal characteristics, left inboard engine not operating. Differential flap deflection; engines spread out; $(\delta_{f1}/\delta_{f2})_L = 30^o/60^o$; $(\delta_{f1}/\delta_{f2})_R = 20^o/40^o$; $i_t = 0^o$; $\delta_e = -50^o$; $\delta a_L = 60^o$; $\delta a_R = 40^o$.

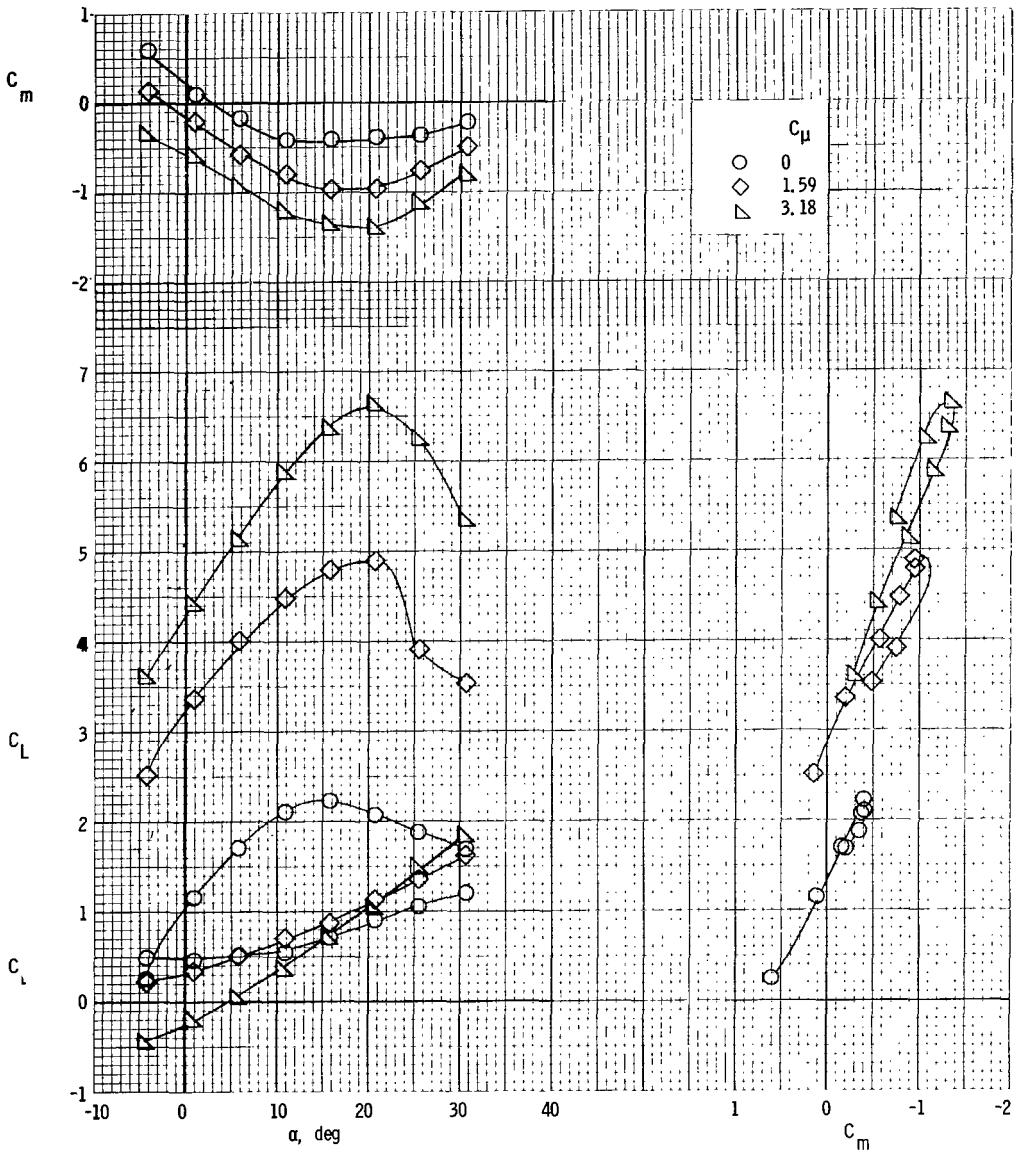

(b) Longitudinal characteristics.

Figure 36.- Concluded.

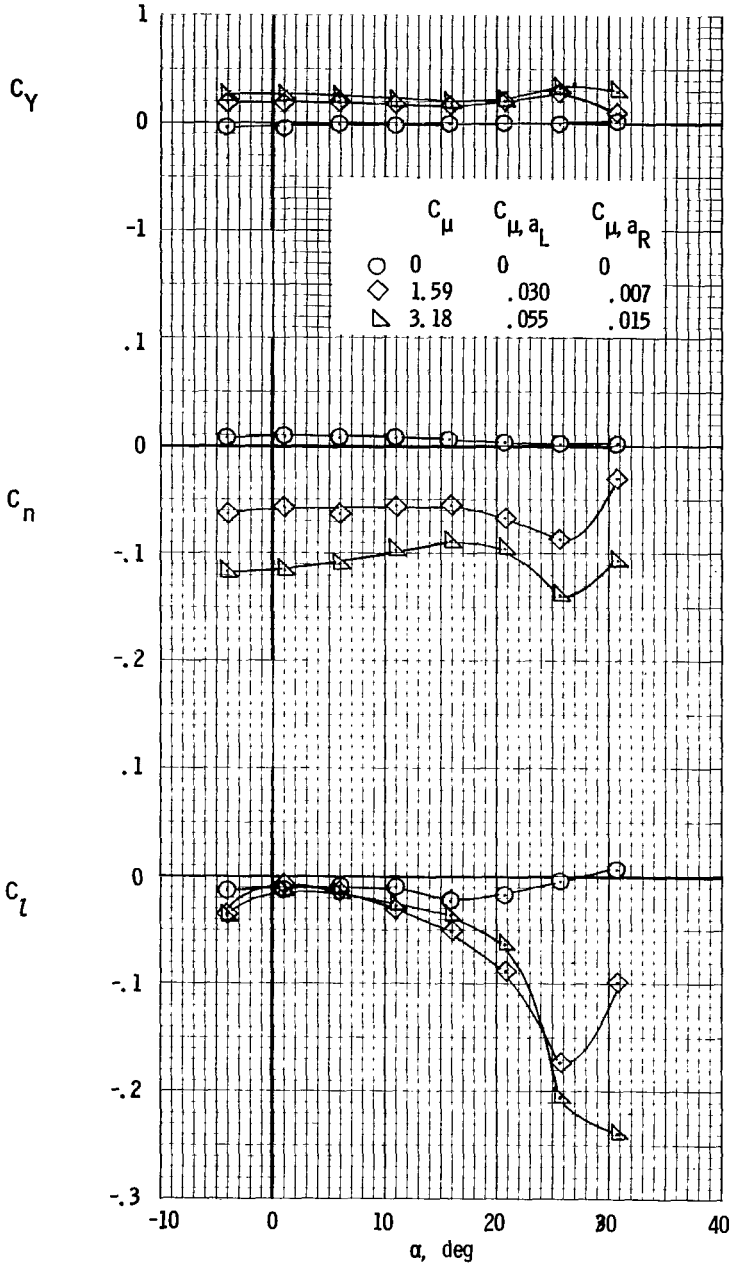

(a) Lateral characteristics.

Figure 37.- Lateral and longitudinal characteristics, left inboard engine not operating. Asymmetric aileron blowing; $\delta_{f1}/\delta_{f2} = 20^o/40^o$; $i_t = 0^o$; $\delta_e = -50^o$; $\delta_{a_L} = 40^o$; $\delta_{a_R} = 40^o$.

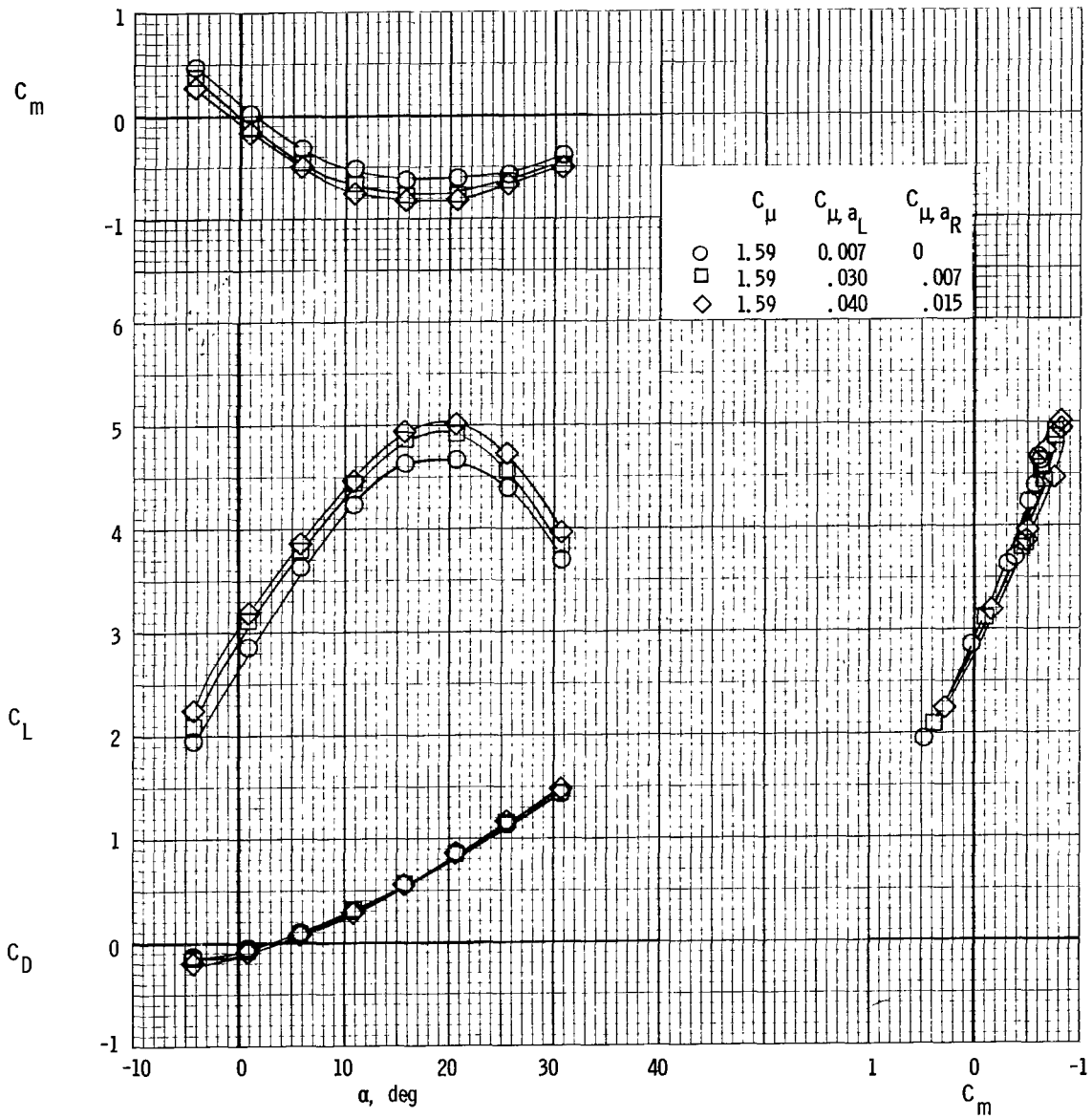

(b) Longitudinal characteristics.

Figure 37.- Continued.

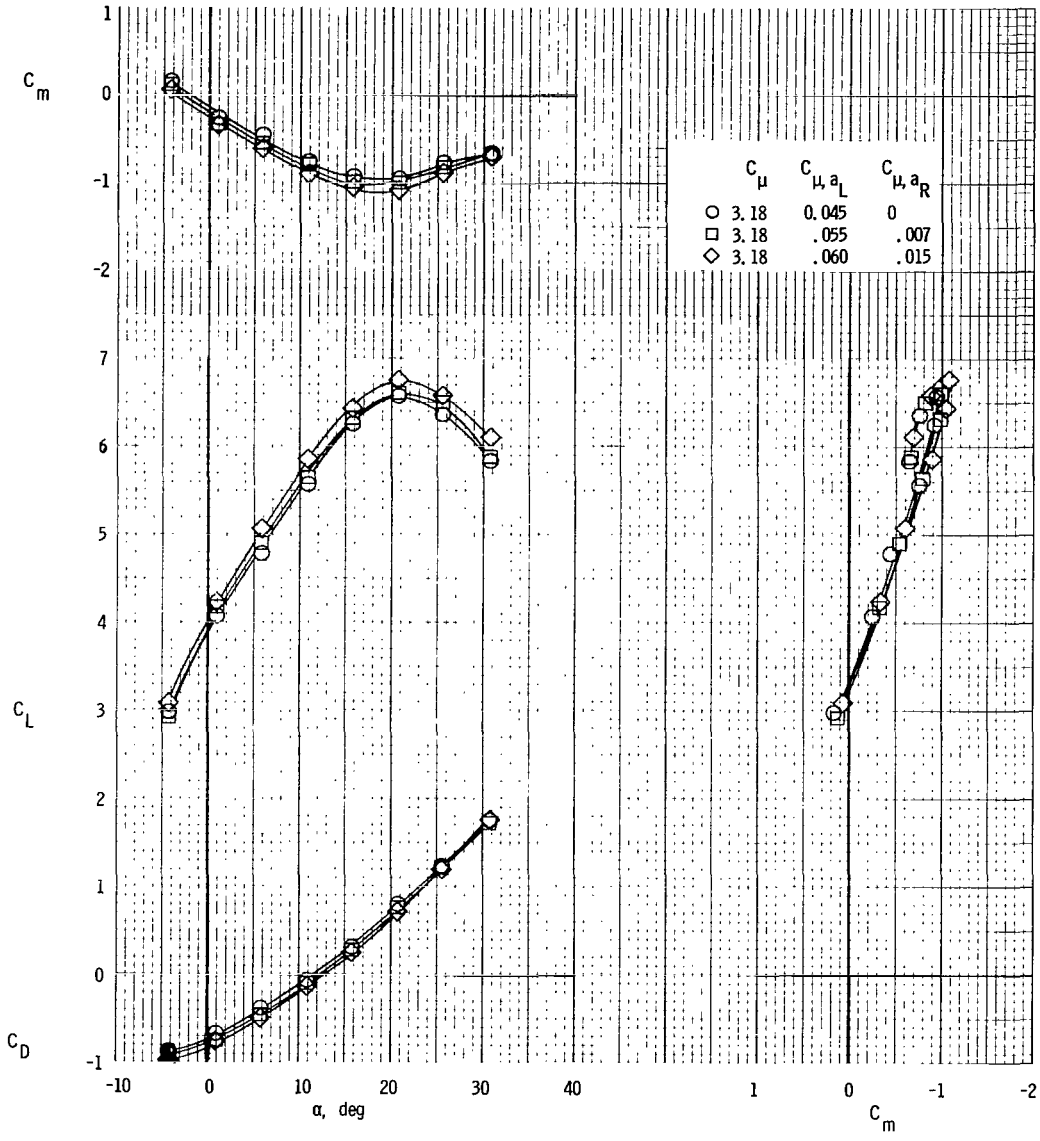

(b) Concluded.

Figure 37.- Concluded.

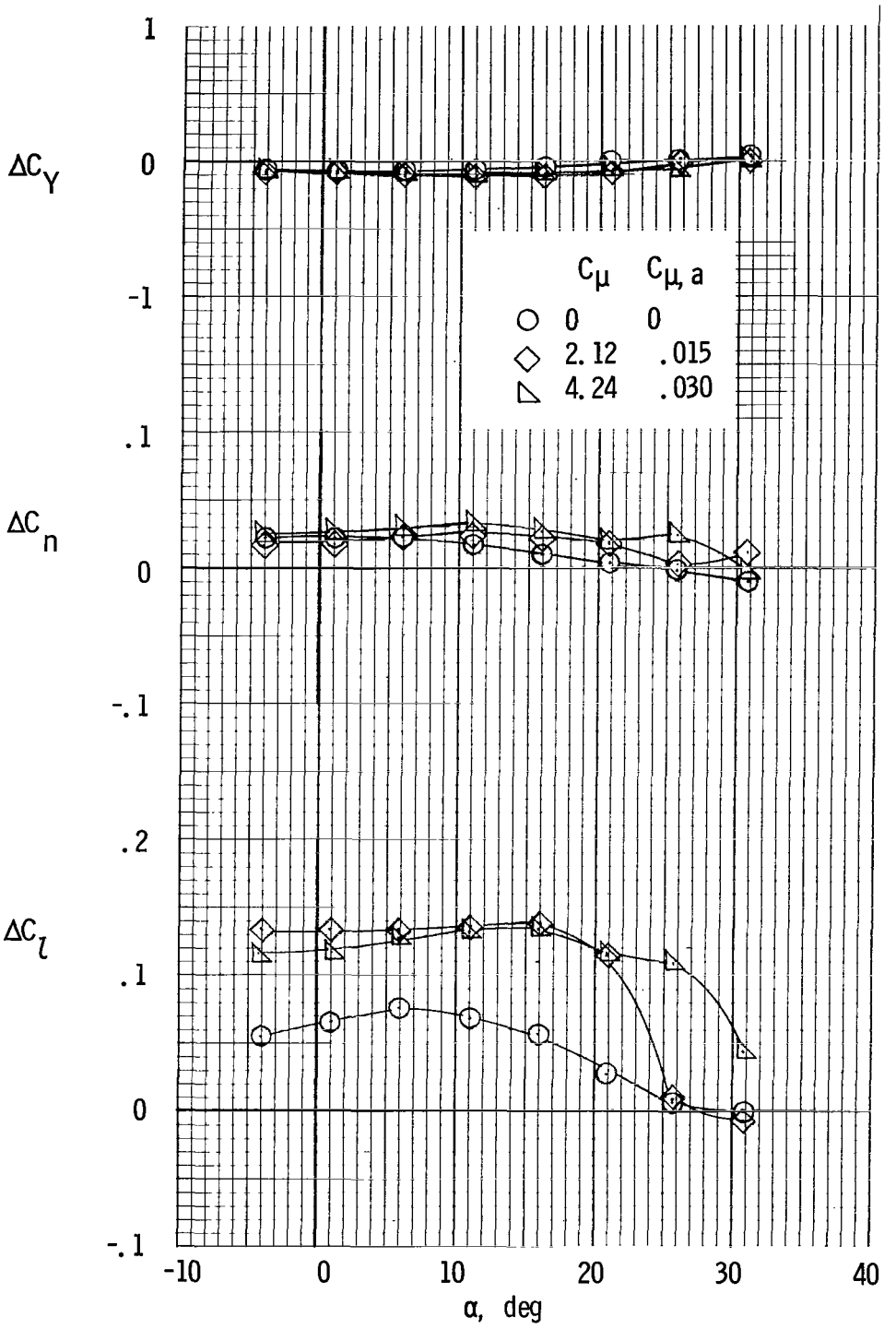

(a) Lateral characteristics, wing spoiler.

Figure 38.- Spoiler effectiveness. $\delta_s = 60^o$; $i_t = 0^o$; $\delta_e = -50^o$; $\delta_a = 60^o$; $\delta_{f1}/\delta_{f2} = 30^o/60^o$.

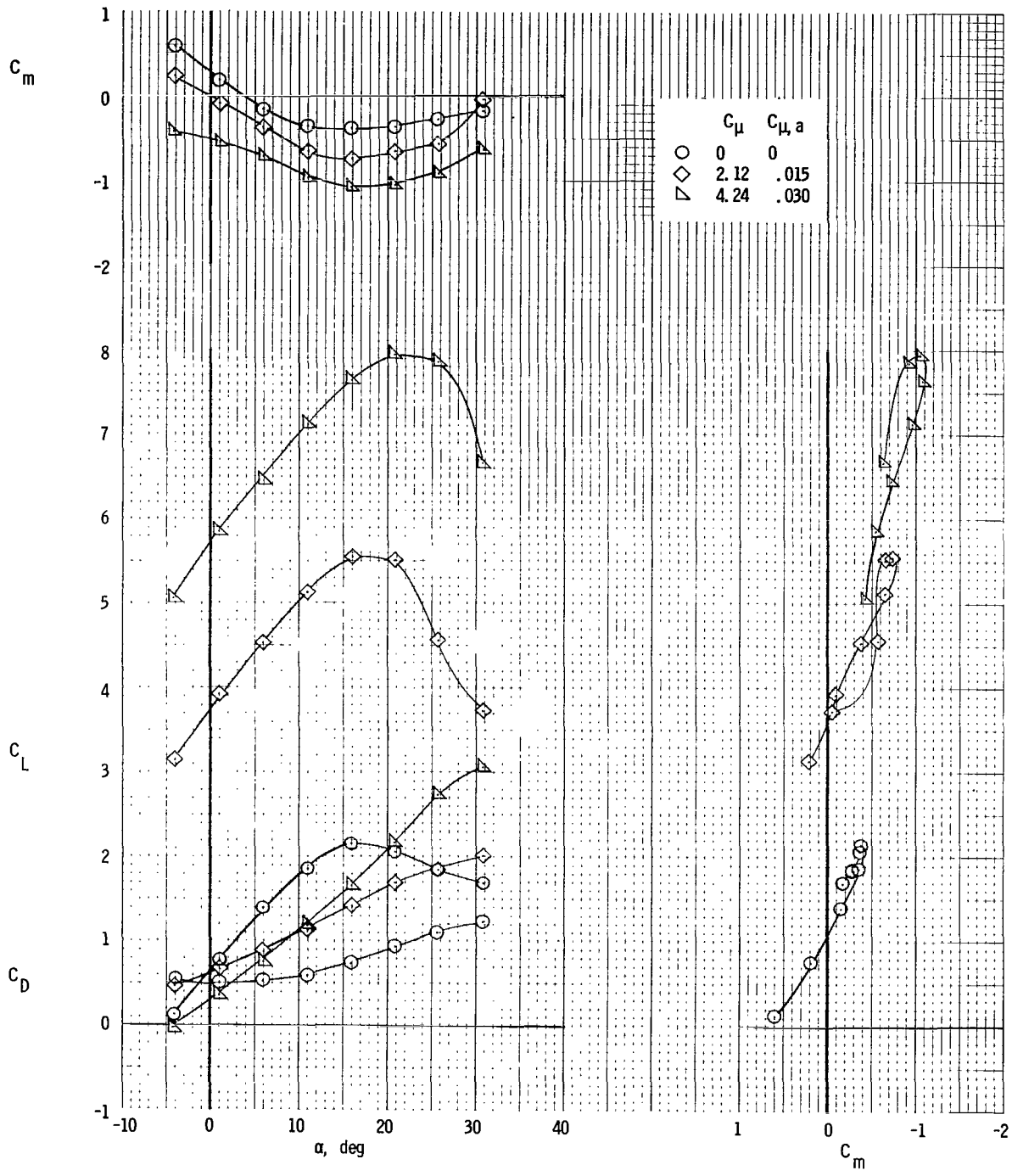

(b) Longitudinal characteristics, wing spoiler.

Figure 38.- Continued.

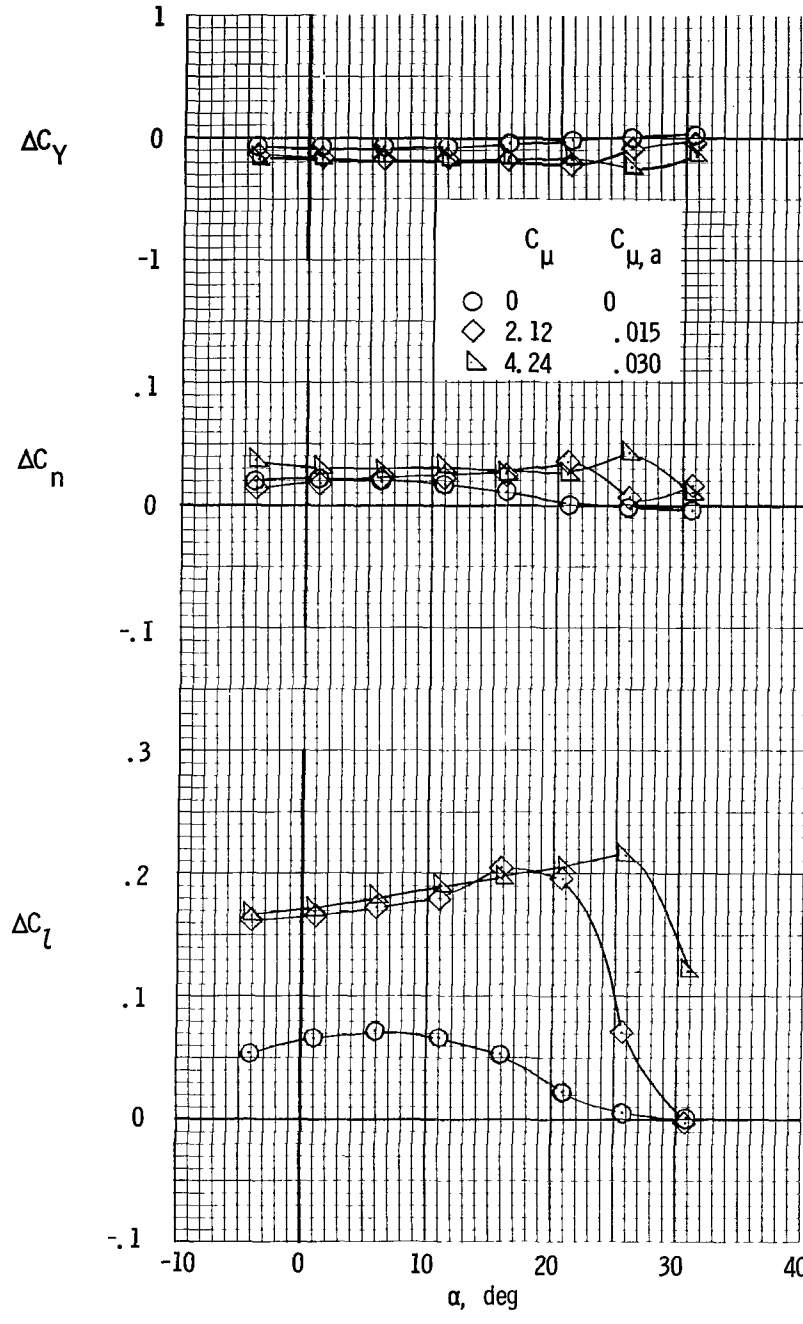

(c) Lateral characteristics, wing and flap spoilers.

Figure 38.- Continued.

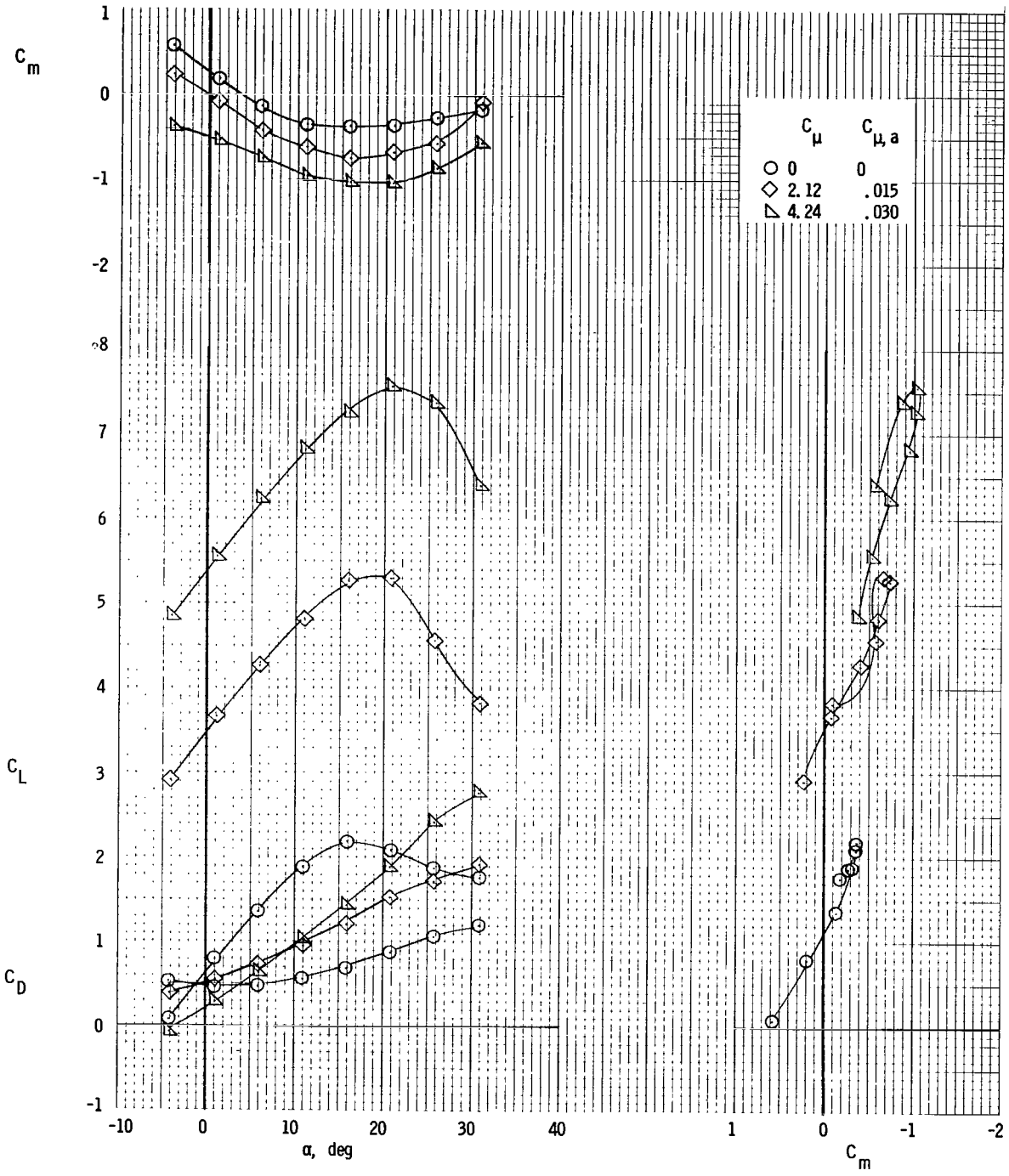

(d) Longitudinal characteristics, wing and flap spoilers.

Figure 38.- Concluded.

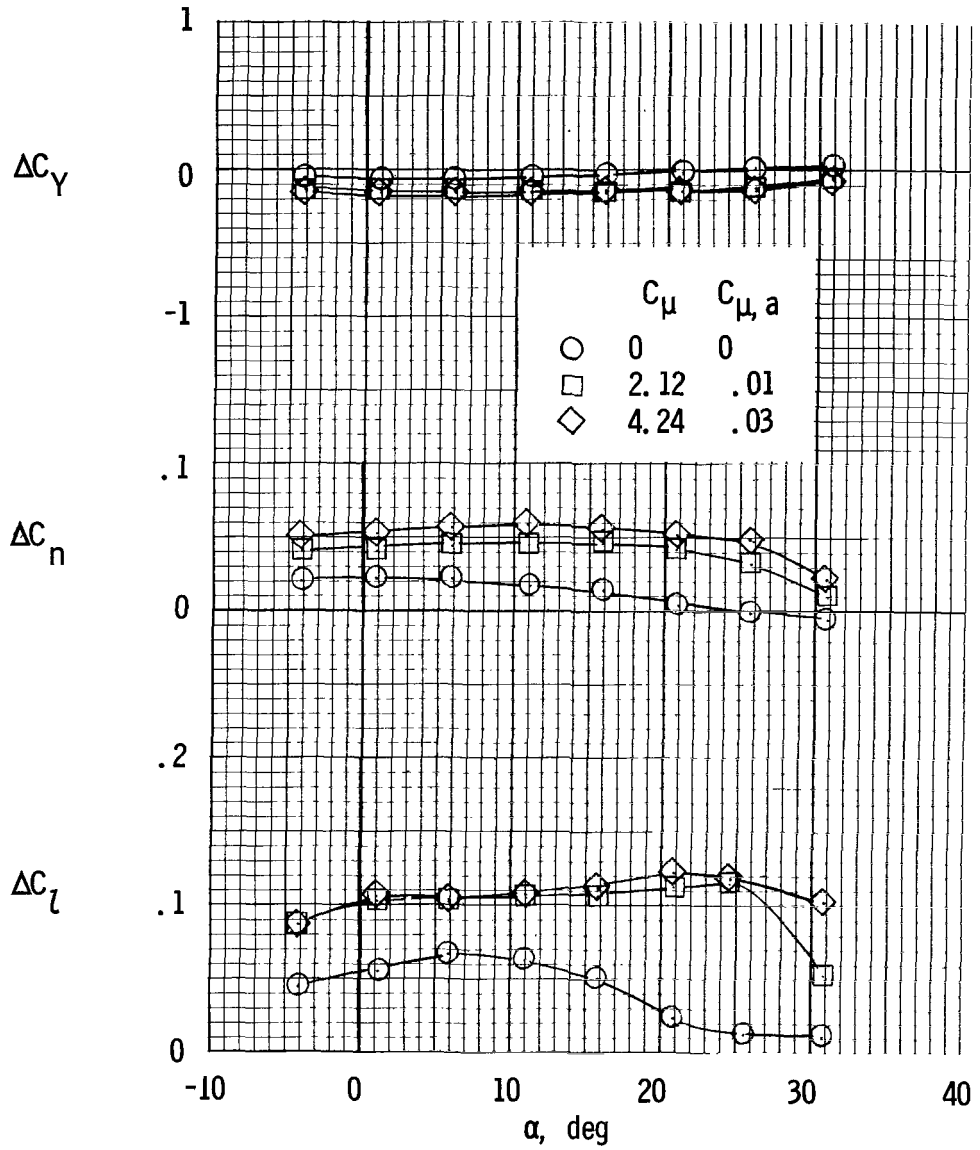

(a) Lateral characteristics.

Figure 39.- Spoiler effectiveness, wing and flap spoilers. $\delta_s = 60^o$; $i_t = 0^o$; $\delta_e = -50^o$; $\delta_a = 40^o$; $\delta_{f1}/\delta_{f2} = 20^o/40^o$.

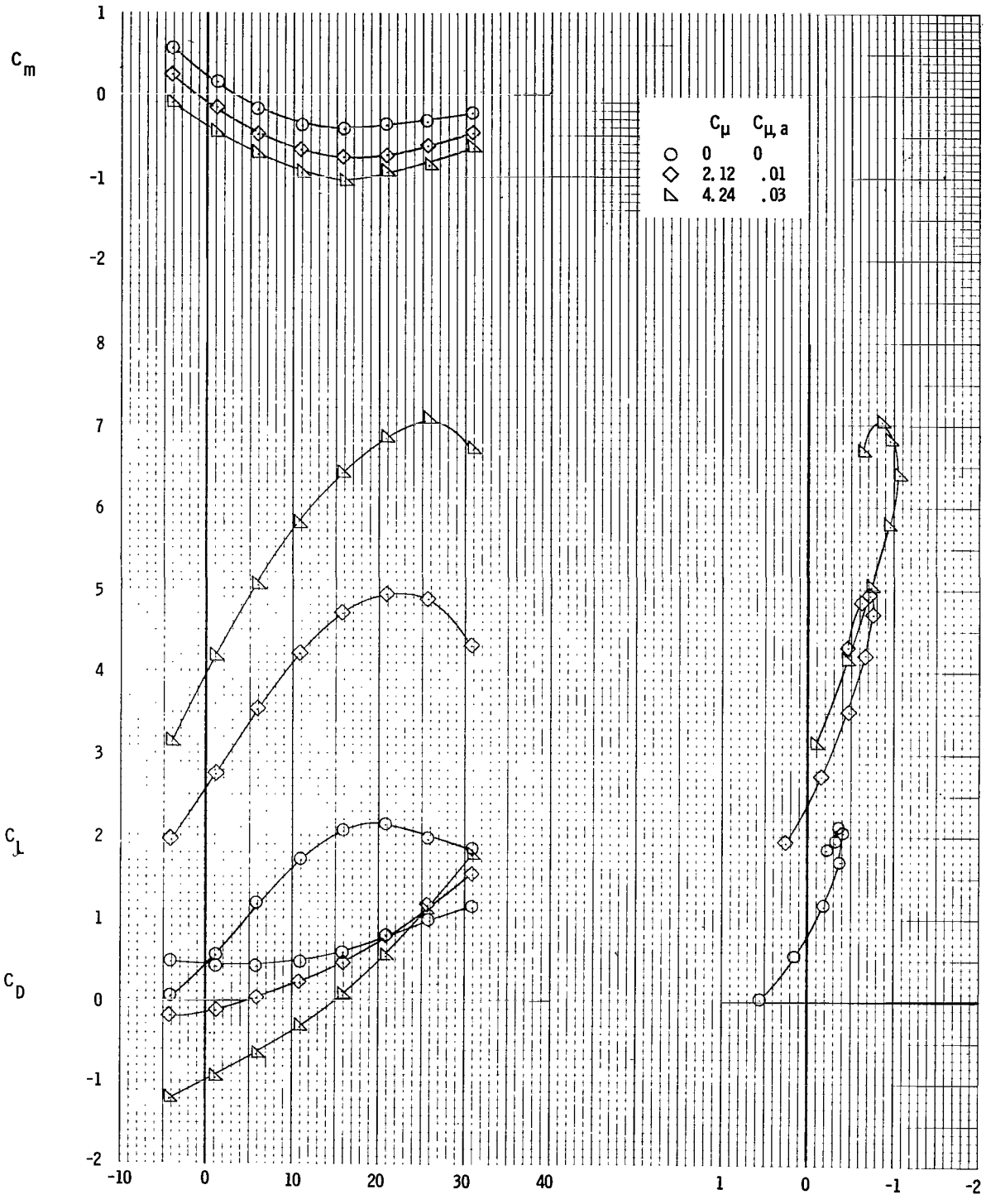

(b) Longitudinal characteristics.

Figure 39.- Concluded.

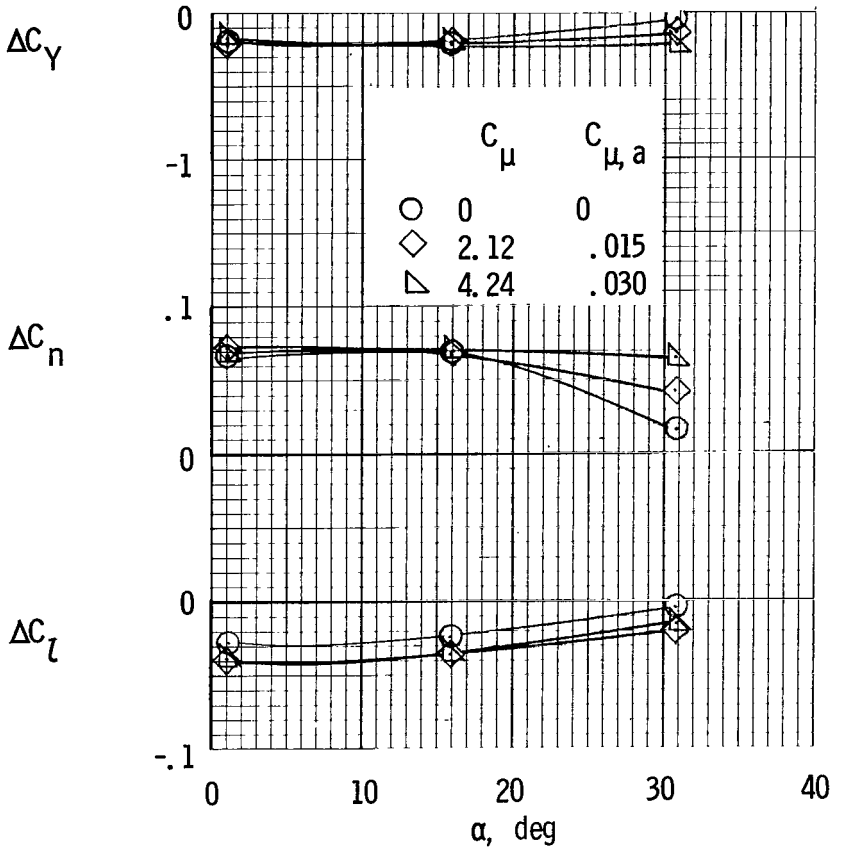

(a) $C_{\mu,r} = 0$.

Figure 40.- Rudder effectiveness. $\delta_r = -42^o$; $\delta_{f1}/\delta_{f2} = 30^o/60^o$; $i_t = 0^o$; $\delta_e = -50^o$; $\delta_a = 60^o$.

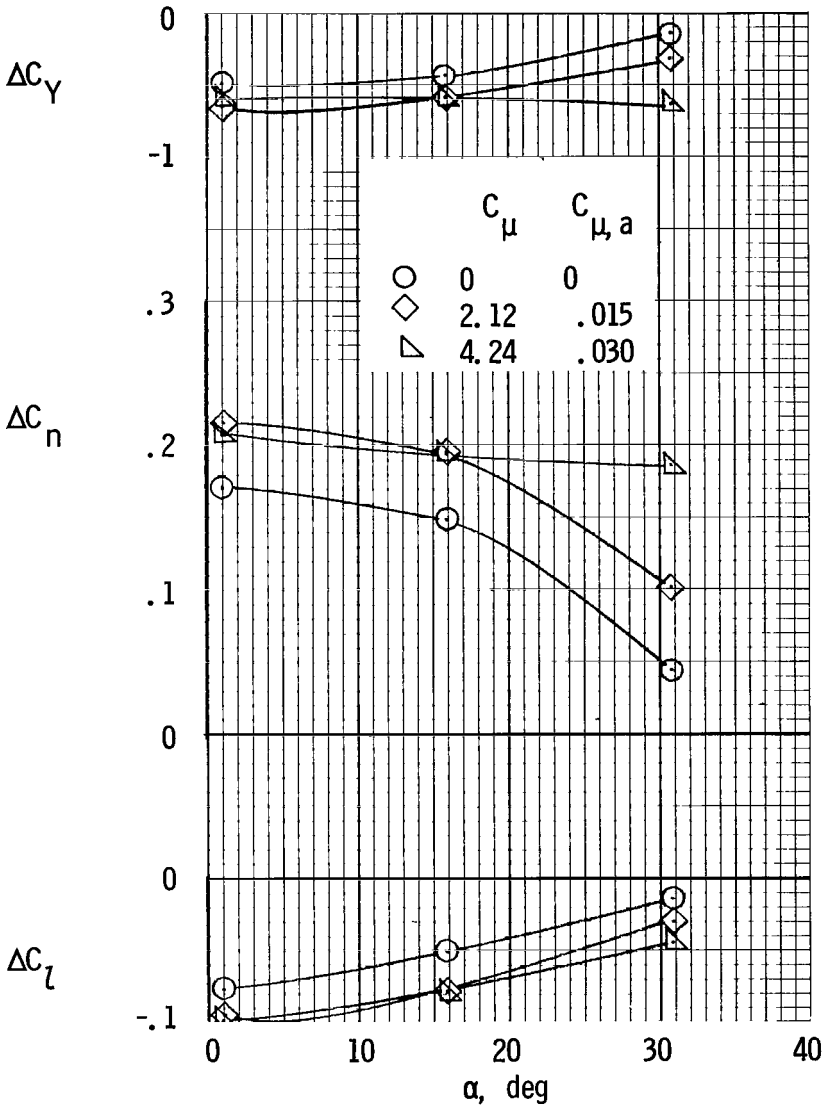

(b) $C_{\mu,r} = 0.021$.

Figure 40.- Continued.

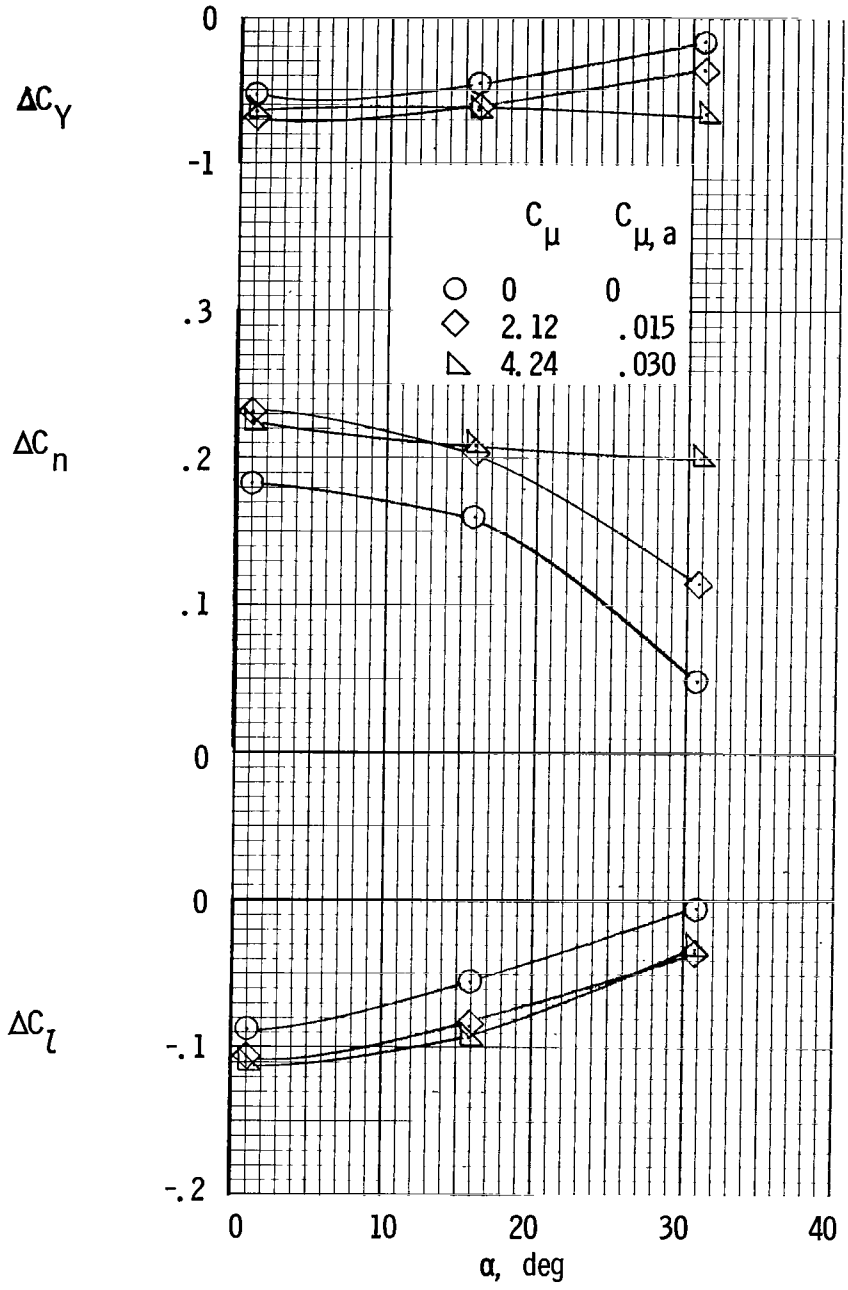

(c) $C_{\mu,r} = 0.027$.

Figure 40.- Concluded.

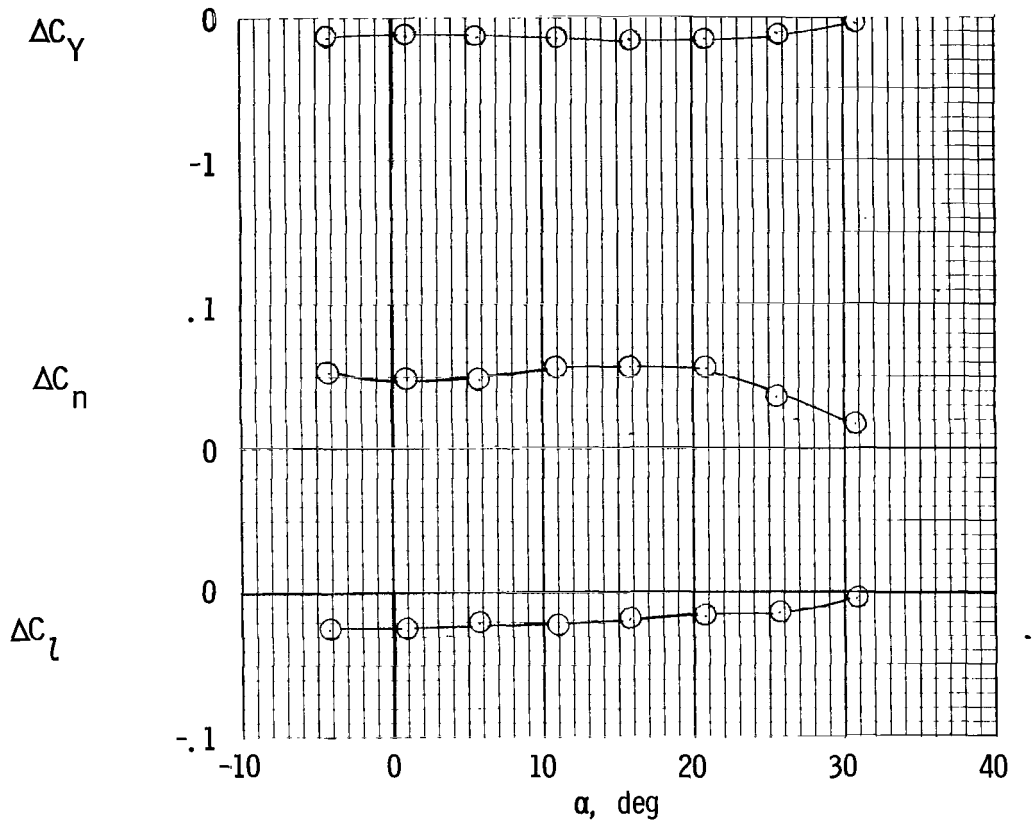

Figure 41.- Rudder effectiveness. $\delta_r = -42^o$; $\delta_f = 0^o$; $i_t = 0^o$; $\delta_e = 0^o$.

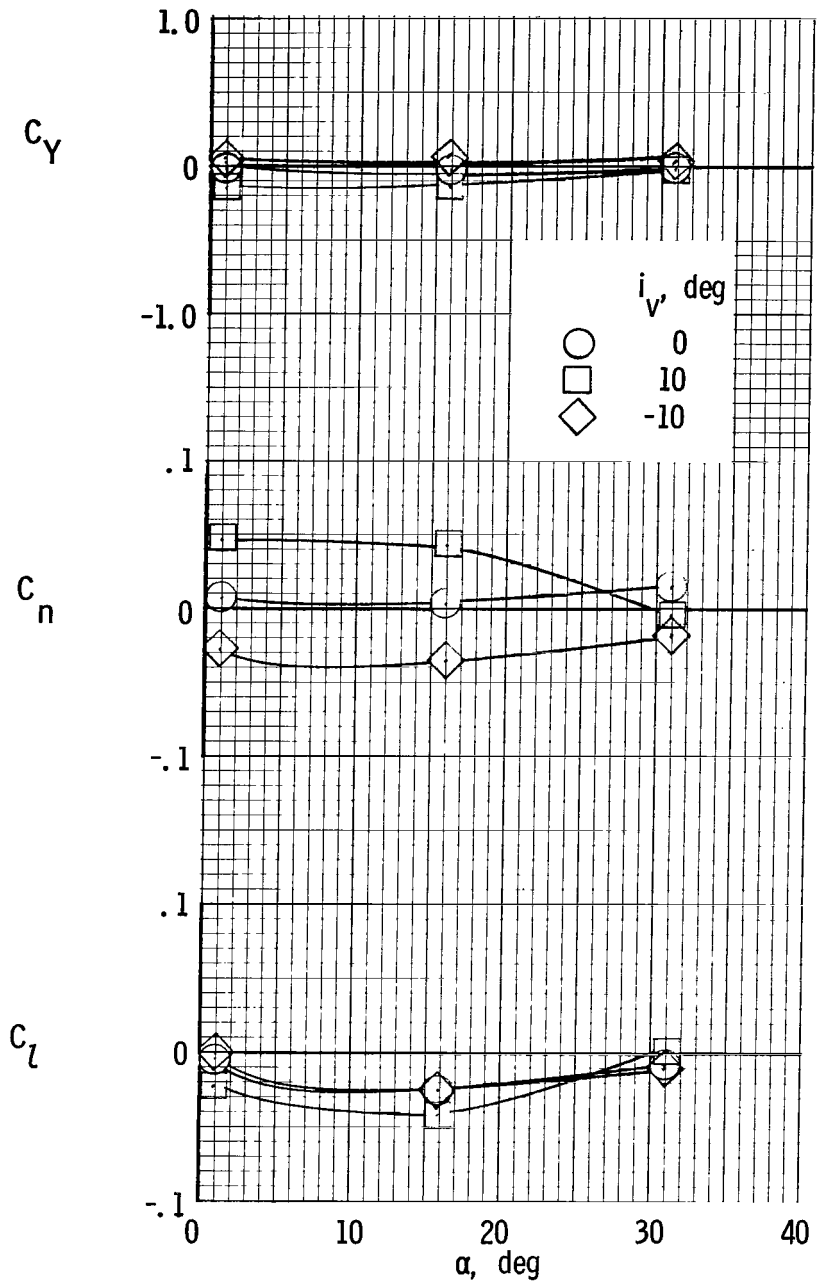

(a) $C_\mu = 0$; $C_{\mu,a} = 0$.

Figure 42.- Variation of lateral characteristics with vertical-tail incidence. $\delta_{f1}/\delta_{f2} = 30^o/60^o$; $\delta_a = 60^o$.

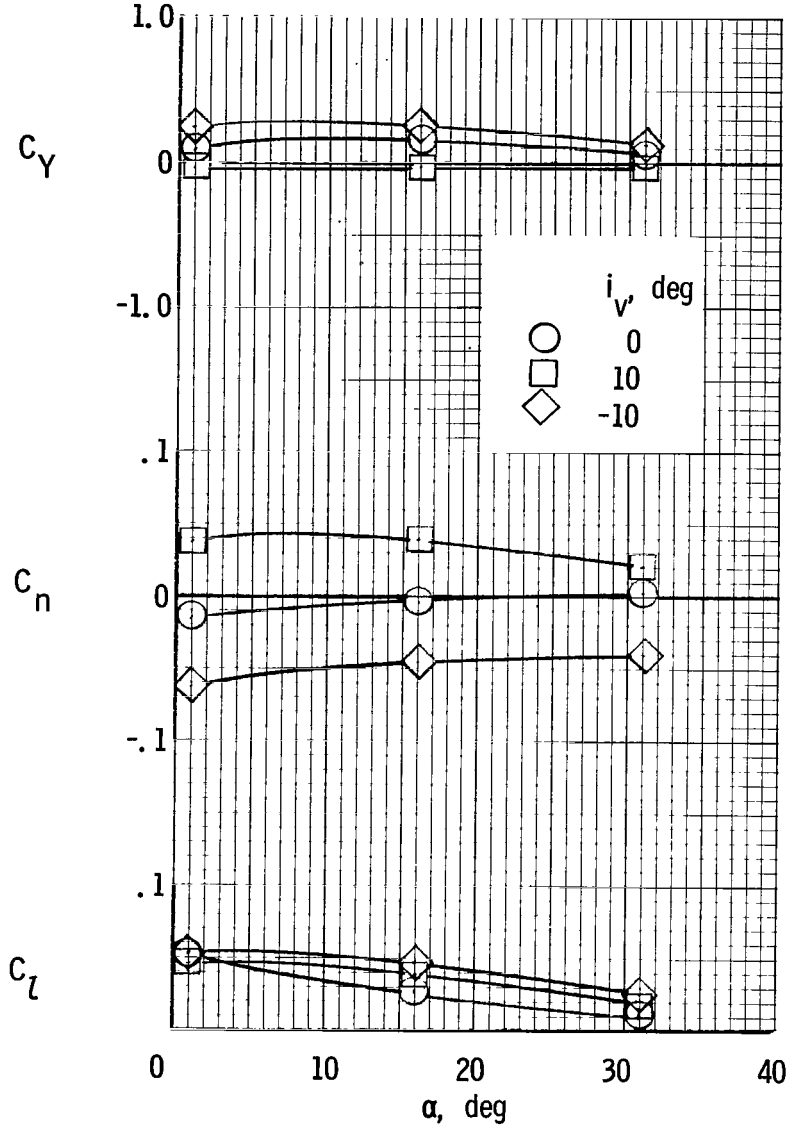

(b) $C_\mu = 2.12$; $C_{\mu,a} = 0.015$.

Figure 42.- Continued.

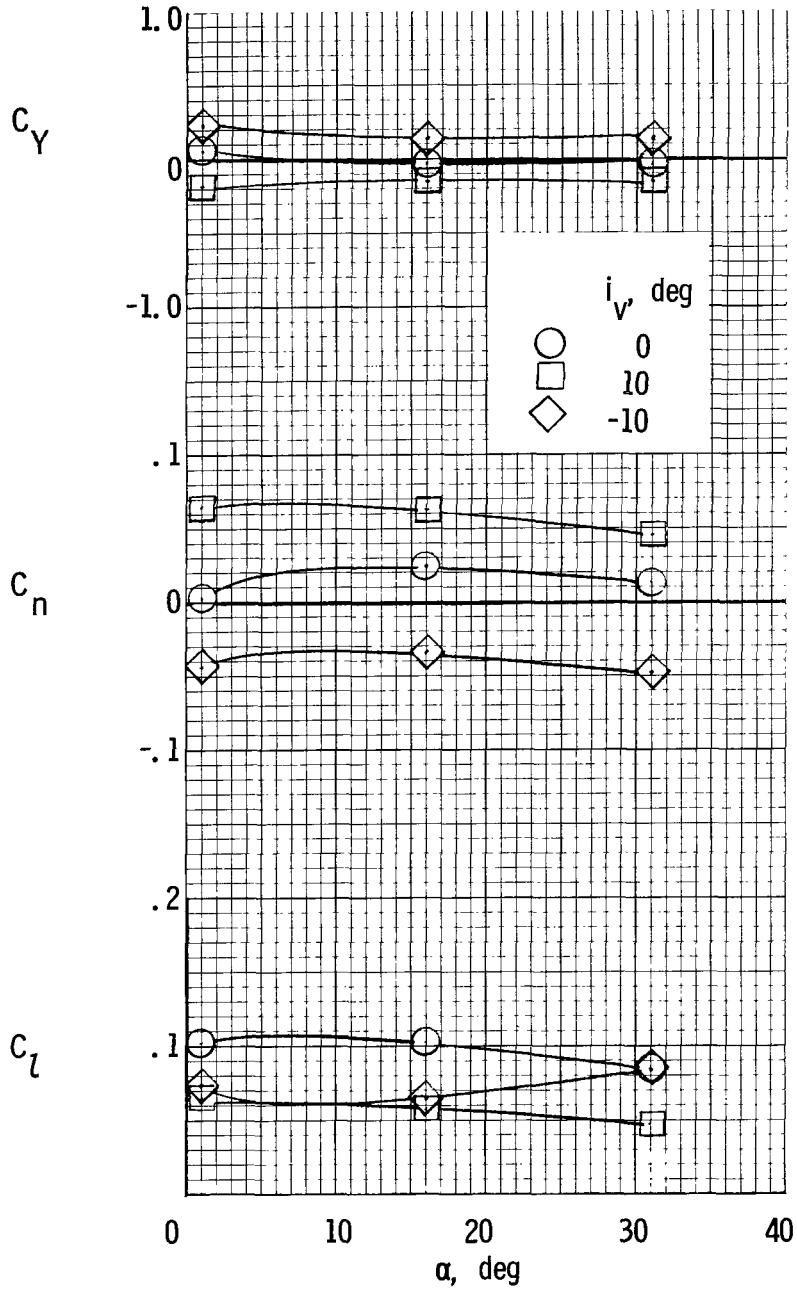

(c) C_μ = 4.24; $C_{\mu,a}$ = 0.03.

Figure 42.- Concluded.

NASA-Langley, 1970 —— 2 L-7403

"The aeronautical and space activities of the United States shall be conducted so as to contribute . . . to the expansion of human knowledge of phenomena in the atmosphere and space. The Administration shall provide for the widest practicable and appropriate dissemination of information concerning its activities and the results thereof."

—NATIONAL AERONAUTICS AND SPACE ACT OF 1958

NASA SCIENTIFIC AND TECHNICAL PUBLICATIONS

TECHNICAL REPORTS: Scientific and technical information considered important, complete, and a lasting contribution to existing knowledge.

TECHNICAL NOTES: Information less broad in scope but nevertheless of importance as a contribution to existing knowledge.

TECHNICAL MEMORANDUMS: Information receiving limited distribution because of preliminary data, security classification, or other reasons.

CONTRACTOR REPORTS: Scientific and technical information generated under a NASA contract or grant and considered an important contribution to existing knowledge.

TECHNICAL TRANSLATIONS: Information published in a foreign language considered to merit NASA distribution in English.

SPECIAL PUBLICATIONS: Information derived from or of value to NASA activities. Publications include conference proceedings, monographs, data compilations, handbooks, sourcebooks, and special bibliographies.

TECHNOLOGY UTILIZATION PUBLICATIONS: Information on technology used by NASA that may be of particular interest in commercial and other non-aerospace applications. Publications include Tech Briefs, Technology Utilization Reports and Technology Surveys.

Details on the availability of these publications may be obtained from:

SCIENTIFIC AND TECHNICAL INFORMATION DIVISION

NATIONAL AERONAUTICS AND SPACE ADMINISTRATION

Washington, D.C. 20546